ENHANCING AGRICULTURAL PRODUCTIVITY BY USING COLD ATMOSPHERIC PRESSURE PLASMA

A THESIS SUBMITTED TO THE

CENTRAL DEPARTMENT OF PHYSICS

INSTITUTE OF SCIENCE AND TECHNOLOGY

TRIBHUVAN UNIVERSITY

NEPAL

FOR THE AWARD OF

DOCTOR OF PHILOSOPHY

IN PHYSICS

BY

ROSHAN CHALISE

October 2024

ENHANCING AGRICULTURAL PRODUCTIVITY BY USING COLD ATMOSPHERIC PRESSURE PLASMA

A THESIS SUBMITTED TO THE

CENTRAL DEPARTMENT OF PHYSICS

INSTITUTE OF SCIENCE AND TECHNOLOGY

TRIBHUVAN UNIVERSITY

NEPAL

FOR THE AWARD OF

DOCTOR OF PHILOSOPHY

IN PHYSICS

BY

ROSHAN CHALISE

October 2024

TRIBHUVAN UNIVERSITY

Institute of Science and Technology

DEAN'S OFFICE

Kirtipur, Kathmandu, Nepal

Reference No.:

EXAMINERS

Institute of Science & Technology
Dean's Office
Kirtipur 2045

The Title of Ph.D. Thesis: "Enhancing Agricultural Productivity by Using Cold Atmospheric Pressure Plasma"

Name of Candidate: Roshan Chalise

Internal Examiner:

Dr. Nurapati Pantha
Central Department of Physics
Tribhuvan University, NEPAL

External Examiners:

(1) Prof. Dr. Raju Bhai Tyata
Khwopa College of Engineering
Bhaktapur, NEPAL

(2) Dr. Mukesh Ranjan
Institute for Plasma Research
Gandhinagar, INDIA

(3) Prof. Dr. Masaharu Shiratani
Center of Plasma Nano-interface Engineering
Kyushu University
Fukuoka, JAPAN

28 October, 2024

(Dr. Surendra Kumar Gautam)
Asst. Dean

DECLARATION

Thesis entitled "**Enhancing Agricultural Productivity by using Cold Atmospheric Pressure Plasma**" which is being submitted to the Central Department of Physics, Institute of Science and Technology (IoST), Tribhuvan University, Nepal for the award of the degree of Doctor of Philosophy (Ph.D.); is a research work carried out by me under the supervision of Prof. Dr. Raju Khanal of Central Department of Physics, Tribhuvan University and co-supervised by Dr. Bhagirath Ghimire of The University of Alabama, Huntsville, AL, USA.

This research is original and has not been submitted earlier in part or full in this or any other form to any University or institute, here or elsewhere, for the award of any degree.

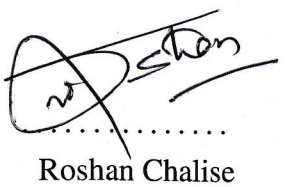

.....

Roshan Chalise

RECOMMENDATION

This is to recommend that **Mr. Roshan Chalise** has carried out research entitled **"Enhancing Agricultural Productivity by using Cold Atmospheric Pressure Plasma"** for the award of Doctor of Philosophy (Ph.D.) in **Physics** under our supervision. To our knowledge, this work has not been submitted for any other degree.

He has fulfilled all the requirements laid down by the Institute of Science and Technology (IoST), Tribhuvan University, Kirtipur for the submission of the thesis for the award of a Ph.D. degree.

.....

Dr. Raju Khanal
Supervisor
(Professor)
Central Department of Physics,
Tribhuvan University,
Kirtipur, Kathmandu, Nepal

Dr. Bhagirath Ghimire
Co-Supervisor
The University of Alabama,
Huntsville, AL, USA

October 2024

TRIBHUVAN UNIVERSITY
CENTRAL DEPARTMENT OF PHYSICS
Kirtipur, Kathmandu, Nepal

☎ 4331054
www.tucdp.edu.np

Ref. No.: (F.No .....) CDP .....

Tribhuvan University Central Department of Physics Kirtipur

Date: 2081-08-16

LETTER OF APPROVAL

Date:

On the recommendation of **Prof. Dr. Raju Khanal**, and **Dr. Bhagirath Ghimire**, this Ph.D. thesis submitted by **Mr. Roshan Chalise**, entitled **"Enhancing Agricultural Productivity by using Cold Atmospheric Pressure Plasma"** is forwarded by the Central Department of Research Committee (CDRC) to the Dean, IoST, T.U.

O.P. Niraula

Dr. Om Prakash Niraula
(Professor)
Head
Central Department of Physics,
Tribhuvan University, Kirtipur,
Kathmandu, Nepal

ACKNOWLEDGMENTS

I have presented lots of results by graphs, pictures, and descriptions in my Ph.D. dissertation. However, this dissertation's success is attributed to the constant encouragement, perceptive feedback, inspiration, criticism, and support provided by various personalities and organizations.

First and foremost, I extend my heartfelt gratitude to Prof. Raju Khanal (Supervisor) and Dr. Bhagirath Ghimire (Co-supervisor) for their invaluable academic guidance, moral support, and a plethora of subject-matter expertise. Without their mentorship and encouragement, my academic progress and the completion of this thesis would not have been possible. I am also deeply thankful to Prof. Eun Ha Choi and his team at the Plasma Bioscience Research Center, Department of Electrical and Biological Physics, Kwangwoon University, Seoul, Republic of Korea. Their hospitality and training were important in enhancing my understanding of plasma production, characterization, and applications, and also essential for establishing a plasma lab at the Central Department of Physics, Tribhuvan University, Kirtipur, Nepal.

I would like to express my sincere thanks to Prof. Dr. Om Prakash Niraula, Head of Central Department of Physics (CDP), Tribhuvan University, Kirtipur, Kathmandu, Nepal and to Prof. Dr. Binil Aryal, Dean of Institute of Science and Technology (IoST), Tribhuvan University, Kirtipur, Kathmandu, Nepal for their guidance throughout the work, and encouragements in the initial phases of the establishment of the plasma lab infrastructure. I would like to extend my sincere thanks to Prof. Dr. Narayan Prasad Adhikari for his encouraging words and for sharing knowledge during my academic years. I got an opportunity to do project work under his guidance in the second semester too. I would like to express my sincere gratitude to Prof. Dr. Hari Prasad Lamichhane for his invaluable guidance and support at every step of my work, from discussions on underlying principles to designing the experimental setup and interpreting the results. Moreover, I am thankful to all the respected teachers and staff of CDP who helped and encouraged me while I had just initiated my research career.

I am thankful to Prof. Dr. Deepak Prasad Subedi, Kathmandu University, Dhulikhel for providing me the opportunity to visit the plasma lab and insight into low-temperature plasma and its applications. In particular, I started plasma treatment of wheat and using a goniometer which also resulted in fabrication and validation of our low-cost prototype goniometer. Dr. Pradeep Lamichhane, currently in the UK, and Dr. Rajesh Prakash Guragain for many rounds of discussions and support particularly in the electric characterization of plasma. I am also thankful to Dr. Deepak Raj Panta, Central Department of Botany, Tribhuvan University, Kirtipur for the suggestions and

cooperation in the measurement of chlorophyll of green leaves. I am indebted to Prof. Dr. Leela Pradhan Joshi, Prof. Dr. Rajendra Parajuli, Mr. Pitamber Shrestha, Dr. Dinesh Kumar Chaudhary, and the entire faculties and staff of Amrit Campus, Tribhuvan University, Lainchaur, Kathmandu for their encouragements and suggestions.

Special thank goes to group members of the plasma lab at CDP and collaborators from international institutions for their invaluable contributions, namely Mr. Sangat Sharma and Dr. Suresh Basnet at CDP, Mr. Sandesh Devkota (USA), Dr. Himali Kalakhety (Texas AM University-Kingsville, USA), and Dr. Satyananda Kar (IIT Delhi, India). I am thankful to all my student colleagues, who worked under my supervision and contributed significantly to my research, including Mr. Abdul K Khan, Mr. Amrit Kumar Yadav, Mr. Angash Niroula, Mr. Asish Dahal, Mr. Asish Tamang, Mr. Avash Kattel, Mr. Deepak Niure, Mr. Oat Bahadur Dhakal, Mr. Prabin Bhandari, Mr. Prakash Kattel, Ms. Pooja Shrestha, Mr. Prajwal Lamichhane, Ms. Roshani Dahal, and Dr. Tirtha Raj Acharya.

I am also grateful to the team of Changing Nepal who supported us in managing necessary instruments for our plasma lab by importing them promptly from abroad on our request, National Innovation Center (NIC), Kirtipur for providing their mechanical lab facilities in designing our various experimental setups, Nepal Agricultural Research Council (NARC), Khumaltar for guiding standard seeds and farming conditions, and Balambu Mushroom Co-operative Ltd, Chandragiri for sharing knowledge and collaboration in mushroom seeds and making mushroom spawns bag.

I am highly indebted to the University Grants Commission (UGC), Sanothimi, Bhaktapur for the Ph.D. fellowship grant: PhD-78/79-S&T-16. The support provided by the Research Coordination and Development Council, Tribhuvan University, Kirtipur, through my supervisor as the Principal Investigator under the National Priority Area Research Grant: TU-NPAR-077/78-ERG-12, which played an important role in the establishment of the plasma physics research laboratory at CDP.

Finally, I have no words to express my thankfulness to my family members, especially my father Mr. Narayan Chalise, my mother Mrs. Maya Devi Chalise, and my wife Mrs. Saru Ghimire, whose unwavering support sustained me through challenging times.

Roshan Chalise
October 2024

कृषि उत्पादकत्वको वृद्धि गर्न प्लाज्माको प्रयोग

रोशन चालिसे
(विद्यावारिधि शोधार्थी)
भौतिकशास्त्र केन्द्रीय विभाग
विज्ञान तथा प्रविधि अध्ययन संस्थान
त्रिभुवन विश्वविद्यालय, कीर्तिपुर
काठमाडौं, नेपाल

शोध सार

क्रमशः वृद्धि भइरहेको जनसङ्ख्या, घट्दै गइरहेको कृषियोग्य जमिन र जलवायु परिवर्तन लगायतका कारणले आवश्यक खाद्यान्न तथा कृषि उपजहरूको उत्पादकत्वमा वृद्धि गर्न विभिन्न प्रविधिको प्रयोग तथा अनुसन्धान भइरहेको सर्वविदितै छ । विगत केही समयदेखि प्लाज्माको प्रयोग गरी कृषिजन्य उत्पादनको वृद्धि, बिउ–बिजनको गुणस्तरमा सुधार, बिरुवाहरूको वृद्धि गर्नका साथसाथै उत्पादित फलहरूको गुणस्तरमा आँच आउन नदिई लामो समयसम्म सुरक्षित राख्न विभिन्न अनुसन्धनात्मक कार्यहरू भइरहेका छन् ।

प्लाज्मा भन्नाले आयोनिकृत अवस्थामा रहेको, एकत्रित (collective) गुण देखाउने पदार्थको अवस्था भन्ने बुझिन्छ, जसलाई ठोस, तरल र ग्याँसपछिको चौथो अवस्था पनि भन्ने गरिन्छ । हाम्रो ब्रह्माण्डका अधिकतम पदार्थहरू प्लाज्मा अवस्थामा रहेको भए तापनि पृथ्वीमा प्राकृतिक रूपमा पाइने प्लाज्मा चट्याङ पर्दा दखिने झिल्काहरू हुन् । यस अनुसन्धानमा वायुमण्डलमा प्राकृतिक रूपमा उत्पन्न हुने चट्याङ (प्लाज्मा) लाई नियन्त्रित रूपमा प्रयोगशालामा तिन भिन्न तरिकाले उत्पादन गरिएको छ । चट्याङ पर्न उच्च मात्राको विद्युतीय शक्ति आवश्यक भए जस्तै कृत्रिम रूपमा प्रयोगशालामा प्लाज्मा बनाउनका लागि पनि उच्च मात्राको विद्युतीय शक्ति (भोल्टेज) चाहिने हुनाले स्थानीय बजारमा पाइने कम खर्चिला सामानहरूको प्रयोग बाट उच्च भोल्टेज दिन सक्ने ट्रान्सफर्मर निर्माण गरी नियन्त्रित रूपमा प्लाज्माको उत्पादन गरिएको छ । यसरी वायुमण्डलीय चापमा उत्पादित प्लाज्माको तापक्रम र घनत्वका साथसाथै प्लाज्मा नै उत्पादन भएको हो भन्ने यकिन गर्न विद्युतीय सूचकहरूको स्थापित वैज्ञानिक विधिहरूबाट मापन गरिएको छ । उत्पादन गरिएका प्लाज्माको तापक्रम र घनत्वले न्यून तापक्रम भएका प्लाज्माका नियमहरू अवलम्बन गरेका र प्रत्यक्ष प्रयोगमा तापमानले पदार्थमा क्षतिग्रस्त नदेखिएकोले यस प्रयोगशालाका प्लाज्माहरूलाई दैनिक जीवनका विभिन्न उपयोगी काममा प्रयोग गर्न उचित पाइएको छ ।

यसरी उत्पादित प्लाज्मालाई कृषि उपज (अन्नबाली, नगदेबाली र हरियो सागपात) को छिटो अङ्कुरण गराउन, बिरुवाको वृद्धि र कृषि उत्पादन बढाउन, पानीमा भएका ब्याक्टेरियालाई नस्ट पार्नका साथसाथै पातको हरियोपनलाई लामो समयसम्म कायम राख्न सकिने उद्देश्यले अनुसन्धनात्मक प्रयोग गरिएको छ । यसका लागि प्रत्यक्ष र अप्रत्यक्ष दुई विधि अपनाइएको छ । प्रत्यक्ष विधिमा बिउ या अनुसन्धान गर्नुपर्ने सम्बन्धित वस्तुलाई सिधै प्लाज्माको सम्पर्कमा ल्याइन्छ भने अप्रत्यक्ष विधिमा पानीमा प्लाज्मा पठाएर प्लाज्मायुक्त पानीको उत्पादन गरी उक्त पानीलाई बिउ–बिजन, बिरुवा तथा सम्बन्धित वस्तुहरूमा प्रयोग गरिएको हुन्छ । लामो समयसम्म प्लाज्माको प्रत्यक्ष प्रयोगले बिउको तापक्रम वृद्धि भई प्रतिकूल असर नपरोस् भनेर तापक्रम र तौलको निगरानी र नियन्त्रण गरिएको छ । प्लाज्मायुक्त पानीमा हाइड्रोजनको क्षमता, नाइट्राइट, नाइट्रेट, हाइड्रोजन पेरोक्साइड, सुचालकता र घुलनशील ठोस पदार्थ (आयोन) को मात्रा कति छ भनी निगरानी र नियन्त्रण गरिएको छ ।

अतः यस अनुसन्धान कार्यको उद्देश्य प्लाज्माको प्रत्यक्ष र अप्रत्यक्ष प्रयोगलाई अनुकूलन गर्नु रहेको छ । यस कार्यमा प्लाज्मा प्रयोगको समय बढाउँदै जाँदा प्लाज्मायुक्त पानीमा हाइड्रोजनको क्षमताको मात्रा घट्दै जाने र अन्य सूचकको मात्रा बढ्दै जाने पाइएको छ । यद्यपि लामो समय प्लाज्माको प्रयोगले केही सूचकहरू पुनः घट्न सुरु गरेको पनि पाइएको छ । गहुँ, धान, फूलगोभी र च्याउ जस्ता प्रत्यक्ष रूपमा प्रयोगमा ल्याइएका नगदेबालीहरूमा प्लाज्माको असरले शीघ्र अङ्कुरण हुने र बिरुवाको वृद्धि एवं उत्पादनमा बढोत्तरी हुने गरेको पाइएको छ । यसो हुनुमा प्लाज्माको असरले बिउ–बिजनहरूको पानी सोस्न सक्ने क्षमतामा वृद्धि हुनु मुख्य कारण रहेको पाइएको छ । पानीमा रहेका ब्याक्टेरियालाई प्लाज्माको प्रत्यक्ष प्रयोगबाट निर्मूल गर्न सकिने पनि देखिएको छ । कीटाणु नष्ट हुनुमा प्लाज्माको प्रयोगबाट तापमानमा वृद्धि, झट्कायुक्त तरङ्ग, उच्च विद्युतीय क्षेत्रको प्रभाव, शारीरिक प्रतिक्रिया र प्रतिक्रियाशील अक्सिजन नाइट्रोजन प्रजातिहरू मार्फत कीटाणुको कोषको भित्ताको झिल्लीलाई रासायनिक प्रतिक्रियाले नष्ट गर्नु हो । अप्रत्यक्ष विधिबाट अन्नबाली (धान), नगदेबाली (गहुँ, आलु, च्याउ र फूलगोभी) र हरियो सागपात (रायो मनकामना, रायो मार्फा, चम्सुर र पालुङ्गो) मा प्लाज्मायुक्त पानीले शीघ्र अङ्कुरण हुनुका साथसाथै र बिरुवाको वृद्धि एवं उत्पादन र हरियोपनमा पनि गुणात्मक र परिणाममुखी वृद्धि भएको पाइयो । त्यसैगरी तेजपातलाई प्लाज्मायुक्त पानीको प्रयोग गरी सामान्य पानीको तुलनामा बढी समयसम्म हरियोपन जोगाइ राख्न सकिने पनि पाइयो ।

यस कार्य सम्पन्न भएसँगै स्थानीय रूपमै विभिन्न प्लाज्माका स्रोतहरूको निर्माण गरी कम खर्चमै यसको प्रयोगबाट कृषि उपजहरूको उत्पादकत्वको शीघ्र अङ्कुरण गराउन र बिरुवाको वृद्धिका साथै उत्पादनलाई पनि वृद्धि गर्न सकिन्छ भने निक्र्यौलमा पुगिएको छ । यसक्रममा प्रयोग भएका न्यून तापीय प्लाज्माले भौतिक परिवर्तनलाई सहयोग गर्ने तर आनुवांशिक परिवर्तन नगर्ने भएकाले हानिकारक पनि नहुने जानकारी गराइन्छ । अन्य विधिको तुलनामा प्लाज्मा विधिले वायुमण्डलमा नकारात्मक असर नपार्ने भएकाले यसलाई पर्यावरणमैत्री विधिका रूपमा लिइन्छ । हाम्रो जस्तो कृषिप्रधान देशमा कम लगानीमा पनि गर्न सकिने यस्ता कार्यबाट देशको अर्थव्यवस्थालाई नै टेवा पुग्ने देखिन्छ । तसर्थ यस कार्यलाई प्रयोगशालामा मात्र सीमित नराखी कृषिसँग सम्बन्धित व्यावसायिक काम गर्ने फर्म र सम्बन्धित निकायहरूसँग समन्वय गरी अभ्यासमा ल्याउनुपर्छ । यसरी पर्याप्त मात्रामा बिउ–बिजनको विकास र प्लाज्मायुक्त पानीको उत्पादन गरी किसानहरूले खेतीपातीमा प्रयोग गर्न सक्ने बनाउन सकियो भने कृषि उत्पादनमा वृद्धि भई सकारात्मक योगदान दिन सकिन्छ भन्ने सुझाव दिन चाहन्छौ ।

ABSTRACT

It is well known that various technologies are being used and researched to increase the productivity of essential food and agricultural products due to the gradually increasing population, decreasing arable land, and climate change. For the past few years, various research works have been carried out to increase agricultural production, improve the quality of seeds, increase plants as well as preserve the produced fruits for a long time without letting the quality degrade by using plasma. Plasma refers to matter showing collective behavior due to its ionized state, which is also called the fourth state of matter after solid, liquid, and gas. It is found naturally on earth as the flash seen when lightning strikes. In this research, naturally occurring plasma in the atmosphere has been produced in three different ways in the laboratory. The cold atmospheric pressure plasma produced in such a way has applications in a wide range of sectors for various purposes, including electronics, food safety, bio-medicine, agriculture, environment, and material science. With the global population growing and agricultural land diminishing, challenges like slow seed germination seedling growth, and crop loss intensify. Nepal is an agro-based economy and addressing agricultural issues is paramount. However, reliance on chemical fertilizers and pesticides harms the soil and environment. Research into cold atmospheric pressure plasma offers promising solutions. In any application involving plasma, the primary concern is ensuring the availability of plasma for the intended purposes. Plasma production requires a high-voltage power source as a prerequisite, after which applications can be explored. In this context, research into the production and application of cold atmospheric pressure plasma holds significant relevance, especially in addressing the aforementioned agricultural problems. Our study focuses on addressing problems for enhancing germination, seedling growth, and agricultural productivity and prolonging their freshness and bacterial decontamination of irrigated water by employing plasma directly and indirectly, to speed up seed germination, better seedling growth as well as improve yield, prolonging greenness and freshness of green leaves and remove contamination from water. Treating the water with plasma enriches the nutrients (such as nitrate/nitrite) in addition to bacterial decontamination caused by hydrogen peroxide.

For plasma production, a fabricated power source made of readily available materials in the local market is capable of producing atmospheric pressure gliding arc discharge which is crucial for those institutions aiming to establish a plasma lab without high operating cost. Additionally, dielectric barrier discharge and plasma jet are produced using a commercially available power supply. The produced plasma is characterized using optical and electrical techniques, adhering to the classical relationship of electron excitation > vibrational > rotational temperature. These plasmas are applied to enhance agricultural production of cauliflower, potato, Basmati rice, and green leafy vegetables

through direct (exposure directly on seeds) and/or indirect (exposure to water and then using this water for irrigation) approaches. The duration of plasma exposure significantly impacts several physico-chemical parameters of water, including the pH, electrical conductivity, total dissolved solids, oxidation-reduction potential, temperature, hydrogen peroxide, and the concentration of nitrite and nitrate. As activation time increases, the pH values of water decrease while other physico-chemical parameters increase synchronously.

Wheat seed wettability increases and contact angle declines noticeably with a longer treatment time of plasma-activated water used for soaking in seeds and direct exposure of plasma which is measured by wettability relation and a self-made prototype goniometer calibrated with a Ramé-Hart goniometer. Plasma-activated water accelerates the germination parameters of cauliflower (*Brassica oleracea*) compared to untreated crops. The seed's wettability is significantly enhanced as the treatment duration increases in plasma-activated water. Basmati rice produces the highest level of seed germination, longer seedling shoots, and heavier plants using plasma-activated water. While for green leafy vegetables, it is observed that plasma-activated water, results in improved germination, production, and greenness. Similarly, the production of oyster mushrooms is beneficial by plasma-treated spawn. Direct plasma treatment also eliminates soluble bacteria like *Scleropages aureus* and *Escherichia coli* in water. Plasma-activated water reduces chlorophyll retention in detached Tejpat (*Cinnamomum tamala*) leaves compared to untreated water and accelerates the dormancy of potatoes. The detached Tejpat leaf could be preserved for longer times than normal water using plasma-activated water. The primary cause of these changes is the physical reaction of the plasma on the surface of the seeds and water, resulting in heat, shock waves, a strong electric field, and the presence of reactive oxygen and nitrogen species. These plasma applications demonstrate the potential of both direct and indirect methods to overcome declining agricultural production.

Hence, cold atmospheric pressure plasma treatment enhances production, accelerates seed germination, retains chlorophyll in detached leaves, and sterilizes water for potential agricultural use. However, prolonged exposure to direct plasma and plasma-activated water can adversely affect agricultural commodities, necessitating optimization. As conventional fertilizers used in agriculture are not economically and environmentally friendly, plasma-based techniques offer a promising alternative for increasing agricultural production and establishing a more sustainable system in agricultural areas.

Keywords: *Cold Atmospheric Pressure Plasma - Electrical & Optical Characteristics - Plasma Activated Water - Physico-Chemical Properties - Reactive Nitrogen and Oxygen Species - Wettability - Germination - Seedling - Chlorophyll - Bacterial Inactivation*

LIST OF ACRONYMS AND ABBREVIATIONS

AC	: Alternate Current
APPJ	: Atmospheric Pressure Plasma Jet
APJ	: Air Plasma Jet
CAPP	: Cold Atmospheric Pressure Plasma
CD	: Corona Discharge
CDBD	: Circular Dielectric Barrier Discharge
CDP	: Central Department of Physics, Tribhuvan University
CFU	: Colony-Forming Units
CP	: Cold Plasma
CDBD	: Circular Dielectric Barrier Discharge
Cy-DBD	: Cylindrical Dielectric Barrier Discharge
DBD	: Dielectric Barrier Discharge
DC	: Direct Current
DI	: De-ionized
FNCCI	: Federation of Nepalese Chambers of Commerce Industry
FDBD	: Floating Dielectric Barrier Discharge
GAD	: Gliding Arc Discharge
GDP	: Gross Domestic Product
HR	: High Resolution
OES	: Optical Emission Spectroscopy
OH	: Hydroxyl Radical
LPM	: Liter Per Minute
LTE	: Local Thermodynamic Equilibrium
MIN	: Minute
NTP	: Non-Thermal Plasma
PAW	: Plasma-Activated Water
PPM	: Parts Per Million
PTM	: Plasma Treated Medium
RF	: Radio Frequency
RMS	: Root Mean Square
RNS	: Reactive Nitrogen Species
ROS	: Reactive Oxygen Species
RONS	: Reactive Oxygen and Nitrogen Species
SDBD	: Spark Dielectric Barrier Discharge

LIST OF SYMBOLS

k_{B}	: Boltzmann Constant
τ	: Collision Frequency
λ_{D}	: Debye Length
d	: Distance Between Two Electrodes
T_{exc}	: Electron Excitation Temperature of Plasma
T_e	: Electron Temperature
e	: Charge of Electron
E	: External Electric Field
α	: Ionization Collision Factor
m	: Mass of the Electron
λ_{mfp}	: Mean Free Path
N_{D}	: Number of Particles in Debye Sphere
ϵ_{o}	: Permittivity of Medium
n	: Plasma Density
ω_{p}	: Plasma Frequency
h	: Planck's Constant
P	: Pressure
T_{rot}	: Rotational Temperature
γ	: Secondary Electron Coefficient
T_{vib}	: Vibrational Temperature

LIST OF TABLES

Page No.

LIST OF FIGURES

Page No.

TABLE OF CONTENTS

CHAPTER 1

INTRODUCTION

1.1 Background of Plasma

The fundamental substances that make up our universe are solids, liquids, gases, and plasmas. The sun, stars, interplanetary, and interstellar space are the primary locations where most of the universe's visible matter is in the plasma state. On earth, however, humans can experience less activity with plasma only in limited activities of atmospheric phenomena such as lightning, northern lights, neon signs, and fluorescent tubes. The earth is a small region of the universe where plasma does not occur naturally (F. Chen, 2016). A change in a material's state from solid to liquid to gaseous and occasionally even plasma is called a phase change or phase transition. Among the states of matter, there are variations in the configuration and energy of particles. Temperature and pressure variations are the primary causes of phase change (Jaeger, 1998).

The system's energy fluctuations are the primary cause of most phase shifts. Increased kinetic energy from rising temperatures allows molecules or atoms to break bonds and separate faster. Similarly, when the temperature lowers, particles slow down and find it easier to form a solid structure. Particles can move apart when pressure decreases, but they can move together when pressure increases. To become plasma, the matter needs to be ionized. Therefore, reducing pressure does not always lead to plasma creation, even if you reduce the pressure. Instead, it can raise the energy to generate an ionized form. There are multiple ways to supply the energy required to create plasma: heat from combustion; laser radiation interacting with a solid, liquid, or gas; or electrical discharges in gases, where free electrons absorb energy and release it as a result of atoms and molecules in the gas being excited and ionized (Blundell & Blundell, 2010).

Energy can change the state of matter; if more energy is added, the constituent parts of gaseous states will not be able to bond together and will instead become plasma or ionized states, which is illustrated in Figure 1. After the sub-sequence of solid, liquid, and gas, the fourth state of matter is called plasma. The general definition of plasma is; "A quasineutral gas of charged and neutral particles that exhibit collective behavior"

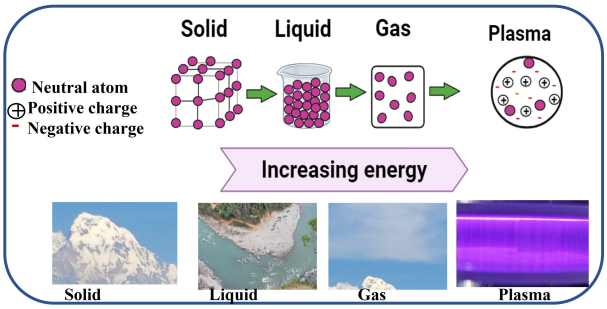

Figure 1: Schematic diagram showing the formation of plasma by adding an energy (F. Chen, 2016)

(F. Chen, 2016). The existence of plasma was first identified by Sir William Crookes in 1879. Later in 1929, Tonks and Langmuir introduced the term "*Plasma*" to describe the glowing ionized gas produced by electric discharge in a discharged tube (Tonks & Langmuir, 1929). The word "*Plasma*" comes from the Greek word "$\pi\lambda\alpha\sigma\mu\alpha$", which means something molded or fabricated that is used to describe macroscopically neutral substances containing interacting ionized atoms or molecules and free electrons (F. Chen, 2016). However, the meaning of the plasma can be found more accurately by looking for a Sanskrit "प्लाज्मा" rather than a Greek word "$\pi\lambda\alpha\sigma\mu\alpha$". The Sanskrit word "pla" or "pra" means very basic, primitive, very high; "z", "s", or "sura" means life or water; and "*ma*" means a collection of energy, i.e., matter (Choi et al., 2022). Thus, a "fundamental and life substance or material in a universe with a highly accumulated state of energy" can be used to describe plasma (Choi, 2015).

However, any ionized gas cannot be called a plasma, even if there is always some small degree of ionization in any gas. Also, an ionized gas must satisfy the following conditions, called a plasma state (F. Chen, 2016):

i). Debye length (λ_D) must be much less than the dimension of the plasma; i.e.

$$\lambda_{\mathrm{D}} << 1 \tag{1.1}$$

ii). Number of particles inside the Debye sphere (N_{D}) must be very very large; i.e.

$$N_{\mathrm{D}} >>> 1 \tag{1.2}$$

iii). The product of the mean time between collision with neutral atoms (τ) in gas and the frequency of plasma collision (ω_{p}) should be greater than unity; i.e.

$$\omega_{\mathrm{p}}\tau > 1 \tag{1.3}$$

where Debye Length λ_{D} is a crucial property of plasma activity and represents the plasma's capacity to block external electric potentials. The distance of shielding is

called Debye length which is calculated by the given relation (Debye & Hückel, 1923):

$$\lambda_{\mathrm{D}} = \sqrt{\frac{\epsilon_o k_{\mathrm{B}} T}{n e^2}} \tag{1.4}$$

where ϵ_o, k_{B}, T, n, and e are the permittivity of the medium, Boltzmann constant, temperature of the electron, plasma density, and charge of an electron.
The number of charged particles inside the Debye sphere is calculated as:

$$N_{\mathrm{D}} = \text{Volume of Debye sphere} \times n \equiv \frac{4}{3}\pi\lambda_{\mathrm{D}}^3 n \tag{1.5}$$

When electrons in a plasma are moved away from a uniform background of ions, electric fields are generated in a direction that pushes the displaced electrons back toward their original positions, restoring the plasma's neutrality. The electrons will overshoot due to their inertia and fluctuate around their equilibrium positions at a distinctive frequency called the plasma frequency (Langmuir, 1928).

$$\omega_p = \sqrt{\frac{n e^2}{\epsilon_o m}} \tag{1.6}$$

where m is the mass of the electron.

1.1.1 Theoretical Scheme of Plasma Formation

Paschen (1889), arguably the earliest plasma experimentalist, provides the experimental background of plasma discharge production on a laboratory scale. A spark/discharge will develop between two electrodes when a high voltage is applied. The required voltage for the argon plasma discharged at atmospheric pressure (10^5) pa at the Central Department of Physics (CDP), Tribhuvan University plasma research lab is related to the gas pressure (p) and electrode distance (d) as shown in Figure 2. The curve is plotted by varying the distance between the electrodes from 1.0 mm to 15.0 mm keeping the atmospheric pressure constant (10^5 Pa), noting the discharge voltage (V_{rms}) from the current-voltage (IV) curve, while the sinusoidal IV curve distorted, i.e., mean distorted sinusoidal curve significance the conformation of breakdown discharge happens between two electrodes in the argon plasma jet. When the distance between electrodes is low, the mean free paths (λ_{mfp}) of electrons are longer, and high voltages are needed to accelerate ions to energies that can liberate secondary electrons from the surface. Voltage increases again when distance is increased because electron collisions with the neutral gas result in electrons losing energy. Paschen curve thus has a minimum breakdown voltage value. Current is not uniform after the gas breakdown between electrodes; instead, it tends to flow in streamers, each of which reaches equilibrium. In this state of equilibrium, the secondary

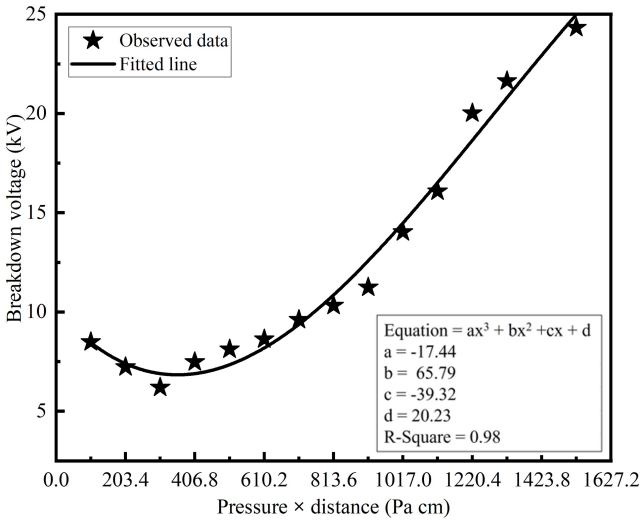

Figure 2: Paschen curve (Paschen, 1889) for atmospheric pressure argon plasma jet (pressure at 10^5 Pa) at an airflow of 2 LPM at CDP plasma research lab

electron emission coefficient (γ), is emitted whenever an ion makes contact with the negative plate or the cathode. The sheath accelerates these electrons into the plasma, clashing with neutral particles to create fresh pairs of electrons and ions. An avalanche will be produced when more secondary electrons are released from the cathode by each new ion that strikes it. Let α be the likelihood of an ionizing collision occurring within a unit of distance, which is proportional to $1/\lambda_{\text{mfp}}$. One electron will produce ion-electron pairs at a distance d. These ions will produce ($e^{\alpha d} - 1$) additional electrons upon collision with the cathode. Therefore, $\gamma(\ e^{\alpha d} - 1)$=1 is needed for stable state (J. S. E. Townsend, 1900).

The applied voltage produces a constant electric field. When primary electrons from neutral sources, are made close to the cathode, they are accelerated by the electric field and come into contact with gas molecules. Impact ionization causes bound electrons to be extracted from the gas molecules, resulting in the formation of positively charged ions. Further gas molecules are ionized by the ejected electrons as they are once more propelled by the external electric field (E). When these processes are repeated, the number of electrons increases exponentially, generating avalanches, as seen in Figure 3. The Townsend ionization coefficient α is frequently used to characterize these ionization avalanches. Conversely, γ indicates that the positively charged ions accelerate in the direction of the cathode, which causes the cathode material to release secondary electrons. Then, more avalanches may be triggered by the secondary electrons. As long as there is an autonomous current established between both electrodes, all of these processes result in a fairly homogenous breakdown known as the Townsend breakdown mechanism (Fridman, 2012). The Townsend breakdown process is restricted to narrow distances and very low pressures (Fridman, 2012), and parallel plate configuration (J. Townsend, 1900).

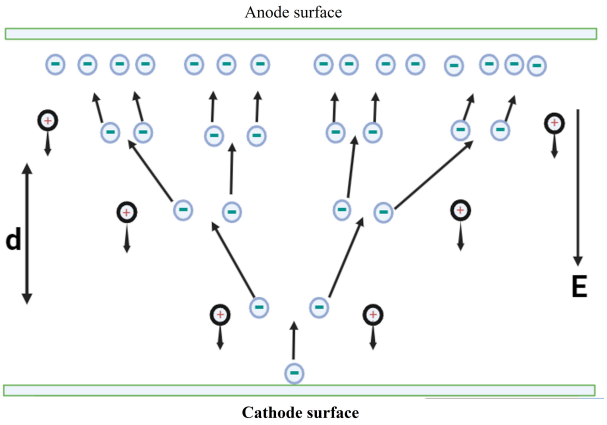

Figure 3: Townsend breakdown and electron avalanche formation between parallel electrodes (J. Townsend, 1900)

If atmospheric pressure is used, the so-called streamer or spark mechanism offers a more precise explanation of the breakdown process. It is essentially based on ionization avalanches, additionally considering the interactions between individual avalanches. A significant local space charge and an extra electric field (E), are produced at the front of the avalanche as a result of the electrons in the head of the avalanche drifting away from the heavier ions in the trail due to their greater mobility. It is possible to augment the resulting field in front of the avalanche by superimposing this additional electric field, over the external electric field. In this area, secondary avalanches mostly grow because of increased ionization processes caused by the higher electric field in front of the original avalanche. A streamer, or narrow ionized channel forming between the electrodes, is the most accurate description for the avalanche that occurs when an additional electric field is equal to or greater than the external electric field (Fridman, 2012). The avalanche-to-streamer transition can only occur when the avalanche reaches the anode's surface at small gap lengths and low voltages (Ollegott et al., 2020). Positive streamers and negative streamers are the two kinds of streamers that can evolve as shown in Figure 4.

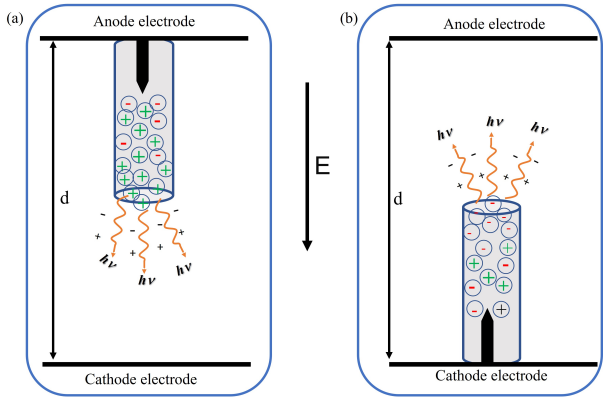

Figure 4: Illustration of formation of discharge phenomena in atmospheric pressure plasma and the propagation of (a) positive streamer and (b) negative streamer (Fridman, 2012)

In the direction of the cathode, positive streamers propagate. Through electron-ion recombination processes, photons having energy $h\nu$ are released in the streamer head, where they cause photoionization to cause secondary avalanches in front of the streamer head. A positive charge remains in the streamer's head after the free electrons are drawn into the ionic trail. In the other direction, negative streamers spread in the direction of the anode. For negative streamers, electrons that move ahead of the initial avalanche and cause electron impact ionization are the main cause of the secondary avalanches. Furthermore, negative streamers may also experience photoionization. Because of the strong electric fields at their tips, both kinds of streamers spread outward. Significantly faster than the electron drift velocity is the related streamer growth velocities. There is a quasi-neutral plasma channel at the streamer's trail, while the space charge layer at the streamer's tip can be either positive or negative depending on the kind (Fridman, 2012).

It is generally possible to divide plasma into those that are in thermal equilibrium and those that are not. According to the theory of thermodynamic equilibrium, all species (electrons, ions, and neutral) have the same temperature. This applies, for instance, to both fusion plasmas and stars. Local Thermodynamic Equilibrium (LTE), which denotes that all plasma species have the same temperature in some limited regions of the plasma, is frequently used. Conversely, interstellar plasma matter, or "non-LTE", is generally not in thermodynamic equilibrium. This indicates that various plasma species have different temperatures, or more specifically, that the temperatures of electrons are substantially higher than those of heavier particles; ions, atoms, and molecules (Bogaerts et al., 2002). So that based on the temperature of particles in plasma, it can be classified into two categories: equilibrium or thermal plasma and non-equilibrium or non-thermal plasma or cold plasma. Low excitation selectivity and high gas temperatures are thermal plasma's primary drawbacks. As a result, the only things that thermal plasma can be used for are cutting, welding, material breakdown, and electric power production. Non-LTE plasma, on the other hand, is typically used for applications where heat is not desirable. In non-thermal plasma, the electron impact process is a key factor in defining the plasma's characteristics. Table 1 displays some key differences between thermal and non-thermal plasma.

Table 1: Comparison of thermal and non-thermal plasma (Indarto et al., 2008)

Characteristic	Thermal Plasma	Non-thermal Plasma
Installation costs	High	Low
Characteristic	High gas temperature	Low gas temperature
Difficulty to handle	Difficult	Easy
Safety	Reactive dangerous	Reactive safe
Example	Fusion, Arc	GAD, DBD, Jet, Glow

Thermal plasma is extensively industrialized. Cold plasma technologies have been developed but their vacuum equipment limits their implementation. Several laboratories have attempted to convert processes that currently operate under vacuum to atmospheric pressure to overcome the disadvantages of vacuum (Tendero et al., 2006). It has been possible to create atmospheric-pressure plasma, and this plasma has many traits similar to traditional low-pressure glow discharges. A partially ionized gas with a temperature that is typically near room temperature is known as non-thermal or cold plasma. Because cold plasma treatment is administered at room temperature, the harmful effects on biological tissues and thermolabile matrices can be reduced without compromising the effectiveness of disinfection and sterilization. Due to this reason, Cold Atmospheric Pressure Plasma (CAPP) is widely employed in many agricultural and life science applications, including plant and food conservation and medicine (Roth, 2001). This work also focuses on the production and applications of CAPP, whose advantages and limitations are shown in Table 2. The question is not "which is bad and which is good", but "suitable for the desired application or not is the main desired thing". We are motivated in CAPP due to the low operating costs, plasma generation in the ambient environment, and environment-friend properties (Roth, 2001).

Table 2: Advantage and limitations of CAPP (Roth, 2001)

Advantages	Limitations
Low-temperature treatment	Large number of samples
Plasma generation in ambient air	Investment costs
Low operating costs	Adaptation mechanisms
Environment friendly	Determination of effective dose
Selective effects	Depth of plasma penetration

1.2 Concept of Plasma Application in Agriculture

The current estimates of the world's population indicate that 7.8 billion people live there (Worldometers, 2024). The amount of arable land available is insufficient to meet the growing population's consumption needs. The only option to satisfy this need is to raise crop yields while improving seed germination and developing drought-resistant seeds. The most widely used techniques to increase seed germination are chemical ones (agrochemicals, fungicides, insecticides, and hormones); yet, these treatments leave behind chemical residues that are bad for the environment and human health. Therefore, to keep up with the rate of the expanding population, innovative alternative technologies for enhancing seed germination must be developed. Plasma has numerous applications in everyday life and real-world experiments, which is shown in Figure 5. Among the various applications of plasma; direct treatment of the seeds and indirect (use of plasma-

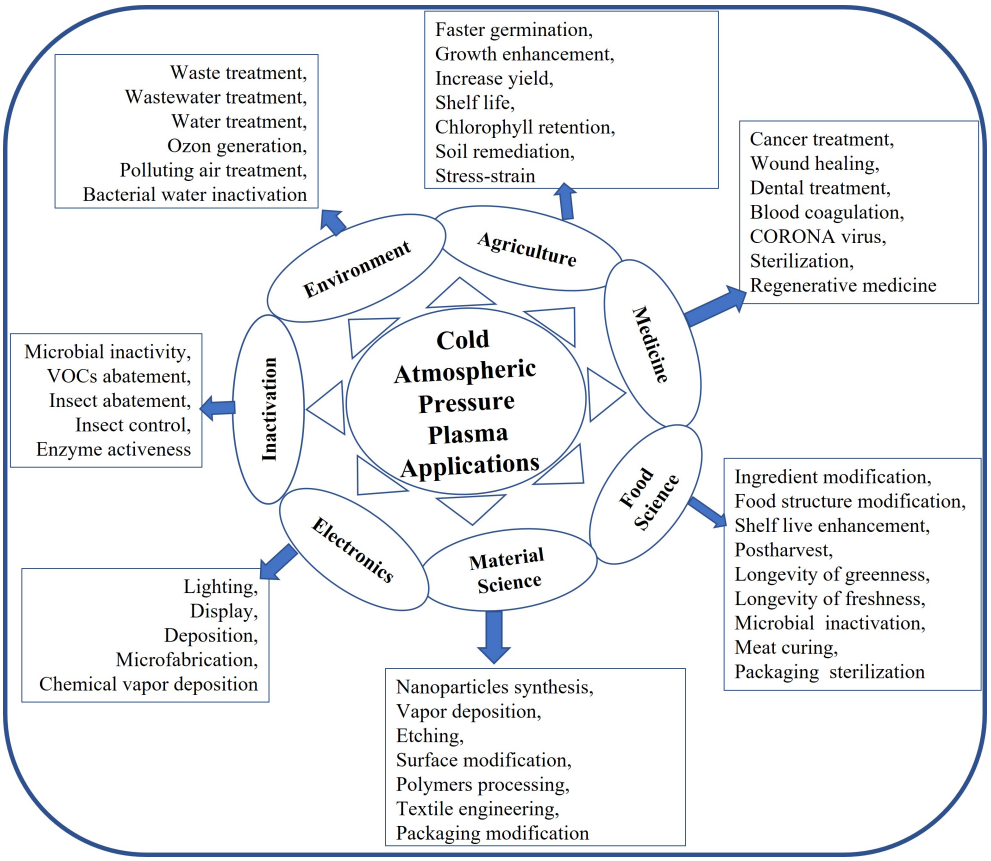

Figure 5: Application of cold atmospheric pressure plasma in different fields

activated water (PAW)) is emerging as a free-from-chemical and eco-friendly method to overcome the limitation mentioned above (Thirumdas et al., 2017). New technologies are actively sought after to overcome the issue shown in Figure 6 and improve seed performance because existing technology has some limitations and obstacles.

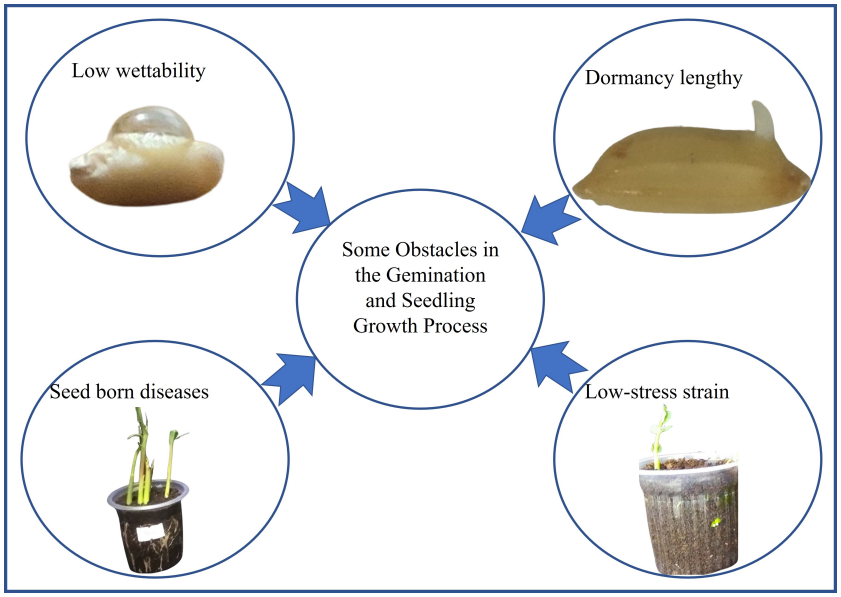

Figure 6: Main obstacles of seedling process in the agricultural field (Shelar et al., 2021)

The lightning phenomenon is one of the best examples of plasma. High voltage develops between storm clouds and is released in the form of lightning, which can produce large amounts of nitrogen oxides (NO_x), critical precursors for ozone and hydroxyl radical (OH^*), the primary tropospheric oxidants. It will also change the background ozone and OH levels in the atmosphere and can deposit a significant amount of nitrates into the soil, those nitrates taken by plants as a fertilizer (Murray, 2016). The plasma species generated during the lightning are responsible for these phenomena but a direct hit by this can often lead to disastrous on humans and agriculture (Khatun et al., 2016).

However, controlled plasma discharge produced in the laboratory in an ambient environment can be controlled and used to enhance agricultural productivity in different ways as shown in Figure 7. The seeds can be treated with various cold plasma modes depending on the plasma system; either direct mode as shown in Figure 7 (a) and (b) or indirect mode of treatment as shown in Figure 7 (c). When a surface is exposed to a discharge is direct plasma treatment where plasma particles and other excited atoms and molecules emit UV radiation directly on the seed's surface. Even non-equilibrium gas or those discharged exposed to water which creates a reactive mixture of plasma species and water is known as PAW. In indirect plasma treatment, the samples are nevertheless exposed to persistent radicals without coming into contact with the blazing plasma zone. When physical elements like heat, UV light, electromagnetic fields, and mechanical scarification come into contact with the seed coat initially, they can cause subsequent effects (Thirumdas et al., 2018).

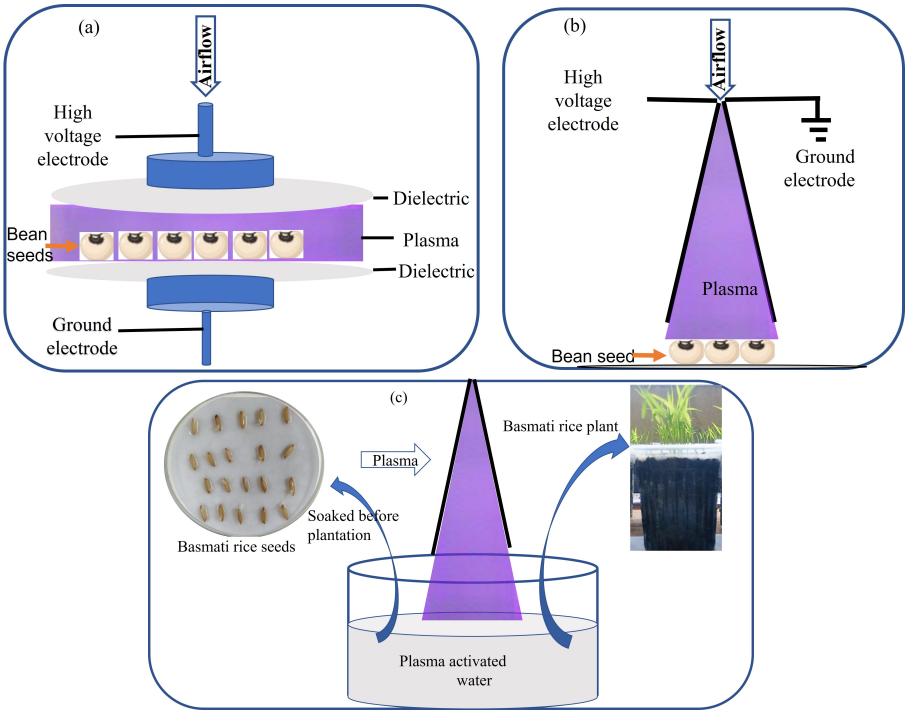

Figure 7: Schematic representation of plasma-based seed treatment methods, illustrating (a) dielectric barrier discharge plasma, (b) gliding arc discharge plasma, and (c) indirect treatment approach.

Numerous chemical processes result in the production of Reactive Oxygen and Nitrogen Species (RONS) in plasma. Plasma is produced by electric discharge in a gas, which is a partly ionized gas that contains both charged and neutral particles. It also contains ions, radicals, excited molecules, and photons emitted by dissolving electrically stimulated molecules. Long-lived species such as H_2O_2, NO_2^-, and NO_3^- with half-lives in milliseconds can be produced by plasma, whereas short-lived species such as hydroxyl radicals (OH^*), nitric oxide (NO), and superoxide ($^1O_2$) can be produced with half-lives in the seconds (Shelar et al., 2022). The chemical processes that take place during the gas phase and gas-liquid interface for PAW generation, which leads to the development of Reactive Oxygen Species (ROS) as well as Reactive Nitrogen Species (RNS) by plasma presented in the following chemical reactions (Thirumdas et al., 2018);

$$H_2O + e \rightarrow OH^* + H^* + e$$

$$H_2O + e \rightarrow H^+ + OH^* + 2e$$

$$H_2O + e \rightarrow H^* + O^* + H^* + e$$

$$O_2 + e \rightarrow O^+ + O + 2e$$

$$O_2 + e \rightarrow O^- + O$$

$$O + O_2 \rightarrow O_3$$

$$O_3 + NO \rightarrow NO_2 + O_2$$

$$N + O_2 \rightarrow NO + O$$

$$O + N_2 \rightarrow NO + N$$

$$O + NO_2 \rightarrow NO + O_2$$

$$2NO + O_2 \rightarrow 2NO_2$$

$$NO_2 + OH \rightarrow HNO_3$$

$$H_2O_2 + h\nu \rightarrow OH^* + OH^*$$

$$3NO_2 + H_2O \rightarrow 2HNO_3 + NO$$

$$H_2O_2 + H^+ + NO_2^- \rightarrow ONOOH + H_2O$$

$$OH^* + OH^* \rightarrow H_2O_2$$

$$NO + NO \rightarrow N_2 + O_2$$

$$NO + OH^* \rightarrow HNO_2$$

$$HNO_2 + OH^* \rightarrow NO_2 + H_2O$$

$$NO_2 + h\nu \rightarrow NO + O^*$$

$$NO_3 + h\nu \rightarrow NO + O_2$$

$$NO_2 + NO_3 \rightarrow N_2O_5 + O^*$$

$$N_2O_5 + H_2O \rightarrow 2HNO_3$$

$$2NO_2 + H_2O \rightarrow NO_2^- + NO_3^- + 2H^+$$

$$3NO_2^- + 3H^+ \rightarrow 2NO + NO_3^- + H_3O^+$$

$$OH + NO_2 \rightarrow [= N - -OOH] \rightarrow O = N - OO^- + H^+$$

where, *, -, and + refer to the unstable, negative charge, and positive charge species. The physical as well as above-discussed chemical reactive species that are produced from gas plasma at the interfaces between gases and liquids as well as in the atmosphere are diagrammatically shown in Figure 8.

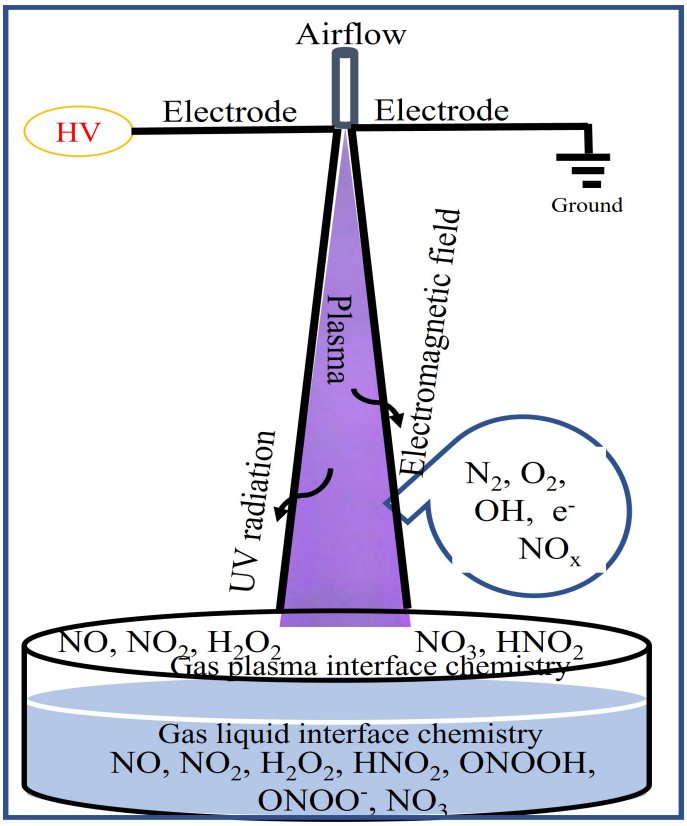

Figure 8: Schematic diagram showing the formation of reactive oxygen and nitrogen species within the plasma discharge region, plasma liquid interface, and within plasma activated liquid (Shelar et al., 2022)

The primary benefit of using atmospheric pressure plasma to produce reactive species is that it can be easily adjusted by varying the target solution, applied voltage, working gas type, working gas flow rate, etc. While long-lived reactive species can be stored in a plasma-activated medium and used at a later time, short-lived reactive species can be used under in-situ treatment circumstances. Overall, they can be applied in a

variety of industries because of their easy-to-use and affordable operation (Ghimire, 2018). ROS and RNS perform a range of regulatory functions during seedling growth and development processes, involving germination, metabolism, signal transduction, absorption of nutrients, aging, and the capacity to endure biotic and abiotic stress. The idea of oxidative stress links the production of ROS to pathogenic modifications in DNA, proteins, and lipids as a result of stressful circumstances (H. Huang et al., 2019).

There are various methods by which PAW can be produced: (i) directly into the water; (ii) directly into the water using multiple electrodes; (iii) gaseous phase discharge onto the water's surface; (iv) gaseous phase discharge into the water; (v) gas phase discharge onto the water's surface using plasma produced on a forward vortex flow reactor; and (vi) bubble releases into the water (Milhan et al., 2022). Compared to PAW produced directly in the liquids, the chemistry and reaction products of PAW generated above the water's surface are different. When water is added to samples during plasma treatment, the water in the sample produces extremely reactive OH radicals as a byproduct. When air is included in the working gas, NO and other nitrogen oxide species may be formed in the air (Grill, 1994).

The first reported case of plasma application of plant seeds is in the USA, patent by Krapivina et al. (1994). When seeds are exposed to plasma, the seed coat erodes, which leads to a cold plasma priming process. Those seeds have a somewhat damaged surface as a result of the cold plasma treatment. If the tough seed coat is cracked or scraped off, moisture from within the seed could pass through and cause germination. Reactive species, such as nitric oxides are produced during plasma discharge as a result of plasma treatment, which ends seed dormancy and speeds up germination. Treatment with plasma makes bacteria and fungi inactive, which reduces the likelihood that seeds will spread disease and cause losses in earnings. Seeds treated with plasma have a lower potential for bacterial contamination, which reduces health hazards (Cui et al., 2019).

The seed priming with plasma might activate molecular processes in seeds, germination chemistry is stimulated and seed coverings are etched by oxygen radicals like O_2^+. ROS are produced as a result of plasma seed priming, which alters the seed coat and induces gaseous and water exchange inside the seed (Mhamdi & Van Breusegem, 2018). The germination signal is stimulated, the amylase enzyme is activated, the phytohormone ratio is modulated, and the reactive oxygen species O_2^+, and water uptake are involved. Plasma priming, however, also influences seedlings in early vegetative stage growth, development, and sustainability by raising the concentration of reactive oxygen and nitrogen species. Reacting species operate as signaling molecules in seed cells, promoting oxidative signaling (Su et al., 2016). ROS also induces the expression of histone modification genes, which are in charge of epigenetic modification, during the growth of seedlings. These epigenetic modifications control several genes related to

stress tolerance, phytohormones, and antioxidants, which improve morphological and biochemical properties (J. J. Zhang et al., 2017). Redox equilibrium is preserved in seedlings by the antioxidant machinery being activated by the up-regulated reactive species. Plasma-primed seedlings showed increased superoxide activity, indicating a larger rate of superoxide radical conversion into hydrogen peroxide. Moreover, superoxide radical is a precursor to extremely metabolically active molecules, such as OH and H_2O_2 (Adhikari et al., 2020).

Among the several factors contributing to crop output reduction, low percentage of germination rates, extended germination durations, loss of seed survival from contamination, and slow seed germination are significant (Mitra et al., 2014). Primary cell elongation of the embryo's axial portion and simultaneous or delayed cell division in the radicle meristem are the two essential processes in seedling growth during germination (Šírová et al., 2011). According to El-Maarouf-Bouteau et al. (2015), ROS and RNS take part in several signaling pathways that are engaged in seed germination in addition to hormones. The cell's mitochondria, which are regarded as active locations for production, create and release these ROS species (Møller et al., 2007). According to Puač et al. (2018), H_2O_2 in the PAW could activate the catalase genes, creating novel proteins that have improved seed germination. A strong correlation between seed initiation and seed dormancy breakdown was discovered in the study by Su et al. (2016) on the enhancement of seed germination in the presence of ROS (via methyl viologen as ROS source). In addition, ROS served as a signal for the reduction of dormancy. According to Y. Liu et al. (2010a), H_2O_2 treatment reduced the abscisic acid hormone, which prevents seed germination and causes seed dormancy. H_2O_2, an exogenous hormone, inactivated the abscisic acid hormone and promoted the germination of slightly dormant seeds (El-Maarouf-Bouteau & Bailly, 2008). Simultaneously, it seems that NO can promote seed germination and break seed dormancy (Šírová et al., 2011).

According to Batak et al. (2002), NO is an active agent in seed germination rate and is greatly impacted by the discovery of substitute NO donor chemicals during seed germination. Additionally, nitrogen molecules such as nitrites, nitrates, and NO alter phytochrome activity in nitrate-stimulated seed germination altering the amount of light required for seed germination. Together with plant hormones and some ROS, the RNS breaks seed dormancy and promotes germination in several pathways. To improve seed germination, the active species generated in PAW act as external donors of NO, NO_2, H_2O_2, and $^1O_2$. As plasma can be formed at diverse temperature, pressure, and density ranges, not all plasma is suitable for use in agriculture. The reactive species from plasma is important for seed germination seedling growth, and production of crops. For agricultural seed applications, the thermal plasma is mostly inappropriate and hence the non-thermal or cold atmospheric pressure plasma is preferred.

1.3 Motivation and Research Gap

For agricultural production to increase, remain stable, and rebound from shocks, seed germination, and development are essential activities. Maintaining a balance between sustainable seed germination and growth is seriously hampered by the usage of chemical fertilizers. Seed germination is fraught with difficulties; for example, seeds absorb very little water, which leads to inadequate hydration and germination of the seed coat. Long seed dormancy, seed-borne diseases, and abiotic environmental factors all reduce the viability and vigor of seeds. The common difficulties faced during seed germination in agriculture have already been shown in Figure 6. It is believed that one of the main factors influencing seed germination is seed water intake capacity. Since water absorption is the initial germination stage, speeding up this process should accelerate germination (Tian et al., 2014). An impermeable seed shows a barrier to water penetration and has poor hydration kinetics. A normal permeable seed takes water easily when it is available to it. However, an impermeable seed (hard) can fail to soak water for several days and even weeks which causes a low amount of germination (Shelar et al., 2022).

Another important feature altered during domestication is seed dormancy, which is essential for crop growth. Many species have the adaptable characteristic of dormancy, which allows their seeds to stay latent until the right circumstances arise for germination. On the other hand, one of the least understood parts of seed biology is seed dormancy, a complicated phenomenon controlled by both endogenous and exogenous stimuli. A complex web of physiological and biochemical processes arises from the involvement of extrinsic and intrinsic stimuli. Among other things, responses to light, temperature, and other environmental conditions, as well as the synthesis of ethylene, and nitric oxide, affect seed dormancy and germination. Dormancy in seed germination increases from either an impermeable seed coat or an insufficiency of enzymes (internal dormancy). The delay caused by the seed's dormancy might result in uneven germination and make it more difficult to sustain crop production (Finch-Savage & Leubner-Metzger, 2006).

Next, abiotic stress or ongoing alterations in the surrounding environment hurt the growth and development of plants, such as heat, cold, salinity, drought, and heavy metals can induce complicated reactions in seeds, leading to decreased growth and crop output (Yadav et al., 2020). These pressures lead to a notable decrease in average crop production of more than 50%. Abscisic acid production can mediate stress adaption responses by activating several signaling cascades and regulating physiological and development processes (K. Chen et al., 2020). Numerous factors impact seed quality, such as viruses that infect seeds and lower their vigor, hence preventing seed growth and resulting in low yields (Nelson, 2018). Increased plant-borne pathogens suppress plant germination capacity, seedling growth, and production (Panth et al., 2020).

The multiple drawbacks of current approaches make new technologies such as Gliding Arc Discharge (GAD), Dielectric Barrier Discharge (DBD), and Plasma Jet (APJ/APPJ) highly desirable for overcoming these obstacles. Researchers have recently evaluated the possibility of cold plasma technology, an eco-friendly, non-thermal technique with special advantages over conventional processing technologies that can enhance germination and accelerate the growth of seedlings (Shelar et al., 2022).

Various plasma modes can be given to the seeds, depending on the plasma system: direct and/or indirect. Direct method: exposure of plasma to the seeds introduces several physical, chemical, and biological effects which result in surface morphology resulting in higher water absorbency, and expansion of embryo size so that faster germination. Enhancing the abiotic stress, antioxidant and fastening nutrient uptake resulted in enhanced metabolism and seedling growth (Shelar et al., 2022), which is illustrated in Figure 9. In PAW, RONS and other physical parameters play an important role in seed sterilization, germination, and seedling growth of plants. Induces chemical and physical characteristics that are created in PAW and their effect indirectly on the seeds and plants when soaked and poured into the plants respectively as shown in Figure 10.

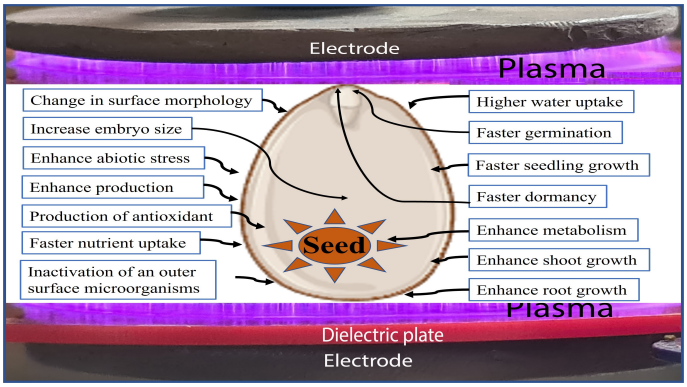

Figure 9: Activity involved when cold atmospheric pressure plasma is directly exposed to the seeds and its subsequent impacts on the physiological, biochemistry, and molecular processes (Shelar et al., 2022)

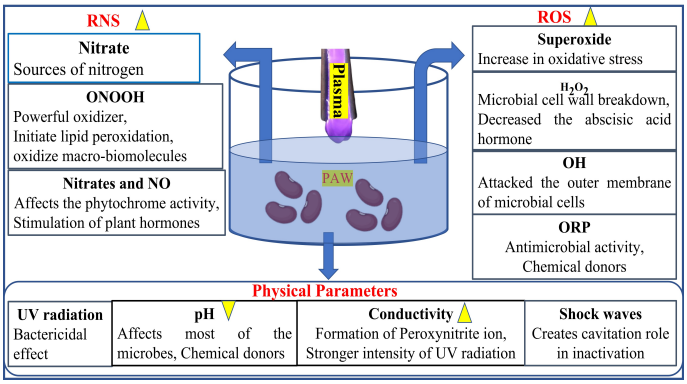

Figure 10: Chemical and physical activities created by plasma exposed to water and affect in the seeds and plants when soaked and irrigated (Thirumdas et al., 2018)

Nepal's economy is largely dependent on agriculture, which accounts for 36% of GDP and absorbs about two-thirds of the labor market using about 30% of the total land for agricultural purposes. For economic growth and sustainability, it is mandatory to increase agricultural productivity in which enhancement of seed germination plays a vital role (FNCCI, 2024). Likewise, seedlings and plant growth as well as their protection against bacteria, viruses, fungi, and parasites are key to increasing productivity. Using chemical methods (agrochemicals, fungicides, insecticides, and hormones) for such purposes harms human health and the environment (Wang et al., 2017). Plasma has been found useful for enhancing agricultural productivity in different cases. The exposure of seeds to the cold atmospheric pressure plasma has substantial effects on physiological, biochemistry, and molecular processes that enhance seed germination and seedling growth. The usage of the cold atmospheric pressure plasma in agriculture is growing and is connected to our daily lives, among other uses.

In this work, cold atmospheric pressure plasma reactors have been developed in various configurations and characterized via electrical and optical methods. To get an understanding of how the plasma or PAW influences growth parameters, the germination of seeds as well as the production of agricultural commodities, the longevity of greenness in green leaf, and bacterial inactivation of water. These facts have been motivational for the production of CAPP using different experimental setups, which are used to treat seeds and use PAW to check faster germination, enhance water absorbency of seeds, higher seedling growth of plants, and increase the productivity of the crops, faster dormancy, longevity of greenness in green leaf and treat bacterial activation water.

Some progress has been already made in argon plasma production and characterization, as well as in its various applications: agriculture, material science, surface modification, wound healing, and water purification at Kathmandu University, Nepal. Thakur et al. (2019) produced arc discharge and characterized it using movable single and double Langmuir probes at the Central Department of Physics, Tribhuvan University, Kirtipur, Nepal. The plasma produced at different gap distances, currents, and electrode materials revealed that its properties could be altered by varying these parameters. However, the arc discharge produced by Thakur et al. (2019) cannot be used for any substrate treatment due to its high temperature. To address this issue, the production of CAPP needs to be realized first, which would enable the direct treatment of heat-sensitive materials (agricultural seeds). This treatment aims to improve agricultural seed germination, seedling growth, and productivity, extend the duration of their greenness without compromising nutritional value or original taste, and achieve bacterial inactivation of water.

1.4 Objectives

General Objective:

To develop and characterize cold atmospheric pressure plasma sources and use them for enhancing agricultural productivity by direct exposure of the seeds to the plasma and indirect treatment (use of PAW).

Specific objectives:

1. To design and characterize CAPP sources; GAD, APJ, and DBD.
2. To study the germination and seedling growth of cereal crops (rice), cash crops (potato), and local Nepali vegetables *Rayo ko sag* (leaf mustard) by direct plasma treatment and using PAW with plasma sources; GAD, APJ, and DBD.
3. To use PAW to improve the yield of rice, potato, and leaf mustard.
4. To use plasma for decontamination of bacteria, viruses, fungi, and parasites in the plants by irrigation and improving freshness of leaves.

1.5 Outline of Thesis

This thesis is structured as follows:
Chapter 1: Introduction, The chapter provides the background of plasma, plasma used in an agriculture application, the motivation of the work, and the objective.
Chapter 2: Literature review, in this part, the comprehensive review of the use of plasma and its applications in the enhancement of agricultural seed germination, seedling growth, and yield in different agricultural seeds has been presented.
Chapter 3: Materials and methods, this chapter outlines the fundamental concept of the production of different types of plasma and its characterization method. The germination and growth parameters of agricultural seeds have also been presented.
Chapter 4: Results and conclusion, the obtained results in the production of the three types of plasma sources, its characterization, and PAW produced from the three sources and also its physico-chemical characterization presented. The applications of produced plasma in cereal and cash crops, green leafy vegetables, greenness, and bacterial inactivation of water and their interpretations have also been discussed.
Chapter 5: Conclusions and recommendations, concluding remarks of the work with limitations, and future extension of the work have been presented.
Chapter 6: Summary, finally summarizes the work.

CHAPTER 2

LITERATURE REVIEW

There will inevitably be a rise in demand for agricultural products as the world's population grows, placing pressure on the supply of these goods worldwide. However, several factors, such as a lack of land, outdated technologies that would enable mass production, crop loss from various diseases, etc., are contributing to the diminishing pace of agricultural output. Many researchers are developing cutting-edge strategies and tactics that will produce more and better-quality vegetable harvests in less time and space (Obaisi, 2017). Similar to this, the lack of food is threatening the earth due to several problems associated with farming. Pasteurization, sterilization, high-pressure processing, irradiation, pulsed electric field, and ozonation are some of the thermal and non-thermal techniques used in food processing to solve this problem. These techniques have a detrimental impact on the nutritional value and quality of the food (H. P. Sharma et al., 2021). The use of pesticides and chemicals in agriculture has a negative influence on the soil, which affects the environment and all living beings (Wang et al., 2017). To improve seed vigor, a variety of techniques have been utilized, including chemical treatment (Guangwu & Xuwen, 2014), ultrasonic scratching (Goussous et al., 2010), electric field treatment (Shi et al., 2014), magnetic treatment (Yao & Shen, 2015), and ion beam scratching (G. Xu et al., 2012). Seed quality is one of the primary determinants of crop yield in agricultural production. High-vigor seeds tend to have a faster germination rate and grow into proportioned, robust seedlings (Miano et al., 2015), which significantly impacts crop yield. By affecting biochemical processes like protein and enzyme activity, physical treatment can increase the vigor of seeds (Moon & Chung, 2000). However, some physical treatments may also harm seed cells, leading to seed loss and uneven treatment (Yao & Shen, 2015). It is necessary because low-temperature plasma leaves no chemical residues on the seeds or in the environment, making it a sustainable alternative to conventional seed treatments (Waskow et al., 2021).

Plasma treatment is used as an affordable and ecologically friendly way to boost production by promoting seed germination, plant growth, seed disinfection, insect control (as insecticides), etc. A new area of agriculture called "seed treatment with plasma

technology" holds the potential for raising crop productivity overall, germination rates, and seed quality and disease resistance (Thirumdas et al., 2018; Choi et al., 2022; Shelar et al., 2022). Enhancing seed germination, plant growth, and eventually agriculture output is believed to be possible with cold plasma treatment quick, affordable, and environmental friendly process (Ling et al., 2014). The non-equilibrium atmospheric pressure plasma produced using different configurations has collected keen interest in agriculture due to its potential to enhance seedling growth and germination rates in various crops (Lotfy et al., 2019). On a global basis, the application of cold or non-thermal plasma in agriculture has grown in popularity lately. Using plasma to increase agricultural product quality and quantity is one new eco-friendly possible tactic (Kučerová et al., 2019).

Generally, two types of plasma treatment are used: indirect approach (generate PAW and use it) and direct exposure to seeds or plants. Various types of laboratory discharge plasma to generate PAW are reported each with a similar basic production principle but useful for different purposes (H. Chen et al., 2021). PAW is used in the treatment of contaminated or polluted water (Takeuchi & Yasuoka, 2020), antimicrobial effect (Chiappim et al., 2021), applicability in the treatment of cancer (Z. Chen et al., 2016), wound healing (D. Xu et al., 2020), dentistry fields (Kaushik et al., 2019), seeds germination and seedling growth, food decay, post-harvest of food and vegetables (C. Liu et al., 2020) and many more. Which PAW is more beneficial for which purpose depends on the formation of reactive species in water due to the reaction in the interaction of water. The actual significance of the reactions, however, is dependent on several factors, including the non-thermal plasma system in use, the ambient environment, and the continuous/pulsed excitation regime (Matějka et al., 2023). The pH, EC, ORP, and nitrate and nitrite concentrations in the water are influenced by reactive species formation in PAW by plasma discharge (Zhou et al., 2020). From direct exposure, the surface is modified and has a positive impact on seed germination in different growing conditions and seed types. Raising a seed's hydrophilicity enhances its capacity to take up water absorbance capacity and development (Volin et al., 2000). However, the outcomes depend on the plasma generation method (Dubinov et al., 2000) and the working gas (Selcuk et al., 2008).

The first known case of plasma application on plant seeds was in a US patent by Krapivina et al. (1994), wherein soybean seeds were treated with CAPP made from a combination of inorganic gases (air, oxygen, and nitrogen) for five to three hundred seconds, resulting in improved germination and growth. In addition to encouraging plant growth and seed germination, the presence of ozone in the plasma treatment chamber has been shown to slow the spread of illness by a ratio of 2.7 when compared to untreated control samples. After this experiment, several studies have demonstrated

that applying atmospheric pressure plasma to various seeds can improve germination and seedling growth by stimulating and speeding up biological processes (Adhikari et al., 2020). Reactive species produced by plasma contact with surrounding air to create RONS (Graves, 2012), which could enhance various seed properties, including increased water intake (Alves Junior et al., 2016), breaking dormancy (Le et al., 2022), eliminating contaminants from seeds (Lee et al., 2021), enhancing seed germination (B. Liu et al., 2018), seedling growth (Ivankov et al., 2020) and improve drought stress tolerance (Ling et al., 2015).

H. H. Chen et al. (2012) treated brown rice by plasma, cooking, textural, and iodine staining qualities enhanced, along with the microstructure of the rice surface. After brown rice is treated with plasma, the surface becomes etched, making it easier for the rice kernel to absorb water after soaking. Brown rice requires less cooking time after plasma treatment, and the cooked grain is softer and simpler to chew. Dobrin et al. (2015) used a surface discharge reactor operating at ambient temperature and atmospheric pressure to study the effects of non-thermal plasma treatment on wheat seeds. They discovered that while plasma affected growth parameters, it had minimal impact on germination rate. Compared to untreated samples, the distribution of roots in the case of plasma-treated seeds was moved towards larger lengths. Thirumdas et al. (2016) found the functional qualities of Basmati rice enhanced by the low-temperature plasma treatment. Pawłat et al. (2018) studied the effects of APPJ on *Lavatera thuringiaca* seed. The seeds stimulated with plasma exhibited the maximum germination parameters after two and five min of exposure; extended exposure caused damage or fracture to certain areas of the cuticle and affected the deeper zone of the cuticle.

Adhikari et al. (2019) compared tomato seedlings treated with PAW with control seedlings, PAW irrigation, or priming, upregulated the growth of the seedlings as well as the levels of endogenous RONS, defense hormones (jasmonic acid and salicylic acid), and important pathogenesis-related (PR) gene expression. Even at concentrations found in 30 min of PAW, RONS can produce harmless signaling. They suggested that PAW irrigation might be beneficial for agriculture since it influences immune response components and plant growth. Iqdiam et al. (2020) investigated how peanut physiochemical quality, aflatoxin level, and sensory characteristics were affected by APPJ treatment. All quality parameters showed minimal alterations, indicating that APPJ is a potential treatment for peanut aflatoxin. Hashizume et al. (2021) found rice seedlings treated with cold plasma have been shown to exhibit improved plant growth, grain yield, and grain quality. Cold plasma has been used effectively to eliminate or render dormant pathogens on the seed surface to reduce the likelihood of disease during germination and the initial stages of plant growth as well as protein content in seeds, and biological nitrogen fixation and modulation (Motrescu et al., 2023).

Locally, some of the works for the development of plasma reactors and their applications for different purposes were done by the Kathmandu University group: APJs developed in the air using argon (Tyata et al., 2012), PAW made by argon plasma and applied on radish, fenugreek, and pea (Guragain et al., 2021d), soybean (Guragain et al., 2021c), paper, barley, mustard, and Rayo (Guragain et al., 2023b) seeds, and directly argon plasma treatment of radish and carrot (Guragain et al., 2021a), and mustard (Guragain et al., 2023) seeds.

In the Tribhuvan University, Thakur et al. (2019) developed arc plasma for the first time at the Central Department of Physics, Tribhuvan University, and characterized plasma parameters using single and double probe methods. However, the produced arc plasma is unsuitable for heat-sensitive applications and it is challenging to use it for substrate treatment. This is because the plasma does not form a plume but rather generates intense heat between the two electrodes, which can destroy the sample. Research on plasma use in agriculture at Kathmandu University has involved argon plasma in all experiments. However, using argon gas as a feeder during the plasma production process is both expensive and impractical for real-world applications. Most literature reports that they utilize gases like argon, nitrogen, and helium, either alone or in combination with air, but rarely use air as the sole feeder gas. There is a gap in studies focusing on using air for plasma production to enhance agricultural productivity. This gap motivated us to implement our findings in practical agricultural applications.

CHAPTER 3

MATERIALS AND METHODS

3.1 Production of Cold Atmospheric Pressure Plasma

3.1.1 Gliding Arc Discharge Plasma

The Schematic diagram of the experimental arrangement for producing and characterizing atmospheric pressure GAD plasma is shown in Figure 11 (a). To understand the discharge parameters variations in different regimes of the discharge, have been discrete into different regions: “O”, “A”, “B”, “C” and “D” as shown in Figure 11 (b). The locally-made power supply (S. Sharma et al., 2024) is used to produce the

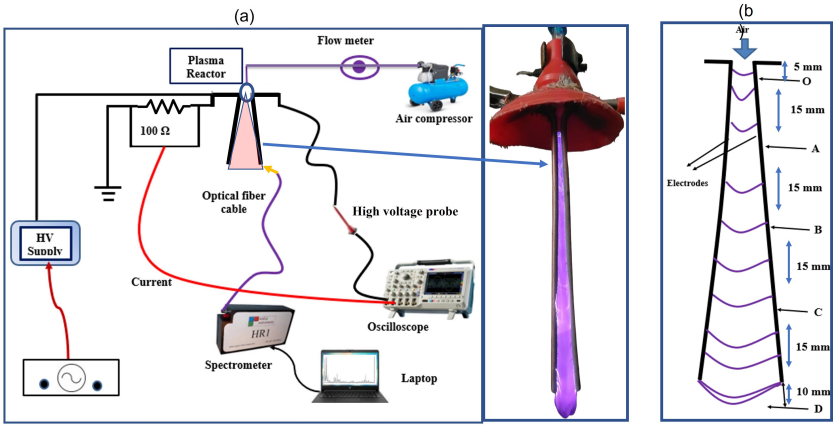

Figure 11: (a) Schematic diagram for the generation and characterization of atmospheric pressure GAD plasma (Chalise et al., 2023) and its real picture of discharge, and (b) different regimes of the discharge: ‘O’, ‘A’, ‘B’, ‘C’, and ‘D’ (S. Sharma et al., 2024)

GAD plasma. The discharge voltage can be varied in the range of 0 to 15 kV DC. The discharge is produced at the air flow rate of (0-15) LPM and the gas flows in between two copper electrodes of 65.0 mm length and 5.0 mm diameter of each, with a separation of 2.0 mm at the inlet and 6.0 mm of outlet position. The arc discharge is produced without air flow in a minimum gap between the electrodes. When air flow pushes the discharge from top to bottom, the discharge is propagated to the O to D region. Due to the air force, the discharge moves or glides from top to bottom, hence the name of the discharge is GAD.

3.1.2 Dielectric Barrier Discharge Plasma

Figures 12, 13 and 14 show the schematic diagram of the experimental arrangement of the three types of DBD plasma with its real picture of plasma generation. An electronic neon transformer type B (neon light model: NTO-500, Neon business, Korea) with an output of 0–20 kV voltage and 34 kHz frequency without load is used to produce the discharge in the Spark Dielectric Barrier Discharge (SDBD) plasma arrangement as shown in Figure 14. A copper wire with a thickness of 0.7 mm is attached to the epoxy glass fiber for a high voltage (HV) electrode. The ground electrode is made of copper with a diameter of 65.0 mm and a thickness of 5.0 mm. The high voltage electrode and ground electrode are facing each other and the spacing between these two electrodes is 8.0 mm. The purpose of this device is the treatment of bacteria which is soluble in water.

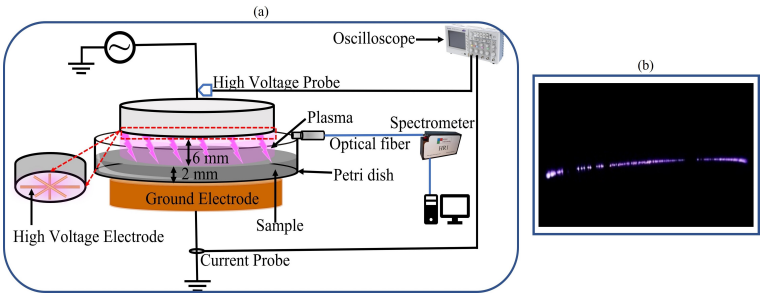

Figure 12: (a) Schematic diagram illustrating the spark dielectric barrier discharge plasma and the characterization mechanism (Dhakal et al., 2023) and (b) real discharge

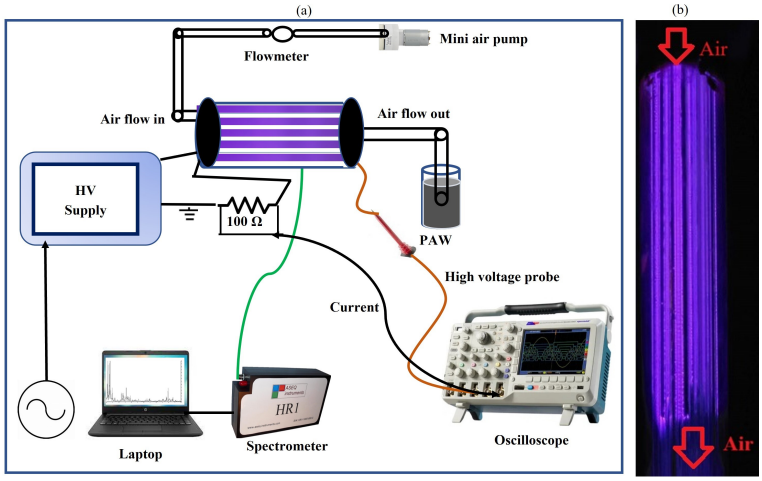

Figure 13: (a) Schematic diagram of the cylindrical dielectric barrier discharge of plasma, and (b) photograph of discharge

The Cylindrical Dielectric Barrier Discharge (Cy-DBD) plasma is produced and characterized as presented in Figure 13. The discharge is produced by electronic neon transformer type B (neon light model: NTO-500, Neon business, Korea) with an output of 0–20 kV voltage and 34 kHz frequency without load. The quartz cylinder has

dimensions of 485.0 mm in length and 45.0 mm in diameter. Inside it, 8-16 electrodes with a gap of 1.5 mm (1.9 mm diameter of brass) are arranged lengthwise with a gap of 2.0 mm. To blow the reactive species produced within the reactor, air is supplied through one end and ejected out of the other, where an external pipe is attached to dipped into the water. The other end of that pipe is dipped in water to generate PAW. This plasma reactor is aimed to produce a large volume of PAW.

Similarly, the schematic diagram of the Circular Dielectric Barrier Discharge (CDBD) setup is shown in Figure 14. The diameter and thickness of the stainless steel circular electrode are (57.2±0.8) cm and (4.6±0.7) cm respectively. The electrode gap is 4.0 mm and the discharges in the air gap between two cylindrical electrodes covered by quartz plate have 2.0 mm thickness and 90.0 cm diameter. This quartz plate works as a dielectric medium and the discharge is produced by a high-voltage power supply (Chengdu Chuangyu Xinjie Technology Co. Ltd.) with an output voltage of 3-30 kV. The center of the 8.0 mm hole provides a 15 LPM air flow on the upper electrode center, which is controlled by a flow meter. Treating the large number of seeds and thin film is the main purpose of this reactor.

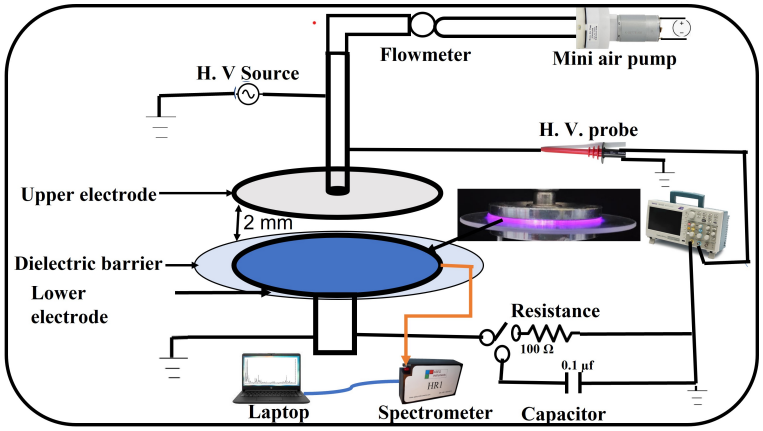

Figure 14: Schematic diagram of the circular dielectric barrier discharge plasma and its photograph of discharge (Chalise et al., 2024d)

3.1.3 Air Plasma Jet

The schematic diagram of atmospheric pressure APJ is shown in Figure 15 (a) and the real picture of the jet is shown in Figure 15 (b). The discharge is produced by electronic neon transformer type B (neon light model: NTO-500, Neon business, Korea) with an output of 0–20 kV voltage and 34 kHz frequency without load. APJ is generated in a quartz capillary tube with an inner diameter of 3.0 mm and an outer diameter of 5.0 mm. The central electrode of stainless steel with a 1.0 mm external diameter is connected with high voltage. The air flow provided by a mini air pump is inserted into the hole of the central electrode. The distance between the lower point of the electrode and the

lower point of the quartz nozzle is 10.0 mm. The grounded electrode (copper foil) is inserted under the 90.0 mm diameter glass and 2.0 mm thick beaker. 40.0 ml water is put in the beaker and the gap between the lower point of the nozzle and the upper surface of the water is 2.0 mm. The air flow can be altered by changing the input voltage of the mini air pump to 0-15 LPM.

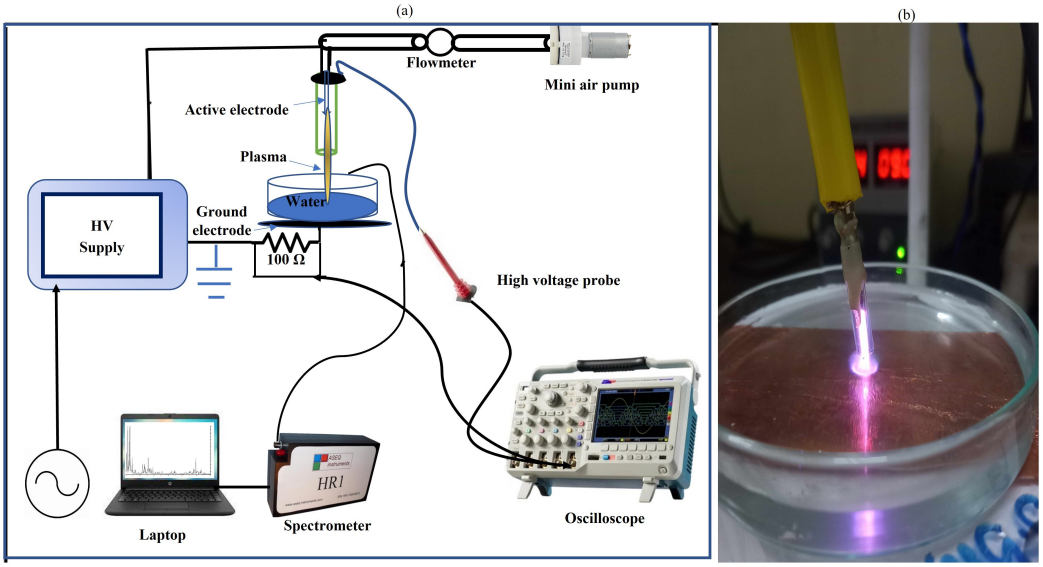

Figure 15: (a) Schematic diagram for the generation and characterization of atmospheric pressure air plasma jet, and (b) photograph of discharge

3.2 Characterization of Plasma

3.2.1 Electrical Characterization

The voltage across the plasma reactor (GAD, DBD, and APJ) is measured using a high-voltage probe (PINTEK HVP-40) and an oscilloscope (Tektronix TBS 1052B). 100 Ω resistor is connected in series with the ground (Tektronix TPP0051, 10 × voltage probe) electrode to measure the discharge current. A capacitor of 10 nF is connected in series with the ground (Tektronix TPP0051, 10 × voltage probe) electrode to measure the transported charge in the DBD plasma in which AC power supply is used for discharge production. Discharge current (I_{dis}) and discharge voltage (V_{dis}) are the corresponding values of the current and voltage of the first discharge observed in the I-V curve cycle. The discharge's peak-to-peak voltage (V_{pp}) is measured from peak to peak value of the sinusoidal current-voltage waveform. However, the discharge waveform is a distorted sinusoidal wave in plasma discharge. V_{p} of the discharge is half of the peak-to-peak value of the V_{pp} (Pourali et al., 2023);

$$V_{\text{p}} = \frac{V_{\text{pp}}}{2} \tag{3.1}$$

Root mean square (V_{rms}) of sinusoidal voltage in discharge is calculated as (Pourali et al., 2023);

$$V_{\mathrm{rms}} = \frac{V_{\mathrm{p}}}{\sqrt{2}} \tag{3.2}$$

The frequency of the discharge is obtained as the reciprocal of the time of one complete cycle of discharge

$$\mathrm{Frequency}(f) = \frac{1}{T} \tag{3.3}$$

Two ways of calculating of energy and power of the discharge are implemented. The first way is to calculate the time-averaged electrical energy of the plasma discharge using voltage and current curves (Pourali et al., 2023):

$$\overline{E} = \int V(\mathrm{t}) \times I(\mathrm{t}) dt \tag{3.4}$$

where $V(\mathrm{t})$ and $I(\mathrm{t})$ are the voltage and current at the respective time. The discharge's time-averaged electrical power consumption can be calculated using (Pourali et al., 2023)

$$\overline{P} = \frac{1}{T} \int V(\mathrm{t}) \times I(\mathrm{t}) dt = f \times \overline{E} \tag{3.5}$$

The electrical power calculated by using this method typically fluctuates from cycle to cycle. After that, several cycles are required to get a converged mean value. In addition, to ensure that the current peaks are correctly recorded and provided, the data must be captured using a high sampling rate (usually a few ns) and a high bandwidth oscilloscope. There is still a problem with this approach, despite its relative simplicity and accuracy: when there are strong current peaks, it can be difficult to resolve the synchronous current accurately because its amplitude is at least one order of magnitude smaller than the current peaks (Benard & Moreau, 2014). Manley et al. (1943) developed another simple method to overcome this issue. This method consists of placing a capacitor between the grounded electrode and the earthing point as shown in previous Figure 14. It is accomplished by plotting the charge curve of the inserted capacitor throughout a full cycle as a function of the applied voltage. Each period's energy dissipated by the discharge is represented by the area inside the closed Lissajous curve. The shape of the Lissajous curve depends on various factors, including the frequency, amplitude, and phase relationship between the two waveforms. So, to obtain the area of the Lissajous curve, accumulated charges versus applied voltages are plotted. If we take one full cycle of discharge data, the area of this curve indicates the energy that the discharge releases

for each cycle. Thus energy dissipated per cycle (Manley, 1943)

$$E = \text{Area covered by Lissajous (Q-V) plot} \tag{3.6}$$

Using the Lissajous (Q–V plot) approach, the power dissipation across the plasma is calculated by multiplying energy with waveform frequency (Manley, 1943):

$$P = (E_{\mathrm{L}} \times f) \tag{3.7}$$

This approach's primary benefit is that it is more reproducible from cycle to cycle and does not suffer from bias caused by high current peaks in the computation. Using this method, calculating the precise amount of electrical power utilized only requires one AC cycle. This makes sense for tests conducted in closed loops where a short loop time is required (Benard & Moreau, 2014).
The root means the square voltage of the non-sinusoidal wave is calculated by (Guofeng & Xinwei, 2012):

$$V_{\mathrm{rms}} = \sqrt{\frac{\int_0^T [V(t)]^2 \, dt}{T}} \tag{3.8}$$

Similarly, the root mean square current of the non-sinusoidal wave is (Guofeng & Xinwei, 2012):

$$I_{\mathrm{rms}} = \sqrt{\frac{\int_0^T [I(t)]^2 \, dt}{T}} \tag{3.9}$$

The average power of the non-sinusoidal wave (Bissell & Chapman, 1992):

$$P_{\mathrm{avg}} = \frac{\int_0^T I(t)V(t) \, dt}{T} = I_{\mathrm{rms}} \times V_{\mathrm{rms}} \tag{3.10}$$

3.2.2 Optical Characterization

Optical emission spectroscopy (OES) is a widely used technique to measure the intensity of different wavelengths of light. It is a simple but contemporary powerful non-destructive diagnostic tool of plasma. Indeed, spectra radiated by plasma enclose a lot of information reflecting the fundamental properties of plasma. OES provides information on excited atomic and molecular states to determine the produced discharge's rotational, vibrational, and electron excitation temperature and density. The population of the excited state involved in the optical emissions arising from the electron impact excitation also influences the intensity of certain lines. The electronic temperature and electron density are therefore related to the emission intensity and the widening of the spectral

lines. These temperature parameters are important as they directly affect the rate of a chemical reaction during plasma applications (S. Huang et al., 2019). OES of the CAPP is detected employing an HR-1 high-resolution spectrometer (ASEQ Instruments), which had a detection range of 200–830 nm, grating element of 300 grating per mm, resolution of 0.176 nm, and a slit width of 10 μm. An integration time of 300 ms is used with an average of 30 samples to obtain the optical emission data. Figure 16 shows the transitional energy diagram for N_2 second positive system (SPS) N_2 $\left(C^3\Pi_u \rightarrow B^3\Pi_g\right)$ (297–400 nm) and N_2 first positive system (FPS) N_2^+ $\left(B^2\sum_u^+ \rightarrow X^2\sum_g^+\right)$ (550–800 nm) (Choi et al., 2022).

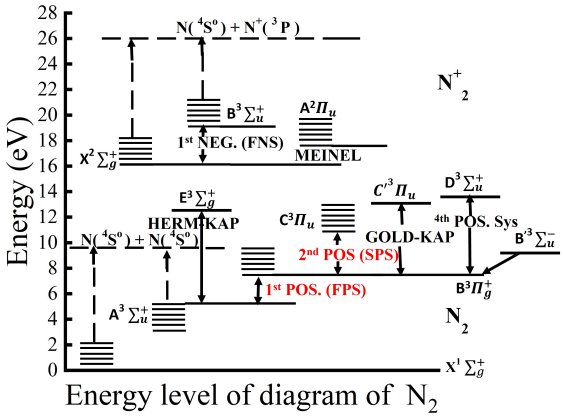

Figure 16: Transitional energy diagram of nitrogen second positive system and nitrogen first positive system (Choi et al., 2022)

The excitation temperature (T_{ex}) for non-equilibrium high-density plasmas can be estimated using the electron temperature (T_e), assuming that heavy particle collisions are not inelastic. A straightforward and effective technique for determining out T_{ex} in atmospheric pressure plasma is the Boltzmann plot (Gulec et al., 2015; Roy & Talukder, 2018). This plot method is one of the most widely used techniques for measuring the temperature in lab plasma. The radiative transfer equation for an optically thin, uniform, and isothermal plasma along the line of sight provides the basis for this calculation. The equation is linearized by taking the logarithm of both portions to get the Boltzmann plot. The argument of the logarithm, a dimensionless transcendental function, must also be dimensionless (Völker & Gornushkin, 2022). The Boltzmann plot technique of N(III) species, which uses the data from the NIST database (Kramida et al., 2023), is used to compute the electron excitation temperature (T_{exc}). Using this approach, the LTE plasma equation is (Aragón & Aguilera, 2008);

$$\ln\left(\frac{\lambda_{ij}I_{ij}}{A_{ij}g_j}\right) = -\frac{E_j}{k_B T_{exc}} + \ln\left(\frac{4\pi Z}{hcN_o}\right) \tag{3.11}$$

The variables in this equation are the intensity of the transition from the i to the j

state (I_{ij}), the wavelength of the transition (λ_{ij}), transition probability (A_{ij}), statistical weight (g_j), higher energy level E_j, electron excitation temperature T_{exc}, Z is the partition constant, c is the speed of light, N_0 is the total population of the species. When we plot the ln $\left(\frac{\lambda_{ij} I_{ij}}{A_{ij} g_j}\right)$ versus E_j, the slope of the obtained graph (Boltzmann plot) is equal to -$\frac{1}{k_B T_{exc}}$ and then the electron excitation temperature is obtained.

The Saha equation is rooted in the principles of statistical mechanics and considers the balance between ionization and recombination processes in plasma at thermal equilibrium. It provides a way to calculate the relative abundances of different ionization states of an element in plasma as a function of temperature and pressure. The plasma density is calculated from the Saha-Boltzmann equation (Unnikrishnan et al., 2010):

$$N_e = 2\frac{I_2 A_1 g_1 \lambda_2}{I_1 A_2 g_2 \lambda_1}\left(\frac{2\pi m_e k_B T_{exc}}{h^2}\right)^{3/2} \exp\left[-\frac{(E_1 - E_2 + E_j)}{k_B T_{exc}}\right] \tag{3.12}$$

The energy of ionization of a neutral atom is denoted by E_j; the intensity of the same species line has a larger gap in upper energy, and the wavelengths are denoted by λ_1 and λ_2; the transition probabilities are represented by A_1 and A_2; and the statistical weights are g_1 and g_2.

Rotational (T_{rot}) and vibrational (T_{vib}) temperatures are calculated by MassiveOES (Voráč et al., 2017a, 2017, 2019) software. The MassiveOES package uses the logarithmic ratio of intensities of different spectral lines to estimate rotational and vibrational temperatures. So that if the given OES data shifted from standard value/fit then software provided with error. When dealing with nitrogen plasmas or plasmas containing nitrogen, Boltzmann plots or fits of the band envelopes of various bands belonging to the first negative system and/or second positive system are commonly employed (Biloiu et al., 2006). The vibrational temperature is calculated by the Boltzmann plot method also. The line intensity of the vibrational transition's spectral is provided as (Wu et al., 2015)

$$I_{\nu' \to \nu''} \propto \frac{hc}{\lambda_{\nu' \to \nu''}} A_{\nu' \to \nu''} N_0 \exp(-\frac{hc G_{\nu'}}{k_B T_{vib}}) \tag{3.13}$$

where $I_{\nu' \to \nu''}$, k_B, h, c, and T_{vib} are the transition frequency from the upper vibrational level to the lower vibrational level, Boltzmann constant, Planck's constant, velocity of light, and vibrational temperature respectively. $A_{\nu' \to \nu''}$, $G_{\nu'}$, and $\lambda_{\nu' \to \nu''}$ are the probability of vibrational transition, spectral term of the vibrational transition, and wavelength which are related to the upper vibrational level (ν') to the lower vibrational level (ν''). The spectral factor can be replaced by the energy difference of the energy levels $G'_\nu = E_{\nu'} - E_0$. The vibrational energy of the excited molecules on the level of N_2 ($C^3\Pi$) in the quantum harmonic oscillator approximation disregarding the anharmonicity

constant (Lamichhane et al., 2023);

$$E_v(eV) = 1.2398 \times 10^{-4}(v + \frac{1}{2})w_e(\mathrm{cm}^{-1}) \tag{3.14}$$

where v is the vibrational quantum number and w_e is the spacing of vibrational energy on the $C^3\Pi$ (-2047.17 cm^{-1}). Using equation (3.14) in equation (3.13) we can get the semi-log equation as (Wu et al., 2015)

$$\ln\left(\frac{I_{v'\to v''}\lambda_{v'\to v''}}{A_{v'\to v''}}\right) = C - \frac{E_{v'} - E_0}{k_B T_{\mathrm{vib}}} \tag{3.15}$$

where $I_{v'\to v''}$ is the intensity of transition from upper to lower state, $\lambda_{v'\to v''}$ is the wavelength of transition, $A_{v'\to v''}$ is the transition probability, $E_{v'}$ is the upper energy level with the vibrational quantum numbers. When we plot the $\ln\left(\frac{I_{v'\to v''}\lambda_{v'\to v''}}{A_{v'\to v''}}\right)$ versus $(E_{v'} - E_0)$, the slope of the obtained graph (Boltzmann plot) is equal to $-\frac{1}{k_B T_{\mathrm{vib}}}$ and then the vibrational temperature is obtained. For the Boltzmann plot method, four vibrational bands are taken: Δv= +1 (1-0, 2-1), Δv= -1 (0-1, 1-2, 2-3), Δv= -2 (0-2, 1-3, 2-4) and Δv= +2 (2-0, 3-1) (Lofthus & Krupenie, 1977). The National Institute of Standards and Technology reference database is the source of the spectroscopic parameters needed for the Boltzmann graphic (Kramida et al., 2023).

3.3 Application of Plasma and Seedling Parameters

The seeds are directly treated below 10.0 mm of the GAD electrode from the GAD plasma and between the two electrode gaps of 7.0 mm over the dielectric in DBD plasma, as shown in Figure 17 (a) and (b) respectively. Where Figure 17 (a) and (b) show the direct treatment of wheat and Basmati rice seeds, respectively. The temperature and

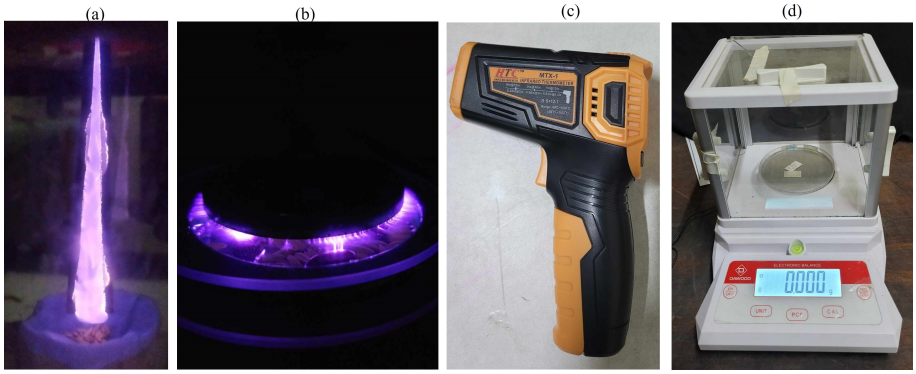

Figure 17: Direct treatment of seeds by (a) gliding arc discharge plasma and (b) circular dielectric barrier discharge plasma, (c) infrared thermometer, and (d) digital weight balance

weight, before and after the plasma treatment are noted by the Infrared (IR) thermometer and digital weight balance (Daewoo Digital) as shown in Figure 17 (c) and (d). The

IR thermometer is used to measure the temperature of seeds from far away so that temperature is not influenced by the measuring system. A digital weight balance with a minimum count of 0.001 gm used for seeds and plant weight. For the observation of directly plasma-treated seed's morphology, a low-cost goniometer is developed and calibrated with the Ramé-Hart goniometer available at Kathmandu University, Nepal for contact angle measurements using drop image analysis (Chalise et al., 2023a) as shown in Figure 18, where (a) macro lens, (b) camera holder, (c) micropipette, (d) final setup, (e) liquid drops image, (f) image of drop, and (g) contact angle measured. The

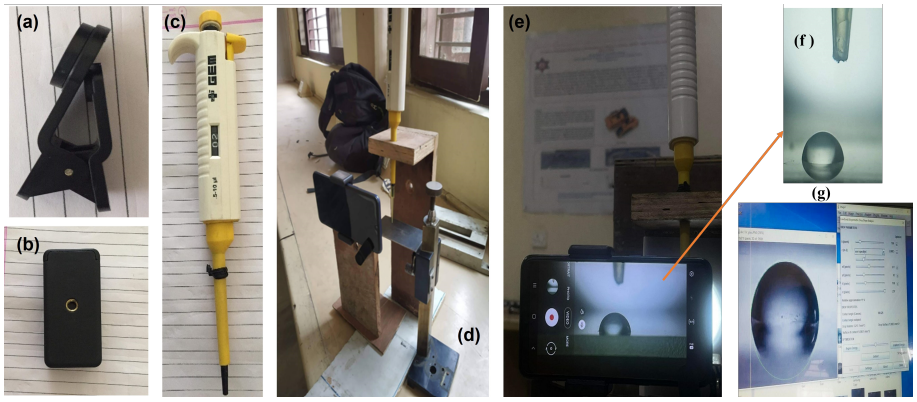

Figure 18: Goniometer configuration: (a) macro lens, (b) camera holder, (c) micropipette, (d) final setup, (e) liquid drops image, (f) image of drop, and (g) contact angle measured (Chalise et al., 2023a)

next method of observing the surface change on seeds due to the plasma is calculating wettability from relation (Lotfy et al., 2019)

$$\text{Wettability or water imitation rate}(\%) = \frac{m_1 - m_0}{m_0} \times 100 \tag{3.16}$$

where m_0 denotes the mass of seeds before they are soaked in water and m_1 denotes after that step. Then treated seeds are planted after 24 hours of the wettability measurement.

For the indirect treatment method, PAW is produced from plasma directly exposed on the water surface from GAD plasma as shown in Figure 19 (a), and the plasma-generated reactive species are delivered inside the water as shown in Figure 19 (b). The physio-chemical characteristics of PAW are investigated for all applications. A 7-in-1 RCYAGO water quality tester is used to measure temperature, electrical conductivity (EC), the potential of Hydrogen (pH), total dissolved solids (TDS), and oxidation-reduction potential (ORP) before and after the plasma treatment as shown in Figure 19 (c). The water quality tester is calibrated in the buffer solution supplied by the tester manufacturer. In every, experiment quality tester is calibrated in buffer solution. Test strips of Purtec medical equipment (Kunshan) Co., Ltd., China are used to assess the concentration of hydrogen peroxide (H_2O_2), as shown in Figure 19 (d), and strips from Changchun MDC Medical Co., Ltd., China are used to measure the concentration of nitrite (NO_2) and nitrate (NO_3) as shown in Figure 19 (e) and (f) respectively. The

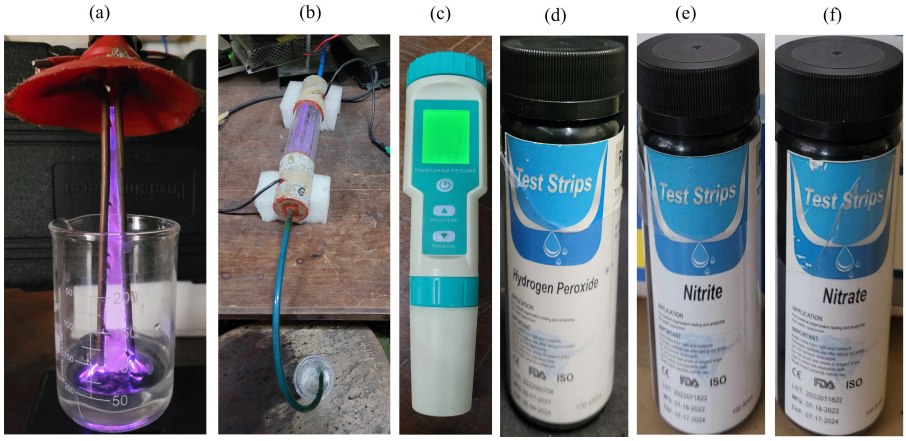

Figure 19: PAW production from (a) GAD plasma and (b) cy-DBD plasma, (c) 7-in-1 water test meter, (d) hydrogen peroxide test stripes, and (e) nitrite and (f) nitrate test stripes

concentrations were quantitatively determined using a color chart on each test strip container, with a test strip efficiency of 99.6%. Water test stripes give the color code chart after inserting it in the PAW. The color code values (in mgL^{-1}) are 0, 1, 5, 10, 20, 40, and 80 for nitrite and 0, 10, 25, 50, 100, 250, and 500 for nitrate, 0, 0.2, 0.5, 1.0, 5.0, 10.0, 30.0, and 100.0 for hydrogen peroxide. The values were noted corresponding to the color change observed in the test strip. Thus, we got the single color code value and it is not necessary to present with error bar during the experiment, and the procedure is consistent with previous works (Gharagozalian et al., 2017).

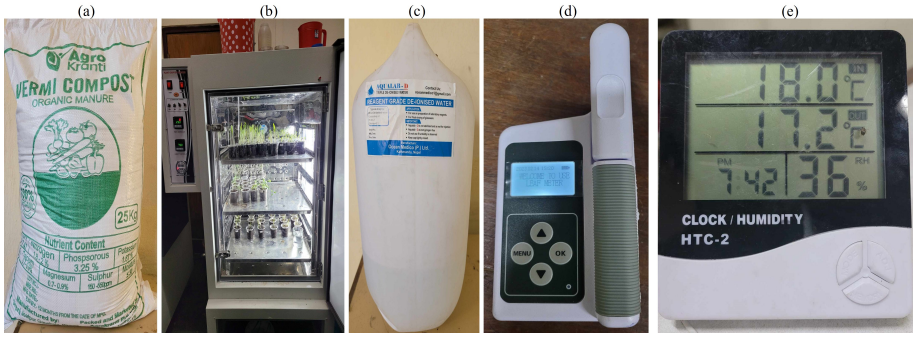

Figure 20: (a) Vermicompost, (b) plant growth chamber, (c) de-ionized water, (d) TYS-B chlorophyll meter, and (e) HTC-2 hygrometer

The seeds are planted in vermicompost as shown in Figure 20 (a), product of Agro Kranti, Nepal, which has 7.41 pH, (1.80-2.00)% nitrogen, 3.25% phosphorous, (0.70-0.90)% calcium, (0.70-0.90)% magnesium, 1.87% potassium, and (150.0-650.0) ppm sulfur and put inside the plant growth chamber at (25.0±1.0)^{o}C temperature and (75.0±15.0)% humidity with 12 hrs 50% light. Most of the research presented in this thesis is in ambient environment conditions. Two plant growth chambers (H. L. Scientific Industries, India) were used to create a regulated environment for plants as shown in Figure 20 (b), which has 280-liter capacity, (50-100)% humidity range, temperature, and control of the daylight system. During the experiment triple de-ionized water (AQUALAB-D of

Ocean Medico. Pvt. Ltd., Nepal having conductivity less than 1.0 and pH 6.5-7.0) is used for soaking and irrigation of plantation time, which is shown in Figure 20 (c). Chlorophyll content in a plant's leaf is measured using a CCM-300 provided by the Central Department of Botany and TYS-B chlorophyll meter device at our lab as shown in Figure 20 (d), but these devices have a limitation in the area of scan of leaves. While experimenting in the ambient environment, the temperature and humidity of the environment are measured by HTC-2 hygrometer as shown in Figure 20 (e).

The following parameters are calculated and repeated with five replications.
The germination rate is calculated using (Lotfy et al., 2019):

$$\text{Germination rate}(\%) = \frac{\text{Seeds germinated in 3 day}}{\text{Total number of seeds}} \times 100 \tag{3.17}$$

The final germination percentage (FGP) is calculated as (Volin et al., 2000)

$$\text{FGP}(\%) = \frac{\text{Number of seedlings germinated}}{\text{Total number of seeds used}} \times 100 \tag{3.18}$$

FGP can be relativized as (Ranal et al., 2009):

$$\text{R}(\%) = \frac{\text{Actual percentage}}{\text{Highest percentage among the group}} \times 100 \tag{3.19}$$

The rate and range of germination are measured by mean germination time (MGT). It indicates the length of time spent watching the sprout emerge. The mean germination rate (MGR) is defined as the reciprocal of the mean germination time. MGT and MGR are calculated as (Ranal et al., 2009):

$$\text{MGT} = \frac{\sum_{i=1}^{k} n_i t_i}{\sum_{i=1}^{k} n_i} \tag{3.20}$$

and

$$\text{MGR} = \frac{1}{\text{MGT}} \tag{3.21}$$

where t_i is the time from the start of the experiment to the i^{th} observation (day for the example), n_i is the number of seeds germinated in the i^{th} time (not the accumulated number, but the number correspondence to the i^{th} observation), and k is the last time of germination. A variance of germination time is expressed as (Jones & Sanders, 1987):

$$S_t^2 = \frac{\sum_{i=1}^{k} n_i (t_i - \text{MGT})^2}{\sum_{i=1}^{k} (n_i - 1)} \tag{3.22}$$

The coefficient of variation of the germination time is given by (Ranal et al., 2009)

$$\mathrm{CV}_t\ (\%) = \frac{\mathrm{S}_t}{\mathrm{MGT}} \times 100 \tag{3.23}$$

where S_t is the standard deviation of germination time. The coefficient of the velocity of germination (CVG) indicates rapidity of germination which increases as the number of germinated seeds increases and the time required for germination decreases (Jones & Sanders, 1987).

$$\mathrm{CVG}\ (\%) = \frac{\sum_{i=1}^{k} n_i t_i}{\sum_{i=1}^{k} n_i} \times 100 \tag{3.24}$$

Uncertainty of the germination process is calculated as (Ranal et al., 2009):

$$\mathrm{U} = -\sum_{i=1}^{k} f_i \log_2 f_i \tag{3.25}$$

where $f_i = n_i / \sum_{i=1}^{k} n_i$ with n_i is the number of seeds germinated on the i^{th} time. Synchrony of germination is calculated as (Ranal et al., 2009):

$$\mathrm{Z} = \frac{\sum_{i=1}^{k} C_{ni,2}}{C_{\sum n_i,2}} \tag{3.26}$$

where $C_{n_i,2} = n_i(n_i - 1)/2$ with $C_{ni,2}$ is the combination of seeds germinated in the i^{th} time, and n_i is a number of seeds germinated in the i^{th} time. During the production of the mushroom the colonization and budding time (days) from the spawning time of the mushroom in noted. The growth potential of the oyster mushroom is given by biological efficiency (Agun et al., 2020) and is calculated by

$$\text{Biological efficiency (BE) (\%)} = \frac{\text{Fresh weight of harvested mushrooms (gm)}}{\text{Dry weight of the substrate (gm)}} \times 100 \tag{3.27}$$

The standard ruler, whose least count is 0.1 cm, is used to measure the plant's root and shoot length. The length from the tip of the plant to the portion above the ground is known as the shoot length; on the other hand, the root length is the measurement from the end of the shoot system to the tip of the longest root. The obtained results are plotted using the student learning edition of MATLAB R2024a, Origin 2024, and Python. The presented values represent mean and standard error (mean ± standard error). However, a one-way ANOVA test is carried out to check the statistical significance of germination and production parameters of wheat as well as the production of mushrooms.

CHAPTER 4

RESULTS AND DISCUSSION

In this chapter, the experimental results obtained for the cold atmospheric pressure plasma generation, its characterization, and its application in cereal crops, cash crops, green leafy vegetables, greenness retention of detached leaves, and bacterial inactivation in water have been presented. The one important objective of the thesis is the generation of cold atmospheric pressure plasma in the Central Department of Physics, Kirtipur, Kathmandu, Nepal. Figure 21 depicts different stages of the development of plasma reactors using local materials that are easily available in the local market for a sustained duration of operations for a longer time. Our quest to produce plasma begins with easily available low-cost materials from our local market, such as hair dryers for air flow and high voltage power supply of plasma reactor from fly back transformer which is used in television to produce cathode ray discharge and is wrapped in a shoe box as depicted in Figure 21 (a). Two master's degree students initiated it; Mr. Sangat Sharma and Mr. Sandesh Devkota. This achievement remarks the initial inflection point in plasma production in a lab suitable for low-temperature atmospheric-pressure applications. As illustrated in Figure 21 (b), the hair dryer is replaced by an air blower

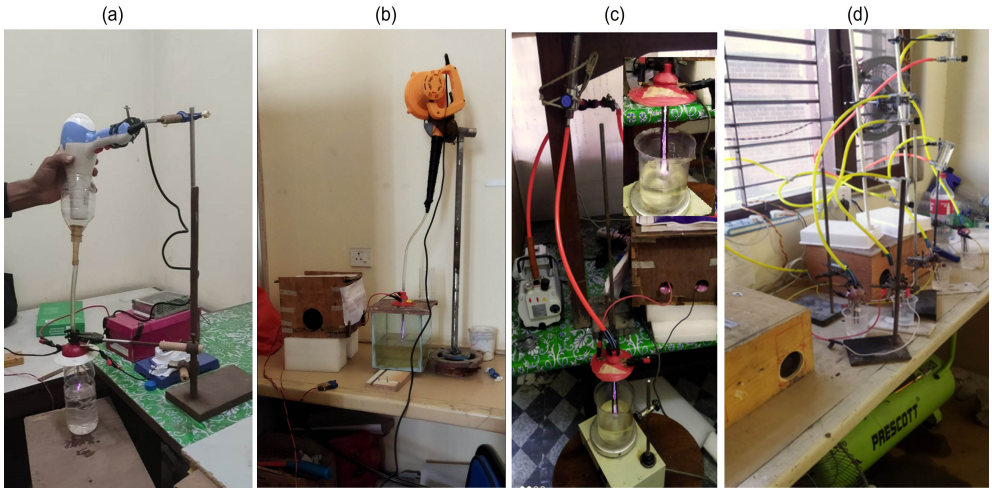

Figure 21: Different stages of development of cold atmospheric pressure plasma in a plasma research laboratory at the Central Department of Physics, Tribhuvan University, Kirtipur, Nepal

due to overheating, which limited plasma operation to under two min. Subsequently, the air blower is replaced with an air compressor to overcome its air flow limitations and provide sufficient pressure for long-length GAD plasma as shown in Figure 21 (c). The increased number of plasma reactors caused the air pump to overheat and generate uneven air flow. Consequently, the air pump is replaced by an air compressor to enable the continuous operation of four GAD plasma reactors from a single air compressor source as depicted in Figure 21 (d).

Following a month-long training (December 2, 2022 – January 2, 2023) at the Plasma Bioscience Research Center, Department of Electrical and Biological Physics, Kwangwoon University, Seoul, Republic of Korea, we are successful in generating two additional types of plasma sources. We established a new plasma research laboratory in our department, as shown in Figure 22. This lab produced three different types of cold atmospheric pressure plasma: GAD, DBD, and APJ. Notably, eight plasma reactors could operate simultaneously in a sustained way for a longer time at an instant. The natural air at atmospheric pressure is a feeder gas in all of the reactors, which could lower the operating costs and it would be applied in the future in the field of agriculture as air is available everywhere. Our needs could easily be met by adjusting the input voltage and air flow rate. Another accomplishment is the power source for the GAD, which we could assemble using readily available materials from the local market, making the cost of producing the GAD plasma more economically feasible. The generated plasma is analyzed and used in various agricultural commodities to address issues such as bacterial water inactivation, extended leaf greenness, seed germination, seedling growth, and enhanced production.

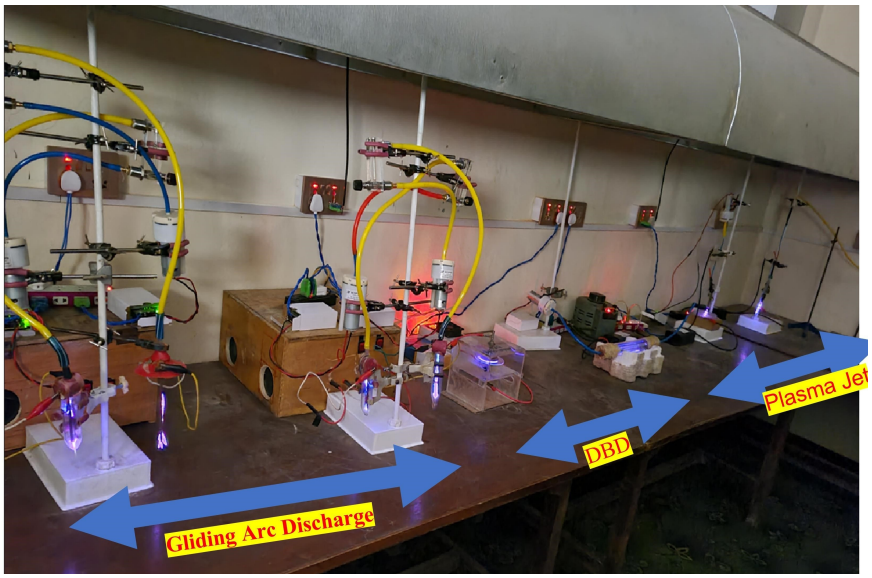

Figure 22: CAPP reactors at plasma research lab at Central Department of Physics, Tribhuvan University, Kirtipur, Nepal

4.1 Plasma Production and Characterization

4.1.1 Gliding Arc Discharge Plasma

Figure 23 (a) and (b) illustrate GAD plasma at atmospheric pressure produced in the laboratory by varying applied voltage and air flow, without enclosing the gliding arc discharge and enclosed gliding arc by borosilicate glass with a 4.0 mm nozzle diameter serves to contain all of the reactive species created during the discharge respectively. It is found that the length of the plasma plume increases as air flow increases and more intense plasma is produced by increasing the input voltage of the plasma power source.

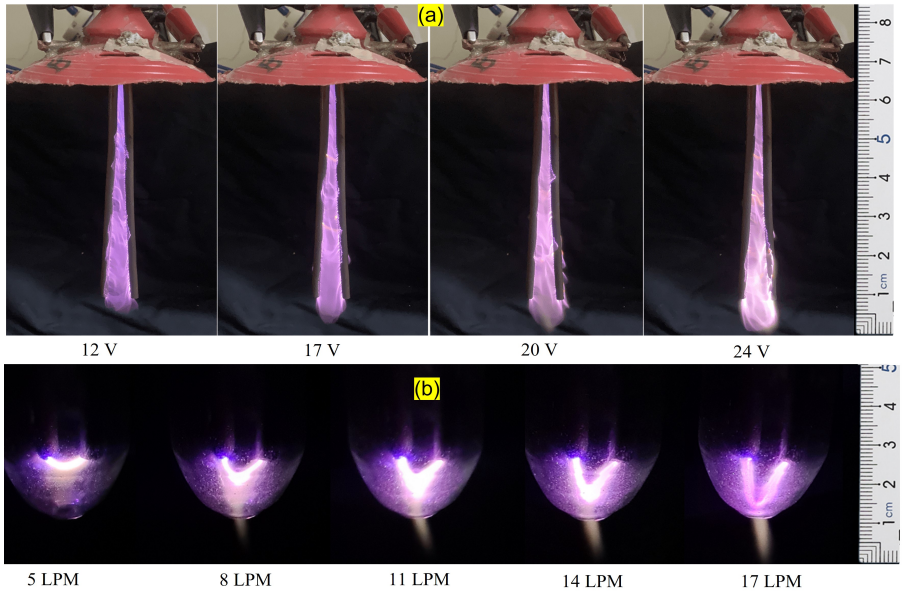

Figure 23: Production of GAD plasma (a) between two copper electrodes at 15 LPM for different input voltage, and (b) enclosed by borosilicate for developing GAD plasma jet at different air flow rates

4.1.1.1 Electrical Characterization

The electrical characterization of the plasma provides details on the configured discharge's property of applied current and voltage, frequency, discharge energy, and power. Figure 24 (a), (b), (c), (d) illustrates the GAD's current-voltage characteristics for various applied DC voltages of power source for 12.00 V, 14.00 V, 17.00 V, and 20.00 V at 15 LPM air flow. The output AC voltage is converted into pulsating DC voltage to create GAD plasma. This method appears to be more cost-effective and secure as DC voltage may be shielded from external influences using dielectrics. Furthermore, the use of DC voltage reduces the corona loss from the sharp tips. The rectified output of the rectifier is the source of the voltage waveform's spikes. The current curve experiences spikes due to the initiation of micro-discharges as the voltage rises. The cycle repeats when the voltage drops quickly and the current rises. Because of the rectification, the pulse frequency is twice that of the AC voltage. Sharp drops in the applied voltage

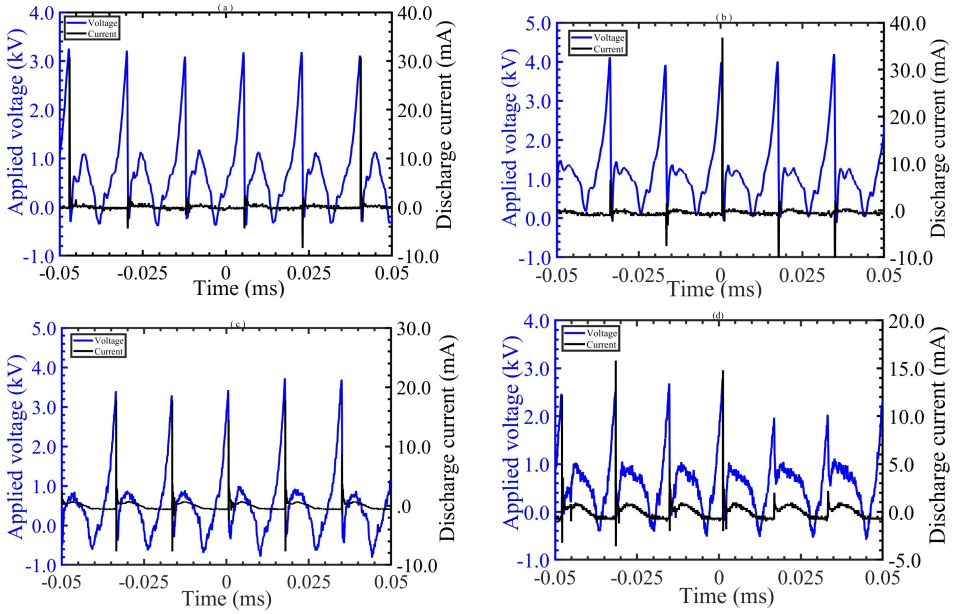

Figure 24: Current-voltage characteristics of GAD plasma for various input voltages; (a) 12.00 V, (b) 14.00 V, (c) 17.00 V, and (d) 20.00 V at 15 LPM air flow rate (S. Sharma et al., 2024)

between the two electrodes occur immediately following the breakdown due to a rise in both the intensity and current of the plasma. In an equilibrium regime, a stable plasma discharge is initiated when the discharge current increases. The plasma arc lengthens as a result of the gas flow pushing the plasma discharge to the opposite end. In this regime, arc current and temperature do not vary significantly (Mutaf-Yardimci et al., 2000). GAD plasma involves arcs that shift positions. The voltage and current levels consequently fluctuate significantly and continuously. Therefore, to determine the discharge power, we must take into account an entire arc cycle. The current-voltage, and power variation for a 12.00 V input is depicted in two complete arc cycles as shown in Figure 25 (a) and (b) respectively. At first, as the arc ignites, the voltage drops to its lowest value and the

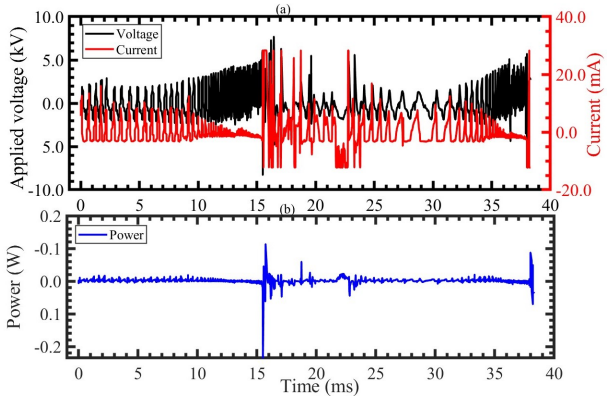

Figure 25: GAD plasma (a) current-voltage characteristics, and (b) power during two cycles at 12.00 V (S. Sharma et al., 2024)

current increases to its maximum value. Following ignition, the current steadily drops until the next cycle, while the voltage across the electrodes progressively rises as the arc

descends. For various input voltages, RMS voltage, RMS current, and RMS power are computed using equations (3.8-3.10) and presented in Table 3. The power source has a large number of winding in the secondary transformer coil so the current value is low in the arc discharge. While increasing the input applied voltage in the transformer the root mean square voltage, current, and power are increased.

Table 3: Electrical parameters of GAD plasma for various input voltage (S. Sharma et al., 2024)

S.N.	Input voltage (V)	RMS Voltage (kV)	RMS Current (mA)	RMS Power (W)
1	12.00	1.62	5.28	11.34
2	14.00	2.26	5.51	14.65
3	17.00	2.48	5.33	18.56
4	20.00	2.87	6.39	20.21

4.1.1.2 Optical Characterization

Figures 26 illustrates the variation of the intensity of GAD plasma for air flow variation of the discharge position "D", where substrates are treated and our interest region for application. The first negative system (390-440 nm) of N_2^+ $\left(B^2\sum_u^+ \rightarrow X^2\sum_g^+\right)$ and the

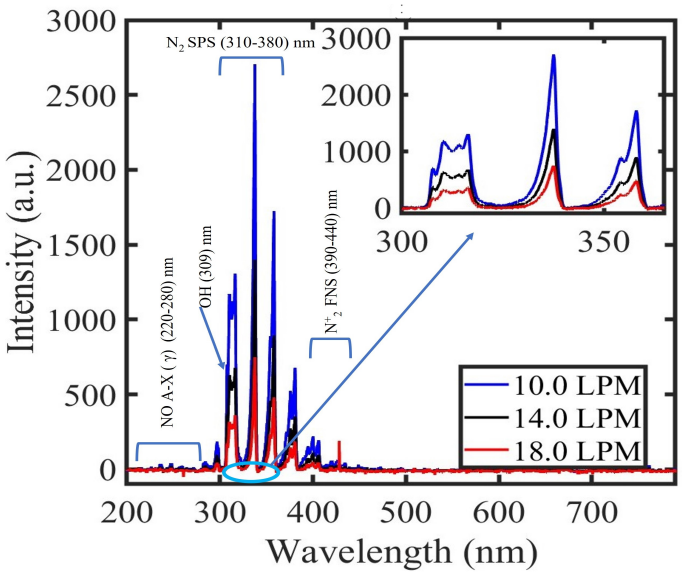

Figure 26: Optical emission spectra of GAD plasma at the discharge position "D" for varying air flow (S. Sharma et al., 2024)

second positive system (310-380 nm) of N_2 $\left(C^3\Pi_u \rightarrow B^3\Pi_g\right)$ are the main observed spectra (Lofthus & Krupenie, 1977). And OH $\left(A^2\sum^+ \rightarrow X^2\Pi\right)$ in the GAD plasma spectrum, which is important for plasma chemical reactions including the oxidation of gas and liquid contaminants, shows radicals prominently at 309 nm. The nitric oxide gamma band NO_γ $\left(A^2\sum^+ \rightarrow X^2\Pi\right)$ is observed in 200 to 280 nm. As the air flow is increased, the intensity of the reactive species is reduced.

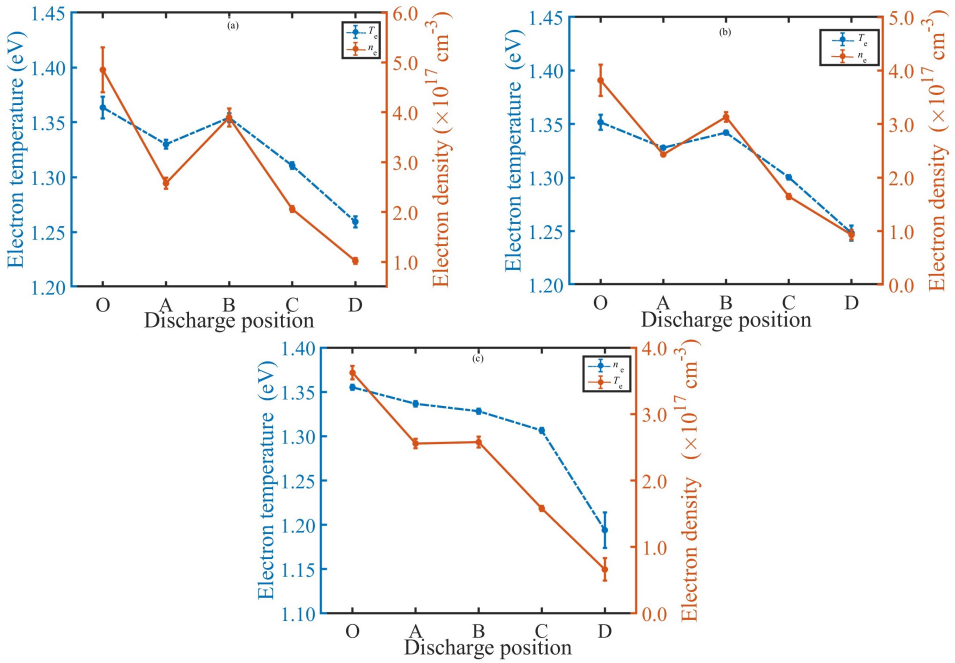

Figure 27: Changes in electron temperature and density at discharge positions "O", "A", "B", "C", and "D" of GAD plasma for different air flow (S. Sharma et al., 2024)

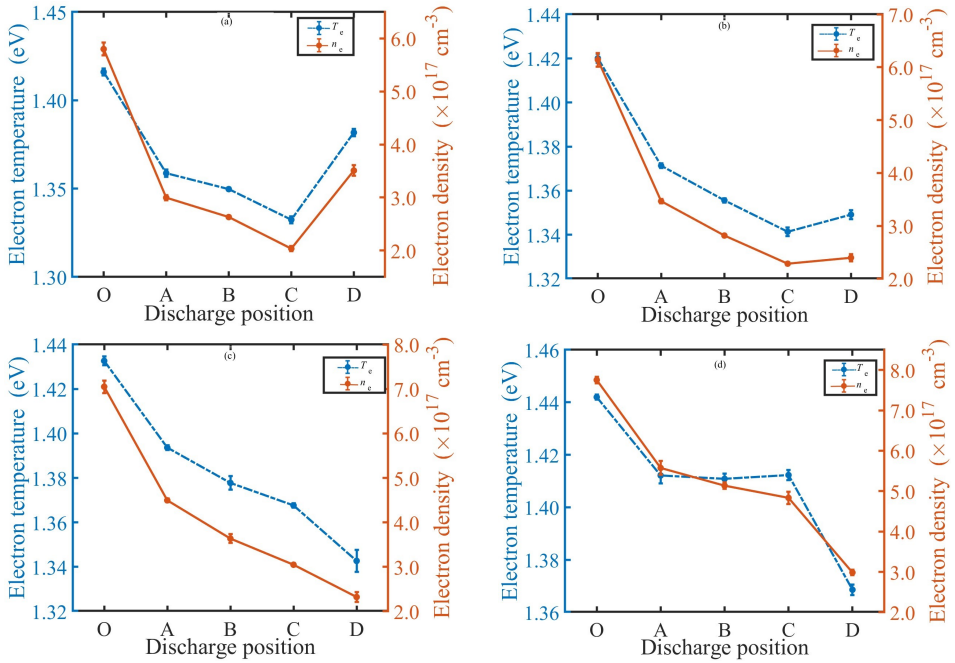

Figure 28: Changes of electron temperature and density at "O", "A", "B", "C", and "D" discharge positions of GAD plasma for various input voltage (S. Sharma et al., 2024)

Figures 27 (a), (b) and (c) and 28 (a), (b), (c), and (d) illustrate the effects of applied voltage and air flow on electron temperature and density calculated using equations (3.11) and (3.12) respectively, at various discharge places of gilding arc discharge. It is found that when one gets farther away from the discharge's ignition point, electron density and temperature both drop. The electron temperature and density are seen to drop toward the discharge outlet (the end of the electrodes) as soon as the ignition occurs (at

position “O”). The discharge position “O” for 10 LPM air flow has the maximum electron temperature and density [(1.364 ± 0.010) eV and $(4.85 \pm 0.45) \times 10^{17}$ cm^{-3}]. and lowest for 18 LPM air flow at point “D” [(1.194 ± 0.024) eV and $(0.66 \pm 0.17) \times 10^{17}$ cm^{-3}]. It is observed that in all situations (air flow rate), the electron excitation temperature and density are lowest at the discharge position “D”. The acquired parameters (density and electron temperature) agree with the findings of earlier studies (Indumathy et al., 2022)

The temperature of the electrons and the discharge density are influenced by variations in the applied voltage. The electron excitation temperature and density decrease toward the electrode ends, as shown in Figure 28 (a), (b), (c), and (d) at locations “O”, “A”, “B”, “C”, and “D” of GAD. For an applied voltage of 20.00 V, the maximum is reached at the discharge position “O” [(1.442 ± 0.001) eV and $(7.75 \pm 0.08) \times 10^{17}$ cm^{-3}]. It is discovered that the temperature and density of electrons rise with an increase in applied voltage. Figures 29 (a), (b), and (c) illustrate how air flow rate affects vibrational and rotational temperatures at various discharge points “O”, “A”, “B”, “C”, and “D” of GAD. It is discovered that at the discharge position “O”, both rotational and

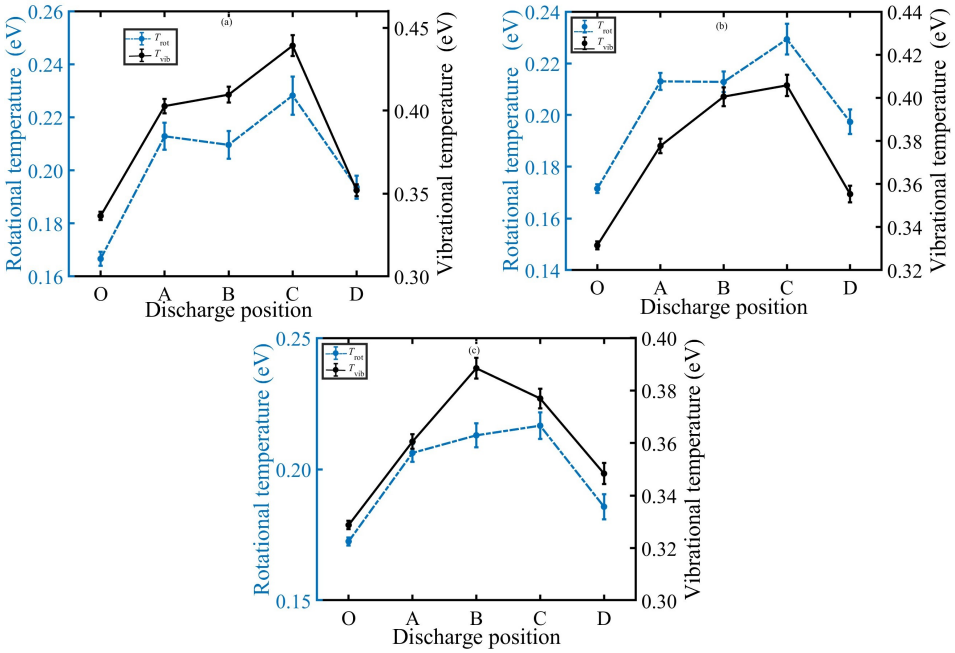

Figure 29: Changes of the rotational and vibrational temperature at “O”, “A”, “B”, “C”, and “D” discharge locations of GAD plasma for various air flow (S. Sharma et al., 2024)

vibrational temperatures are negligible. They then progressively rise to position “C”, after which they fall. This is explained by the plasma’s tendency to lose intensity after it reaches discharge position “C”. As a result, the vibrational and rotational temperatures drop. Additionally, when air flow increases, more air can cool the discharge, which lowers vibrational and rotational temperatures. At the discharge position “O”, the lowest vibration temperature and rotational temperature are (0.336 ± 0.002) eV and (0.167 ± 0.003) eV, respectively. More fluctuation in rotational temperature is observed,

due to the air flow produced by the GAD plasma in discrete form so the fluctuation observed in optical spectra corresponds to calculations. The results obtained are in agreement with the earlier research (T. L. Zhao et al., 2013).

4.1.2 Dielectric Barrier Discharge Plasma

We have produced the three types of atmospheric pressure DBD plasma which are shown in Figure 30. The purpose of the spark DBD (SDBD) plasma is to treat the bacteria in water as shown in Figure 30 (a), circular DBD plasma for large number of seeds, thin and flat surface treatment as shown in Figure 30 (b), and cylindrical DBD plasma for a large volume of water treatment as shown in Figure 30 (c). Because of the wire electrode in the upper electrode, the spark discharge is produced in SDBD plasma.

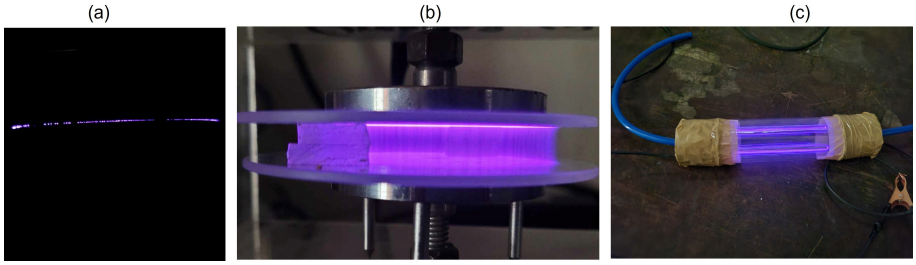

Figure 30: Production of dielectric barrier discharge plasma (a) spark, (b) circular, and (c) cylindrical

4.1.2.1 Electrical Characterization

Figure 31 (a), (b), (c), and (d) show the plot of the discharge current-voltage waveform of various air flows. It is observed that with increasing the air flow multiple micro discharges are increased in the current-voltage plot. So that more and more filamentary discharge is observed during the discharge region. The number of current pulses rises and the discharge current intensity falls as flow rates increase (Mangolini et al., 2002). The breakdown voltage is also reduced because, when air flow is introduced into the discharge region, the breakdown moment gradually shifts towards the lower time values. The breakdown voltage drops as air flow increases in the discharge space. Concurrently, the number of filaments rises while the intensity of the discharge current falls (Z. Fan et al., 2016). Because of the lower breakdown voltage, more filamentary discharge with lower intensities is produced in the discharge region (Osawa & Yoshioka, 2012). Figure 32 (a) and (b) represent the Lissajous curve for different LPM at constant voltage and varying voltages with constant air flow. Five cycles are carried out to calculate the energy and power from the voltage-current curve and Lissajous plot, and results are presented per cycle with mean values with standard error. The energy carried by discharge has also decreased increasing the air flow. It is observed that the power delivered by the DBD also decreased in increasing the air flow as shown in Table 4. The increase in input

voltage has increased the frequency. The energy and power of the DBD plasma increase with increasing the voltage.

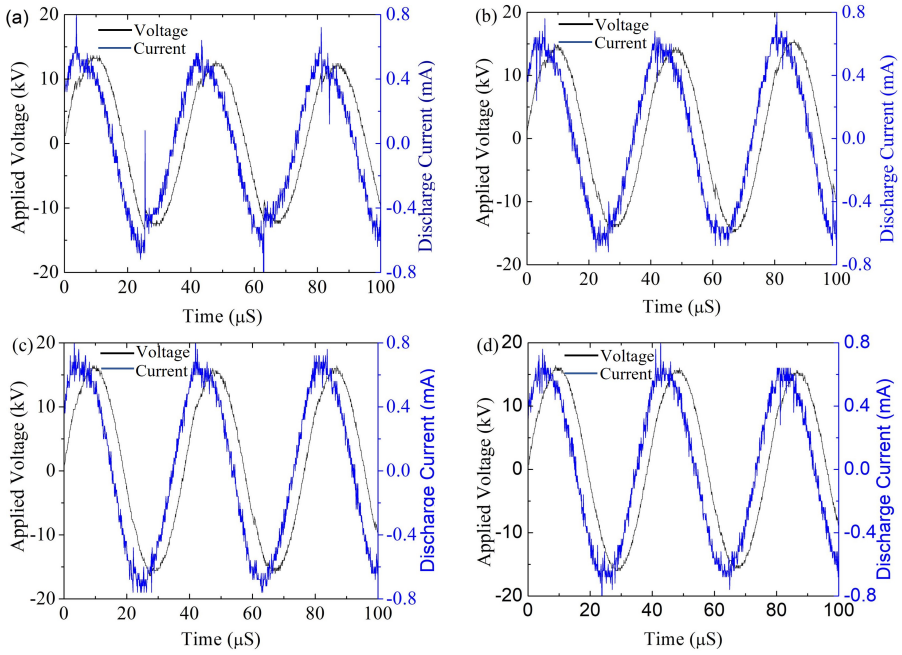

Figure 31: Time variation with current-voltage for the flow variation of (a) 0 LPM, (b) 5 LPM, (c) 10 LPM, and (d) 15 LPM respectively of DBD plasma (Chalise et al., 2024d)

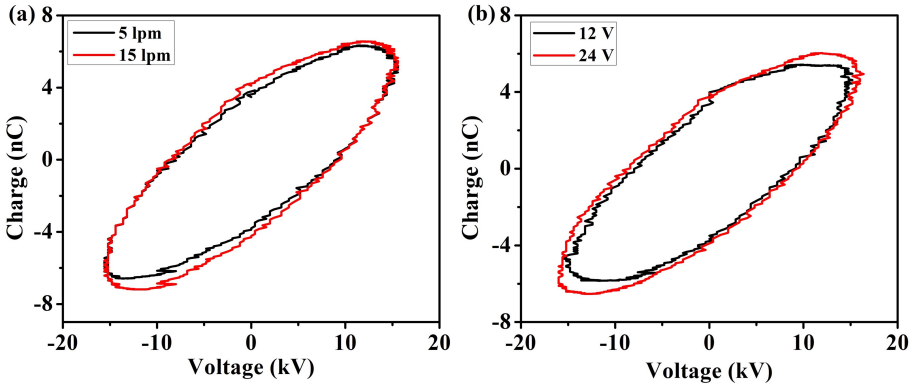

Figure 32: Lissajous plot for (a) different air flow at 24.00 V input voltage of power source, and (b) different input voltage at 15 LPM air flow of DBD plasma (Chalise et al., 2024d)

All the electrical parameters of discharge for variation of air flow and input voltage of power source are calculated using equations (3.1-3.7) and presented in Table 4 and 5. There is the fluctuation of energy from calculated time-averaged and the Lissajous plot method up to 10% fluctuation in air flow and 2% fluctuation in input voltage. Due to the fewer number of cycles measured from our oscilloscope, more fluctuation of energy occurred, these limitations result in agreement with previous results (Benard & Moreau, 2014). However, the fluctuation of energy per cycle is 4% in air flow variation and less than 1% in input voltage variation, when calculated from Lissajous plot methods. When comparing this power estimating process to the time-averaged integration of the voltage

and current product over five AC cycles, the deviation of value per cycle is far more up to 10% by calculating the averaged method and nominal standard deviation found in the Lissajous plot method is used, which is an agreement with Manley (1943).

4.1.2.2 Optical Characterization

Figure 33 (a) and (b) show the OES of DBD plasma at different air flow and input voltages. The intensity of the spectra decreased with increasing the air flow and increased with increasing applied voltage in the power supply. The population of excited species,

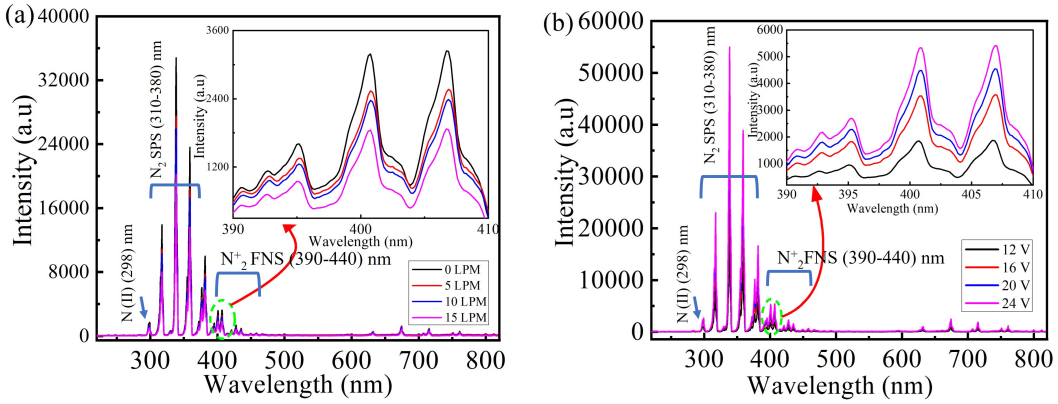

Figure 33: Optical emission spectroscopy of dielectric barrier discharge plasma: (a) at varying air flow rates with a constant input voltage of 24.00 V, and (b) at varying input voltages with a constant air flow rate of 15 LPM (Chalise et al., 2024d)

which can be produced by discharge depending on the plasma conditions, is shown by the emission intensity. More energetic electrons are produced in the discharge zone as the electric field strength increases. As a result, when the applied voltage increases, the intensities of the corresponding emission spectra of from the discharged increased (M. Zhang et al., 2023). In atmospheric air, there is approximately 78% nitrogen and 20% oxygen. Thus, the peak of OES spectra in DBD plasma has almost nitrogen and oxygen species. The major observed spectra are the second positive system (310-380 nm) of N_2 $\left(C^3\Pi_u \rightarrow B^3\Pi_g\right)$ and the first negative system (390-440 nm) of N_2 $\left(B^2\sum_u^+ \rightarrow X^2\sum_g^+\right)$ (Lofthus & Krupenie, 1977). In the context of DBD plasma, which is a type of low-temperature plasma, a Boltzmann plot can be used to understand the energy distribution of excited states of atoms or molecules in the plasma (Kim et al., 2023). The slope of Boltzmann's plot for electron excitation temperature of 12.00 V input of high voltage transformer of DBD at 0 LPM air flow is shown in Figure 34 (a). The range of electron excitation temperature and density of produced DBD plasma is in the range of DBD (Eliasson & Kogelschatz, 1991). T_{rot} is typically utilized as an approximation of the gas temperature (T_g) since it is representative of the rotating population of the ground state and provides information on the global temperature of the plasma (Roy & Talukder, 2018). The average kinetic energy brought on by the rotating

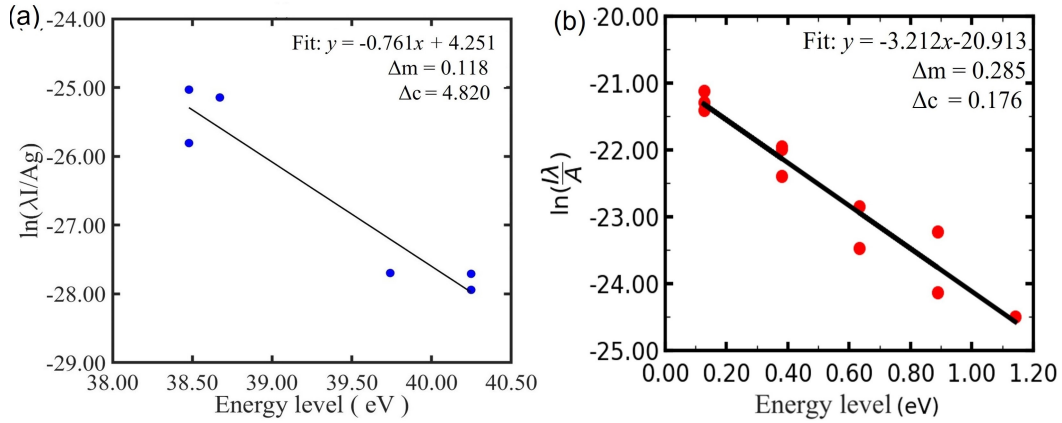

Figure 34: Boltzmann plot for the determination of (a) electron excitation temperature, and (b) vibrational temperature for the input voltage of 12.00 V of 0 LPM in DBD plasma (Chalise et al., 2024d)

of particles in the plasma is referred to as rotational temperature. The molecular axes of plasma molecules can spin. The energy distribution between these rotating degrees of freedom is shown by the rotational temperature (Bruggeman et al., 2014). On the other hand, electron collisions are the primary source of molecular specie's vibrational states. The non-equilibrium plasma's chemical kinetics are significantly influenced by the vibrationally excited species (Fridman & Kennedy, 2004) because vibrational excitation plays the role of an energy reservoir (T. L. Zhao et al., 2013). Figure 34 (b) shows the Boltzmann plot of the relative intensity distributions for vibrational energy using the nitrogen second positive system for 12.00 V input of high voltage of 0 LPM in DBD plasma. The vibrational temperature is correlated with the average kinetic energy of the oscillating motion of the plasma's particle constituents. Atoms and molecules can oscillate about their equilibrium locations as well as other sorts of vibrations that can occur in plasma. The quantity of energy involved in these oscillations is described by temperature variations. After taking into account the scattered data points and fitting errors, the vibrational temperature is obtained.

Table 6 and 7 show the optical parameters of DBD plasma calculated using equations (3.11, 3.12, 3.15) and MassiveOES software (Voráč et al., 2019) for increasing air flow at 24.00 V input voltage and different input voltages at 15 LPM air flow. While increasing the input voltages of the power supply electron excitation temperature, density, vibrational, and rotational temperature are increased. As an increase in the air flow electron excitation temperature, and rotational temperature are decreased, but density and vibrational temperature increase. The gas breakdown between the high-voltage electrodes is more likely to occur as the applied voltage increases. Following the disruption in the discharge region, the electron density rises (M. Zhang et al., 2023). The plasma power grows with applied voltage, and the energy input into the discharge zone rises as well, increasing the likelihood of electron-heavy particle collisions raising the rotational temperature, and highlighting the Joule heating effect (Kunhardt, 2000).

Table 4: Electrical parameters of DBD plasma for different air flow rate of 24.00 V input voltage

LPM	V_{PP} (kV)	V_{rms} (kV)	I_{dis} (mA)	V_{dis} (kV)	$\overline{E}$ (μJ)	E_L (μJ)	f (kHz)	$\overline{P}$ (W)	P_L (W)
0	24.45	8.64	0.41	8.44	116.12±11.98	190.02±1.44	25.60	2.97±0.11	4.86±0.14
5	28.77	10.17	0.75	13.97	158.13±17.01	191.26±7.96	26.10	4.12±0.17	4.98±0.79
10	30.91	10.93	0.87	16.38	160.23±9.68	193.41±6.65	26.70	4.16±0.96	5.02±0.66
15	31.21	11.03	0.88	16.40	179.00±5.35	197.70±4.93	26.90	4.68±0.54	5.15±0.49

Table 5: Electrical parameters of DBD plasma for different input voltage at 15 LPM

V_{in} (V)	V_{PP} (kV)	V_{rms} (kV)	I_{dis}(mA)	V_{dis} (kV)	$\overline{E}$ (μJ)	E_L (μJ)	f (kHz)	$\overline{P}$ (W)	P_L (W)
12.00	30.87	10.91	0.63	5.98	172.99±4.98	156.52±2.57	22.17	3.83±0.11	3.47±0.05
16.00	32.58	11.52	0.68	7.60	172.01±3.22	162.48±3.12	22.98	3.95±0.07	3.73±0.07
20.00	33.03	11.67	0.76	8.70	176.17±4.40	174.96±5.78	24.15	4.25±0.11	4.23±0.13
24.00	33.55	11.86	0.91	9.26	165.63±8.35	186.76±9.39	25.77	4.26±0.21	4.99±0.49

Table 6: Optical parameters of DBD plasma for different air flow rate of 24.00 V input voltage

LPM	T_{exc} (K)	N_e ($\times 10^{23} m^{-3}$)	T_{vib} (Boltzmann Plot) (K)	T_{rot} (MassiveOES) (K)	T_{vib} (MassiveOES) (K)
0	15272.40	1.39	3260.87	492.51 ± 15.13	2759.99 ± 17.59
5	15226.10	1.45	3284.08	486.17 ± 17.95	2762.64 ± 18.19
10	15248.80	1.49	3307.29	474.78 ± 15.93	2777.78 ± 18.35
15	15240.90	1.54	3349.27	464.84 ± 13.56	2787.04 ± 17.85

Table 7: Optical parameters of DBD plasma for increasing input voltage at 15 LPM

V_{in} (V)	T_{exc} (K)	N_e ($\times 10^{23} m^{-3}$)	T_{vib} (Boltzmann Plot) (K)	T_{rot} (MassiveOES) (K)	T_{vib} (MassiveOES) (K)
12.00	15241.50	1.52	3149.27	450.35 ± 16.23	2743.46 ± 18.57
16.00	15279.10	1.51	3214.45	468.44 ± 16.59	2753.47 ± 18.79
20.00	15293.60	1.53	3291.24	486.01 ± 17.75	2754.24 ± 18.99
24.00	15342.80	1.54	3337.66	496.67 ± 16.49	2787.27 ± 17.85

4.1.3 Air Plasma Jet

Two types of atmospheric pressure plasma jets are produced, as shown in Figure 35. The first, depicted in Figure 35 (a), used argon as the feeder gas, while the second, shown in Figure 35 (b), used air as the feeder gas. An effective method for converting electrical energy into chemically reactive plasma species, such as extremely energetic electrons, ions, and radicals, is the main feature of APJ. The treated material's surface chemistry is altered through chemical processes facilitated by these reactive plasma species. Due to the high cost and purity with difficulty in proper management of the argon cylinder, so more motivated toward the air feeder plasma jet. Another reason for that, the use of atmospheric air is reasonable in practical (farm) field applications. To prove the Paschen curve used for argon plasma jet.

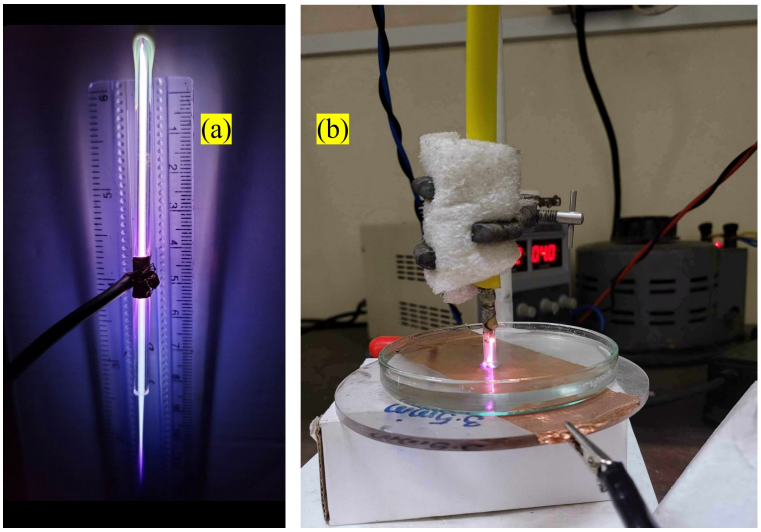

Figure 35: Atmospheric pressure plasma jet of (a) argon flow at 2 LPM, and (b) air flow at 5 LPM

4.1.3.1 Electrical Characterization

Figure 36 (a), (b), and (c) show the voltage-current waveform of an APJ at air flow rates of 3 LPM, 5 LPM, and 8 LPM, respectively. The time reference in the x-axis indicates negative time, representing the discharge initiation before the oscilloscope data capture. The time representation can be customized and adjusted according to our preferences and needs. Increasing air flow results in a more stable discharge, demonstrating that air flow optimization enhances the stability of APJ production. As the applied voltage increases, several breaks between the electrodes result in the multi-discharge pulses that are recorded. Table 8 shows the comparison of the electrical parameters of an APJ operated at different air flow rates which are calculated using equations (3.1, 3.2, 3.3, 3.6, 3.7). Applications in plasma science and technology depend on an understanding of the complex relationship between the energy of a discharge in an APJ and the dynamics of gas flow. When increasing the air flow more voltage, energy, and power are required

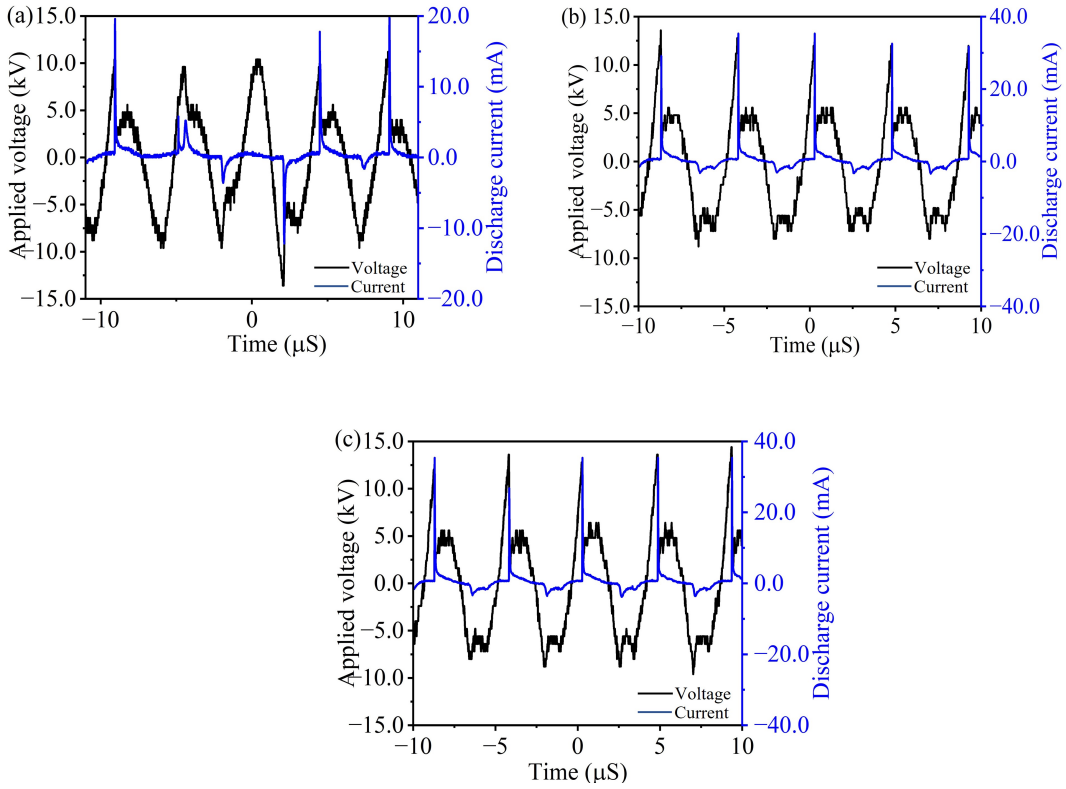

Figure 36: Voltage-current waveform of APJ for air flow rate of (a) 3 LPM, (b) 5 LPM, and (c) 8 LPM

but the frequency of the discharge is independent of air flow variation. While increasing the air flow, the transported charges during the APJ discharge are increased. The flow of charged particles, such as ions and electrons, within the APJ is connected to the transported charge. These particles are essential to plasma–surface interactions and contribute to the overall transmission of energy.

Table 8: Electrical parameters of APJ for various air flow rate at fixed input voltage

Flow (LPM)	V_{pp} (kV)	V_{rms} (kV)	Energy (μJ)	Frequency (kHz)	Power (W)
3	19.20	6.78	375.22	2.24	0.84
5	20.80	7.35	406.94	2.17	0.88
8	21.48	7.59	511.20	2.22	1.13

4.1.3.2 Optical Characterization

Figures 37 show the optical emission spectroscopy of the APJ for 3 LPM, 5 LPM, and 8 LPM air flow rates. The strength of discharge in an APJ is influenced by several parameters, including air flow rate. The properties of an APJ's discharge are mostly determined by the air flow rate. The discharge intensity typically decreases with higher air flow rates. The effect of the turbulent mode could be the cause of this negative association. Because of the fluctuating gas flow rate, charged species (such as ions

and electrons) are forced away from the electrode at variable velocities in this effect. Consequently, as the air flow rate rises, the discharge intensity falls, this result is supported by Sansan et al. (2021). The optical emission spectra are in agreement with the similar atmospheric pressure APJ Dimitrakellis et al. (2021).

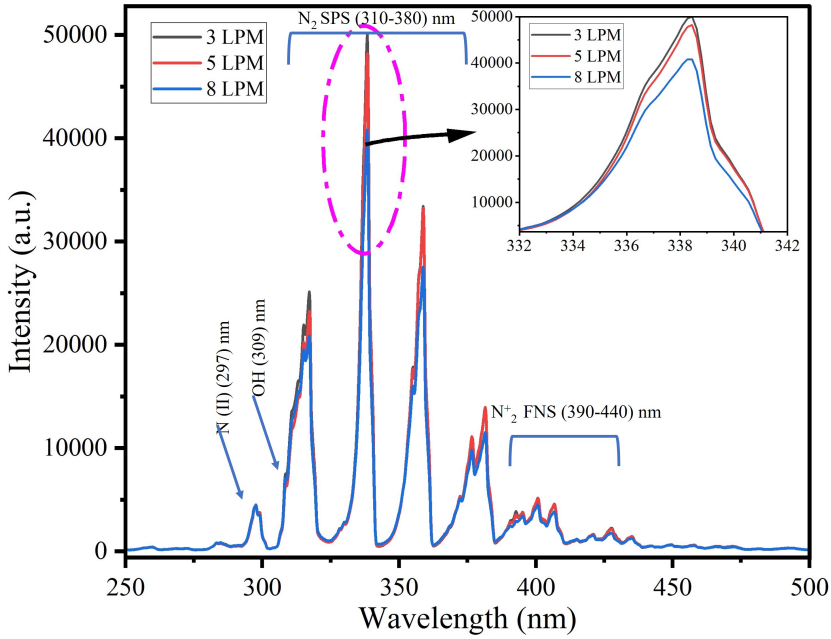

Figure 37: Optical emission spectrum of APJ for (a) 3 LPM, (b) 5 LPM, and (c) 8 LPM air flow rate

Table 9 illustrates the comparison of the optical parameters calculated by using equation (3.12) and MassiveOES software (Voráč et al., 2019) in air flow variation. It is found that when increasing the air flow, the electron excitation temperature and plasma density decrease but rotational and vibrational temperature increase. Greater numbers of charged particles (electron and ion) are present at high plasma densities. In the plasma, this raises the rates of ionization and recombination. With more energy transferred to the surrounding air, the APJ becomes more intense due to the increasing density. The density of the plasma is dependent on the air flow rate, or the gas conveying the plasma. Consistent vortex formations may be seen in the plasma jet at low gas flow rates. Vortices like this can improve reactive species mixing and movement. Higher gas flow rates, however, cause turbulence because they degrade the plasma jet's shear layer. This turbulence can affect the distribution of plasma density (Russ et al., 1994).

Table 9: Optical parameters of APJ for various air flow rate at fixed input voltage

Air flow (LPM)	T_{exc} (K)	N_e ($\times 10^{23}$ m^{-3})	T_{rot} (K)	T_{vib} (K)
3	16129.56	2.82	1398.46 ± 105.03	3808.00 ± 99.88
5	15920.10	1.73	1365.02 ± 105.63	3672.03 ± 95.90
8	15820.80	1.72	1500.19 ± 106.16	4102.52 ± 107.62

4.2 Characterization of Generated Plasma Activated Water

4.2.1 Gliding Arc Discharge Plasma

The physico-chemical parameters such as pH, electrical conductivity, oxidation-reduction potential, total dissolved solids, temperature, hydrogen peroxide, and nitrite and nitrate concentration of PAW for different activation times of GAD plasma are shown in Figure 38. When the plasma exposure time increases, electrical conductivity, oxidation-reduction potential, and total dissolved solids significantly increase, whereas activated water's pH value decreases. As the plasma treatment time increases, the production of oxidizing species and active ions on the PAW increases. The addition of discharge causes the pH value to decrease over the increase in treatment time. This is due to the addition of nitrate and nitrite ions, which makes the water more acidic. The variation of pH value against plasma treatment time is shown in Figure 38 (a). The pH value is found to decline with an increment of discharge exposure time. The pH values decrease from about 5.60 to 3.80 for the increase in treatment time from 0 to 20 min. These factors are implicitly important because they are related to the germination and growth of the seeds. One of the important components for the fast germination and growth of plants is the ability to move ions, increasing the uptake of ions and dissolved oxygen (Oehmigen et al., 2010). For the increment of activation time, the movement of ions increases due to the energy of plasma which helps to increase the conductivity of the water and plays a vital role in plants' germination and growth process as shown in Figure 38 (b).

The formation of reactive oxygen and nitrogen species after the application of plasma in water increases the total dissolved solids (Zhou et al., 2020; Mitra et al., 2014) is shown in Figure 38 (c). The oxidation-reduction potential increases with the increase in the activation time as shown in Figure 38 (d). Since the temperature is a function of energy, it is applied in the form of sparks, and the temperature of the water is found to be increased as shown in Figure 38 (e). The nitrite and nitrate concentration increases with the increase in the activation time as shown in Figure 38 (f). The nitrate concentration reaches from 25.00 to 250.00 mg/L when the activation time increases from 0 to 20 min. For the same increment of plasma exposure time, the nitrite concentration increases from 0 to 40.00 mg/L. The change in concentration of nitrate is more significant than that of nitrate. Because the conversion of nitrite to nitrate is accelerated under acidic circumstances, the absence of nitrate compared to nitrate can be explained (Mitra et al., 2014). As the reaction shows, two OH radicals interact during the plasma treatment procedure to form the potent oxidizing agent hydrogen peroxide. The observed value of H_2O_2 concentration throughout the GAD plasma treatment for water is shown in Figure 38 (g). The physio-chemical characteristics of water are caused by the creation of RONS.

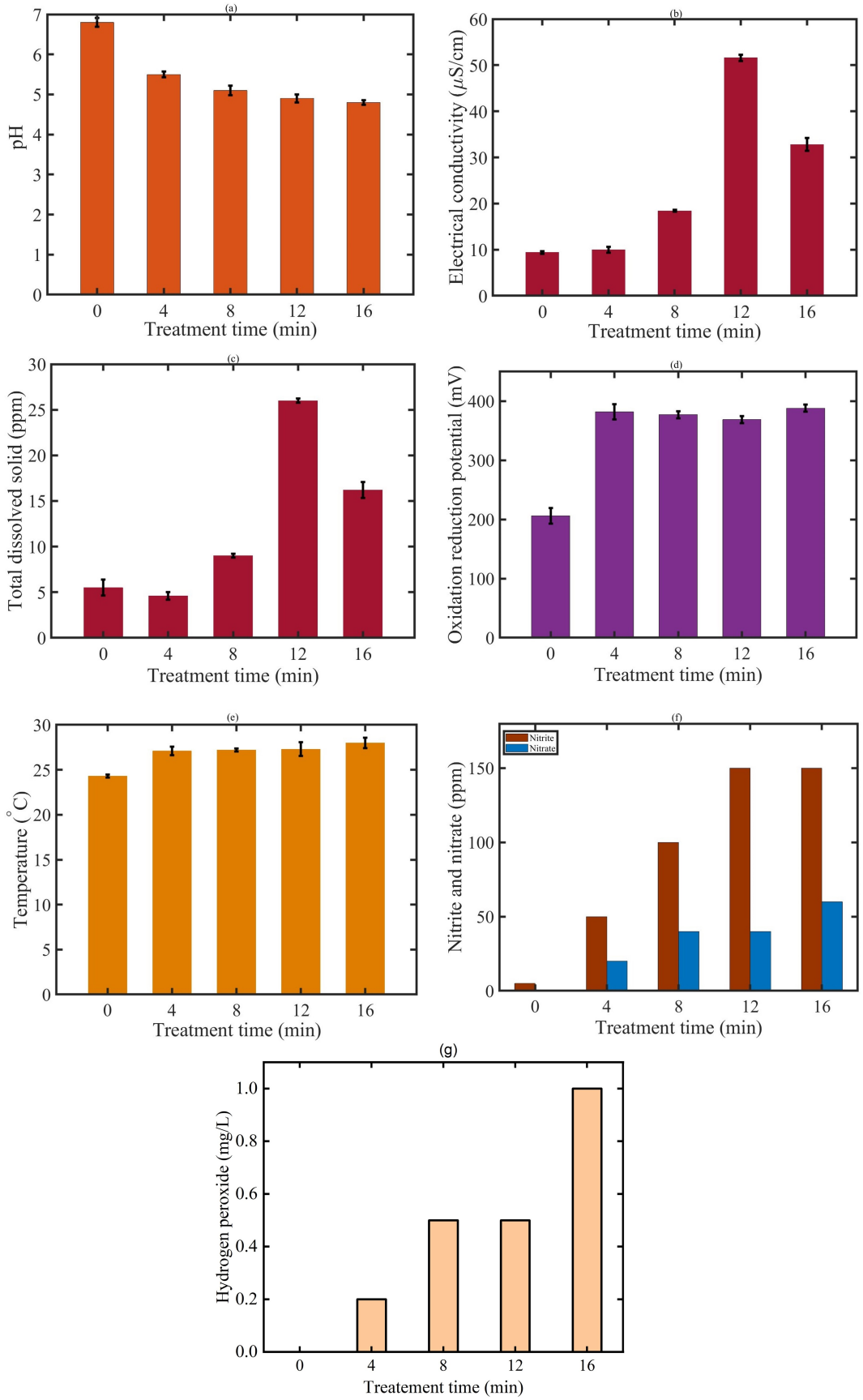

Figure 38: Variation of physio-chemical parameters of GAD PAW for 0-16 min plasma exposure time in water; (a) pH (b) EC, (c) ORP, (d) TDS, (e) temperature, (f) nitrite and nitrate concentrations (Chalise et al., 2024) and (g) hydrogen peroxide concentration

4.2.2 Dielectric Barrier Discharge Plasma

As the test medium during this work, de-ionized water and regular saline (8.50 gm of salt per 1000.0 ml of de-ionized water) are utilized. The physio-chemical parameters of two water samples; regular saline is plasma-treated medium (PTM) and the other is plasma-treated de-ionized water (PTW) following SDBD plasma treatment are presented here. The PTM and PTW at different exposure times are shown in Figure 39. Throughout

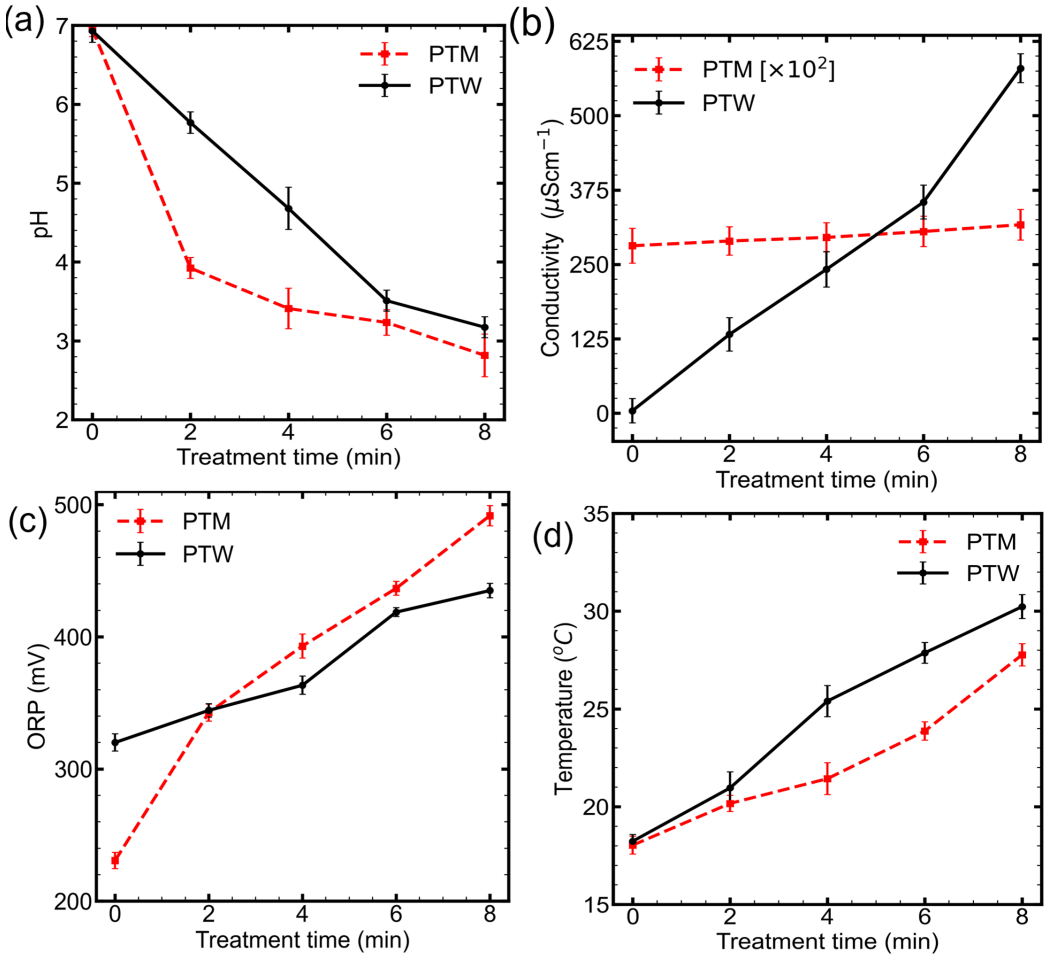

Figure 39: Changes in (a) pH (b) EC (c) ORP (d) temperature in DBD PAW and PTM for 0-8 min exposure times (Dhakal et al., 2023)

the plasma treatment, the pH of the water and medium is progressively monitored. Figure 39 (a) shows that after eight min of treatment, the medium's pH dropped to 2.39 and the PTW's pH dropped to 3.15. The pH of water treated with plasma lowered to 3.80 in that study, which is agreed with previously published (Gharagozalian et al., 2017). Nitric acid and nitrous acid produced by reactive oxygen species (ROS) are responsible for the pH drop. According to earlier research findings, the plasma treatment procedure is responsible for the acidity of the liquids that is noted in this investigation (Oehmigen et al., 2010; Ma et al., 2015). A liquid's ability to conduct electricity is determined by its electrical conductivity. Figure 39 (b) illustrates how the electrical conductivity

of water improves after eight min of plasma treatment from 4.00 μScm^{-1} to 607.00 μScm^{-1}, and that of the medium from 28000.00 μScm^{-1} to 32000.00 μScm^{-1}. The PTW and PTM have higher electrical conductivity because of the reactive species that are produced in large quantities during the plasma treatment. The oxidizing and reducing power of solutions is measured in ORP. The plasma's RONS species function as potent oxidants, increasing the ORP of the liquid in the process. Hydrogen peroxide, which is predominant among the reactive oxygen species (ROS) generated in PTW can operate as an oxidant with an electrochemical potential of 1.77 V (Lukes et al., 2012). Figure 39 (c) shows that the ORP values for medium and de-ionized water increase from 230.00 mV to 491.00 mV and 320.00 mV to 435.00 mV, respectively. Increased ORP enables solutions to oxidize the bacterial cell membrane more effectively, causing the cell to become leaky and unstable and ultimately leading to rapid death (Kawano et al., 2020). High-energy electrons and ions contact liquid surfaces from the plasma, which transfer their energy to the liquid and increase its temperature. The temperature rise of the water and media are shown in Figure 39(d). While the temperature of de-ionized has grown from 18.00 to 29.00°C, the temperature of the medium has increased from 18.00 to 27.00°C. The a chemical change in PTM and PTW is shown in Figure 40. The two

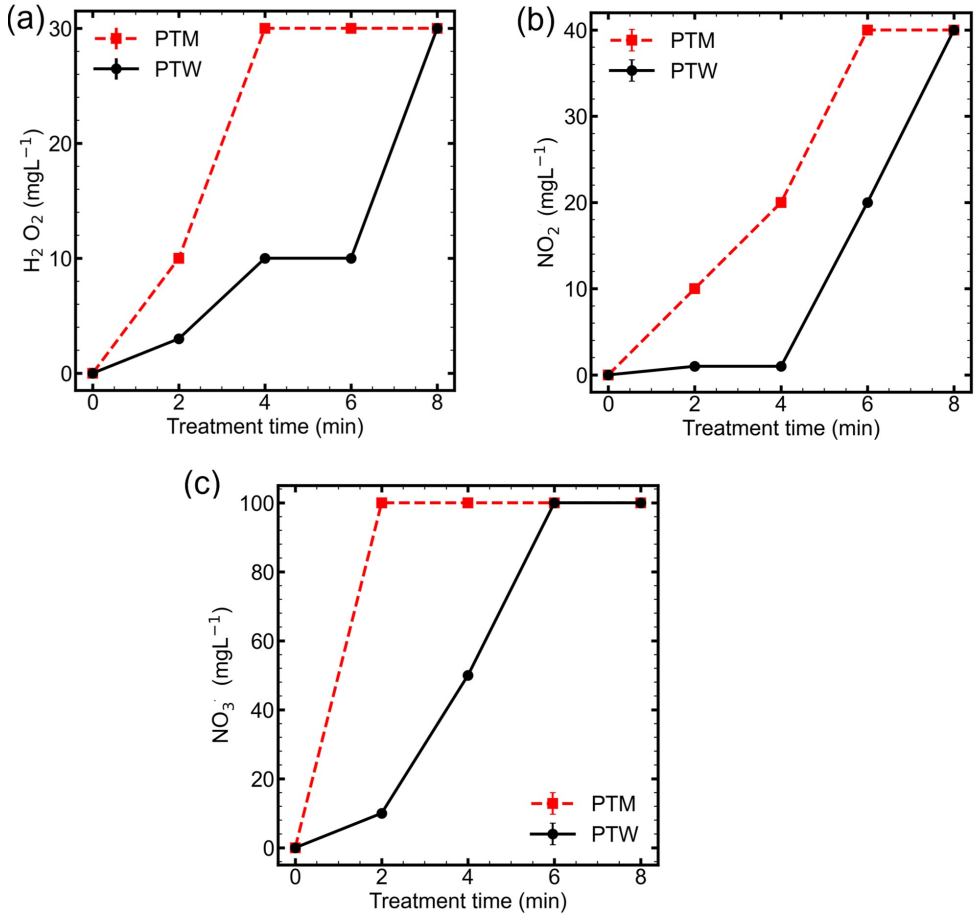

Figure 40: Concentration of (a) hydrogen peroxide (b) nitrite (c) nitrate in PAW generated by DBD for 0-8 min plasma exposure times (Dhakal et al., 2023)

OH radicals interact during the plasma treatment procedure to form the potent oxidizing agent hydrogen peroxide. The fluctuation in H_2O_2 concentration throughout the plasma treatment for PTW and PTM is shown in Figure 40 (a). The test kit has 100.00 mgL^{-1} after 30.00 mgL^{-1}, therefore such a level of H_2O_2 is not formed for up to eight min. The generation of the H_2O_2 concentration is exhibiting a constant due to the test kit range limit. concentration rises from 0 to 30.00 mgL^{-1} in about four min, reaching medium saturation. For de-ionized water, the H_2O_2 concentration increases from 0 to 30.00 mgL^{-1} and reaches saturation after eight min of plasma treatment. RNS is formed by a chemical reaction, as indicated by the presence of nitrites and nitrates in PTM and PTW. As the period of plasma treatment increases, the quantities of nitrite and nitrate radicals in PTW and PTM vary, as depicted in Figures 40 (b) and (c). Nitrite saturation occurs in PTM at 40.00 mgL^{-1} after six min of plasma treatment, while it takes eight min in PTW. Similar to this, PTM becomes saturated with nitrates at a concentration of 100.00 mgL^{-1} after two min of plasma treatment, whereas PTW requires 6 min. Similar results are seen in earlier research by Oehmigen et al. (2010).

4.2.3 Air Plasma Jet

When the air jet plasma is activated in the water, the formation of various primary and secondary reactive oxygen and nitrogen species changes the physio-chemical properties of PAW. The understanding of physical parameters is crucial for various purposes of any plasma applications. So, measuring the physical parameters such as the potential of hydrogen, electrical conductivity, total dissolved solids, oxidation-reduction potential, hydrogen peroxide, and temperature of PAW for different plasma exposure times which are shown in Figure 41, the obtained results pattern is in agreement with Rathore et al. (2021). The highly energetic electrons from the discharge react with molecules of the gas and dissociation occurs leading to the creation of mainly oxygen and nitrogen species (Bradu et al., 2020). As water is treated with air-jet plasma, the presence of additional ions like nitrates, nitrites, etc. affects the physical properties such as pH, EC, TDS, ORP, and temperature.

The variation of pH of PAW for different treatment time is shown in Figure 41 (a). It is found that the value of pH declined sharply up to the four min activation time of the plasma jet, and after that slightly declined. The concentration of hydrogen ions in a solution is determined by pH. The primary cause of pH value may be the production of ONOOH, which is produced from the NO, NO_2, and NO_x created in the plasma phase, as well as nitric and nitrous acids. The production of acidic hydronium ions (H_3O^+) by the interaction of water molecules with H_2O_2 produced in liquid or air is a factor in the pH value dropping. As a result, an acidic pH is essential for PAW to inactivate germs (Ercan et al., 2013).

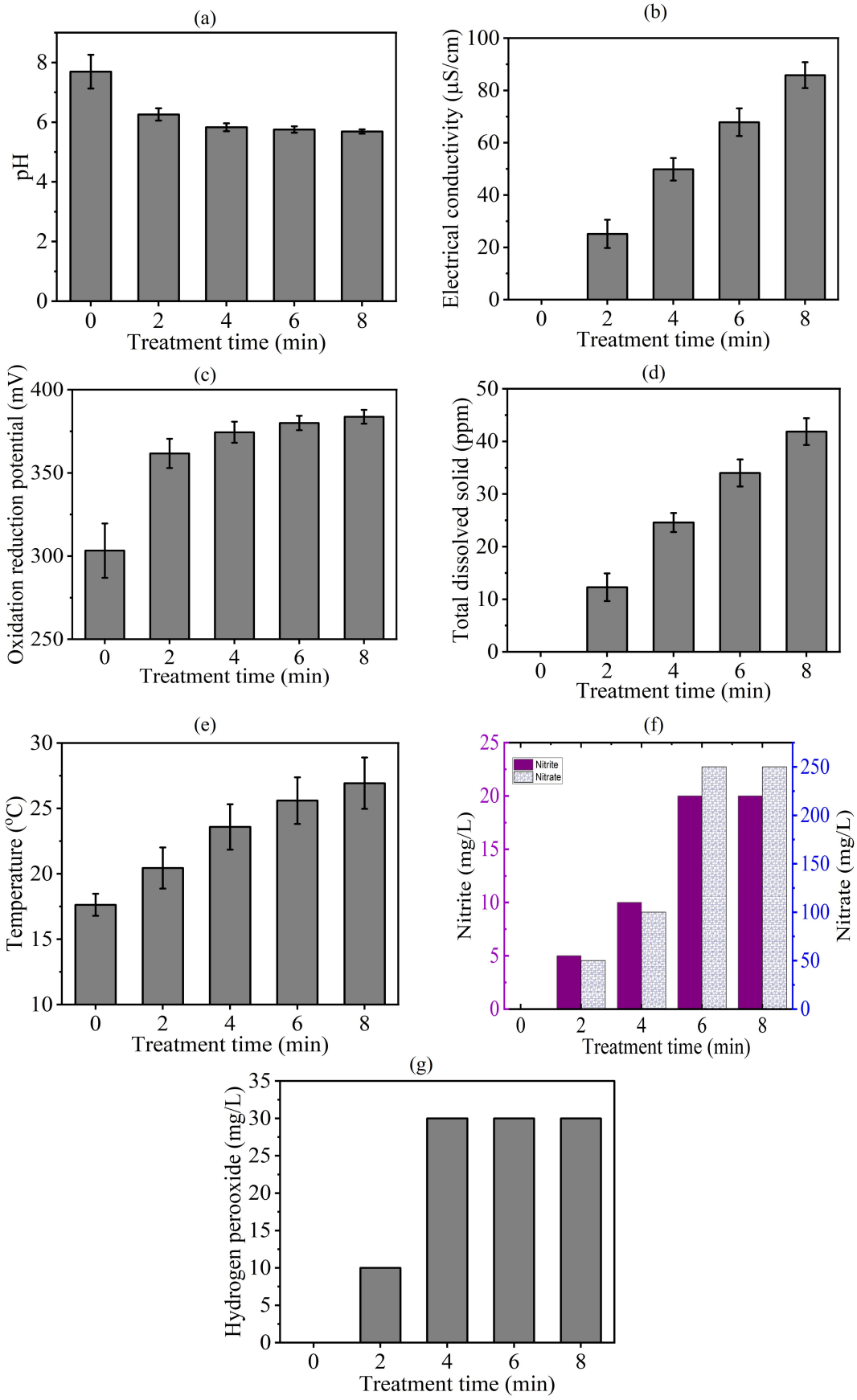

Figure 41: Variation of physico-chemical parameters of APJ activated water for 0-16 min plasma exposure time (a) pH, (b) EC, (c) ORP, (d) TDS, (e) temperature, (f) nitrate, and nitrite concentration, and (g) hydrogen peroxide concentration

The variation of EC of PAW for different treatment time is shown in Figure 41 (b). The application of plasma on the water surface increases the EC. The types of ions present, their concentrations, and the temperature of the solution all affect an aqueous solution's electrical conductivity, which is a measure of its capacity to conduct electricity. Water's conductivity is significantly impacted by the presence of foreign ions. When water is plasma-activated, ROS and RNS are formed, which will raise PAW's conductivity. With an increase in activation time, PAW's electrical conductivity rose significantly. Because H^+ ions move more readily than OH^- ions, the solution's electrical conductivity rises as the pH lowers (H. P. Sharma et al., 2021).

The variation of TDS in PAW for different treatment time is shown in Figure 41 (c). It is found that the addition of plasma to water causes to increase in total dissolved solids in water as well. The ionized charge particle soluble in the solution is the major cause of the increase in the EC of water. The variation of ORP of PAW for different treatment time is shown in Figure 41 (d). It is found that the oxidation-reduction potential of treated water increases with the increase in treatment time. ORP measures a solution's capacity for oxidation or reduction and is correlated with the oxidant's concentration, strength, and activity. The ORP values of PAW showed a notable rise, mostly as a function of plasma activation time. H_2O_2 is thought to be primarily responsible for ORP out of all the ROS produced in PAW since it can function as both a reducing agent and an oxidizing agent). Greater ORP values correspond to better oxidizing capacity and higher antibacterial properties (Y.-M. Zhao et al., 2020). The variation of temperature of PAW for different treatment time is shown in Figure 41 (e). It is found that the treatment of the APJ causes a slow water temperature increase.

The nitrite, nitrate, and hydrogen peroxide formation in the APJ are effectively observed in PAW as shown in Figure 41 (f) and (g). The test kit has 100.00 mgL^{-1} after 30.00 mgL^{-1}, therefore such a level of H_2O_2 is not formed for up to eight min. The generation of the H_2O_2 concentration is exhibiting a constant due to the test kit range limit. The values are noted corresponding to the color change observed in the test kit. Thus, the single color code value during the experiment and the concentration formation in PAW are not sufficient to change the next color, at that time concentration data showed the constant in nitrite, nitrate, and hydrogen peroxide.

4.3 Application of Produced Plasma

The results of applying the three types of produced cold atmospheric pressure plasma, both directly and indirectly to the seeds of cash crops, cereal crops, and green leafy vegetables, as well as the results of bacterial activation in water and the greenness longevity of detached leaves, are presented in this section.

4.3.1 Cereal Crops

We have applied plasma on the cereal crops, namely the Basmati rice (Khumal-12, Khumal-14, and Khumal-16) seeds provided by the Nepal Agriculture Research Council (NARC), Khumaltar, Nepal. This is the indirect application of plasma; generation of PAW from GAD plasma and utilized in soaking seeds and irrigation on plants. The obtained results of faster germination and seedling growth are in agreement with earlier reports by Billah et al. (2021).

4.3.1.1 Basmati Rice

The PAW is made below 10.0 mm from the lower point of the electrode of GAD plasma by treating 40.0 ml of de-ionized water with different treatment times 0, 5, 10, 15, and 20 min, which are denoted by 0PAW, 5PAW, 10PAW, 15PAW, and 20PAW. On the other hand, 0PAW represents the control de-ionized water (untreated). The healthy and similar types of Basmati rice seeds are selected. From the selected seeds, each thirty seeds are soaked in 0PAW, 5PAW, 10PAW, 15PAW, and 20PAW water. The seeds are weighed and placed in separate petri dishes for each experimental group and soaked in 40.0 ml of respective water. These soaked seeds are removed from the water cleaned with a paper towel, and weighed. The water uptaking rate by the seed is calculated by equation (3.16). The 10 seeds were planted in each plastic container and each glass had 80.00 gm of a mixture of 50% soil 25% vermicompost and 25% sand. The planted seeds are kept in the window side of the room in an ambient environment and 10.0 ml of respective water is poured into a glass every two days. The temperature and humidity are in the range of 5-18^{o}C and 30-50% respectively of the environment. The obtained results are presented here.

4.3.1.1.1 Wettability: The water absorbency rates of Basmati rice seeds using equation (3.16) in different PAW for different soaking times are demonstrated in Figure 42 (a), (b), and (c) of varieties of Basmati rice; Khumal-14, Khumal-16, and Khumal-12 seeds respectively. Specifically, increasing the plasma activation period from 0 to 15 min increased the seed's water imbibition rate while a decrease is seen when the treatment time is lengthened to 20 min. The highest water imbibition after 8 hrs of soaking in water is seen in the group containing 10PAW. In Khumal-14, the water imbibition rate of the 10PAW is found to be (22.80 ± 1.60)% which is an 11.80% increment when compared to the control group. The seeds of Khumal-16 had the highest water imbibition rate in 10PAW too, with the average value of (12.52 ± 0.63)% which is an increment of 30.13% from the control group which had a water imbibition rate of (9.74 ± 0.65)%. The seeds of Khumal-12 followed a similar pattern with the highest water imbibition rate as (16.84 ± 0.93)% in the 10PAW group which is an increment of 6.36% when

compared with the control group which had water imbibition rate of (15.87 ± 0.81)%.

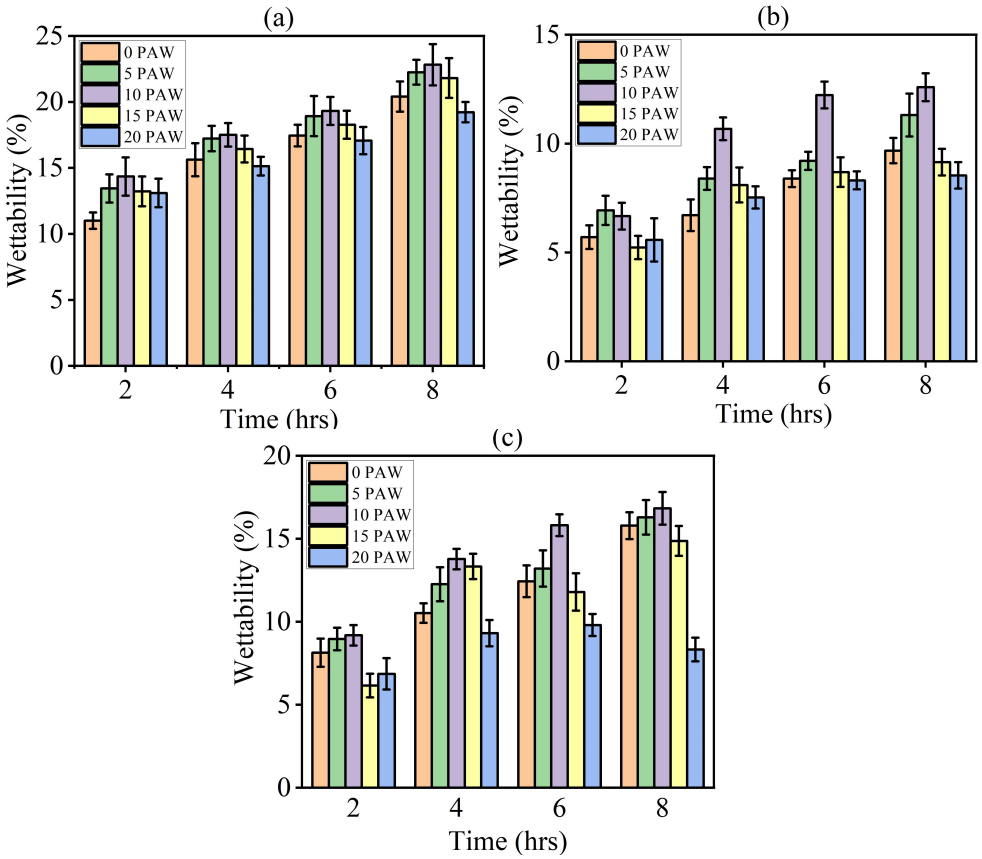

Figure 42: Water absorbency rate of Basmati rice of (a) Khumal-14, (b) Khumal-16, and (c) Khumal-12 seeds soaked in PAW at activation times of 0-20 min

4.3.1.1.2 Germination: The germination rate of Basmati rice is calculated using equation (3.17) after three days of plantation and is presented in Figure 43 (a), (b), and (c) of varieties of Basmati rice; Khumal-14, Khumal-16, and Khumal-12 seeds respectively. In all three samples, the germination rate is recorded as highest for the 10PAW group. In Khumal-12, the germination rate of the 10PAW group is recorded as (93.75 ± 5.81)% which is 212.35% increment from the germination rate of a control group which is recorded as (30.03 ± 3.49)%. Similarly, in Khumal-14 the 10PAW group had the highest germination rate of (90.09 ± 3.42) which is 50% higher than the control group rate recorded as (60.04 ± 5.41)%. Khumal-12 followed a similar pattern with the highest germination rate in the 10PAW group. The 10PAW group in Khumal-14 seeds had a germination rate of (93.39 ± 4.71)% which is 27.32% more than the germination rate recorded in the control group which is (73.34 ± 3.10)%. Thus significant improvement in the germination rate of PAW-supplied samples is observed.

4.3.1.1.3 Seedling Growth: Figure 44 displays the real picture of the plantation area and seedling growth of Basmati rice seeds in plastic glasses.

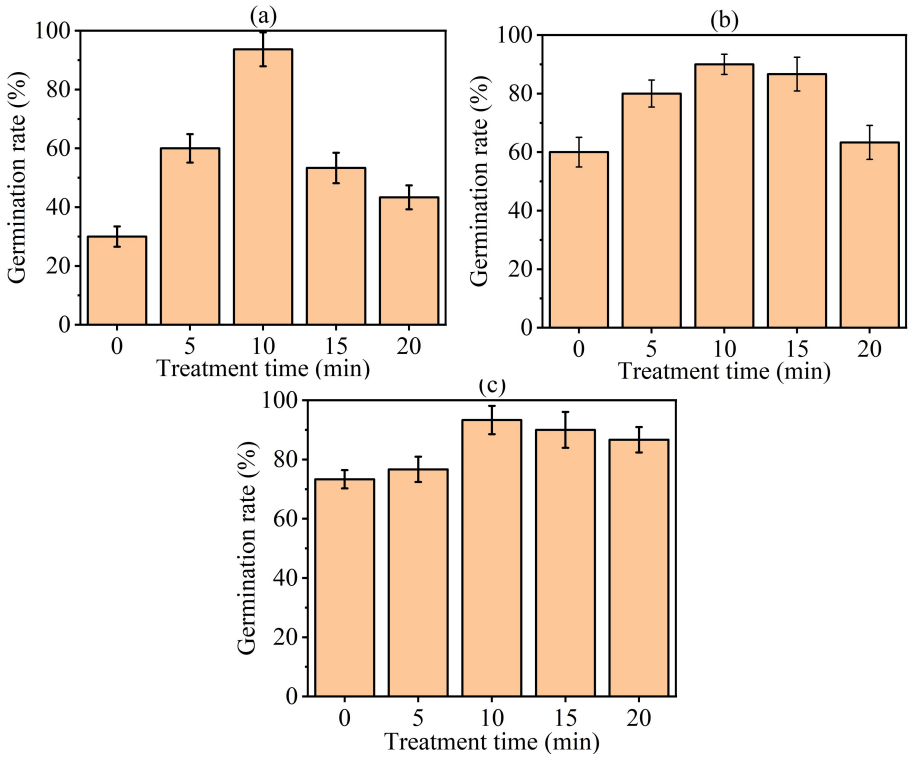

Figure 43: Percentage of germination after three days of being planted of Basmati rice (a) Khumal-14 (b) Khumal-16 (c) Khumal-12 seeds after activation with 0-20 min PAW

Figure 44: Planting area and seedling growth of Basmati rice plant

The longest and shortest plant is shown in the real picture in Figure 45 (a) and (b), (c) and (d), and (e) and (f) of varieties of Basmati rice; Khumal-14, Khumal-16, and Khumal-12 seeds respectively. It is observed that the seedling growth of the plant is highest in the longest and shortest category in 10 min plasma treated water used plant.

The average root and shoot length of the Basmati rice plant in different plasma activation times of water after 21 days is presented in Figure 46 (a), (b), and (c) of varieties of Basmati rice; Khumal-14, Khumal-16, and Khumal-12 seeds respectively. The pattern in root length, however, is not consistent. In all three varieties of Basmati rice seeds,

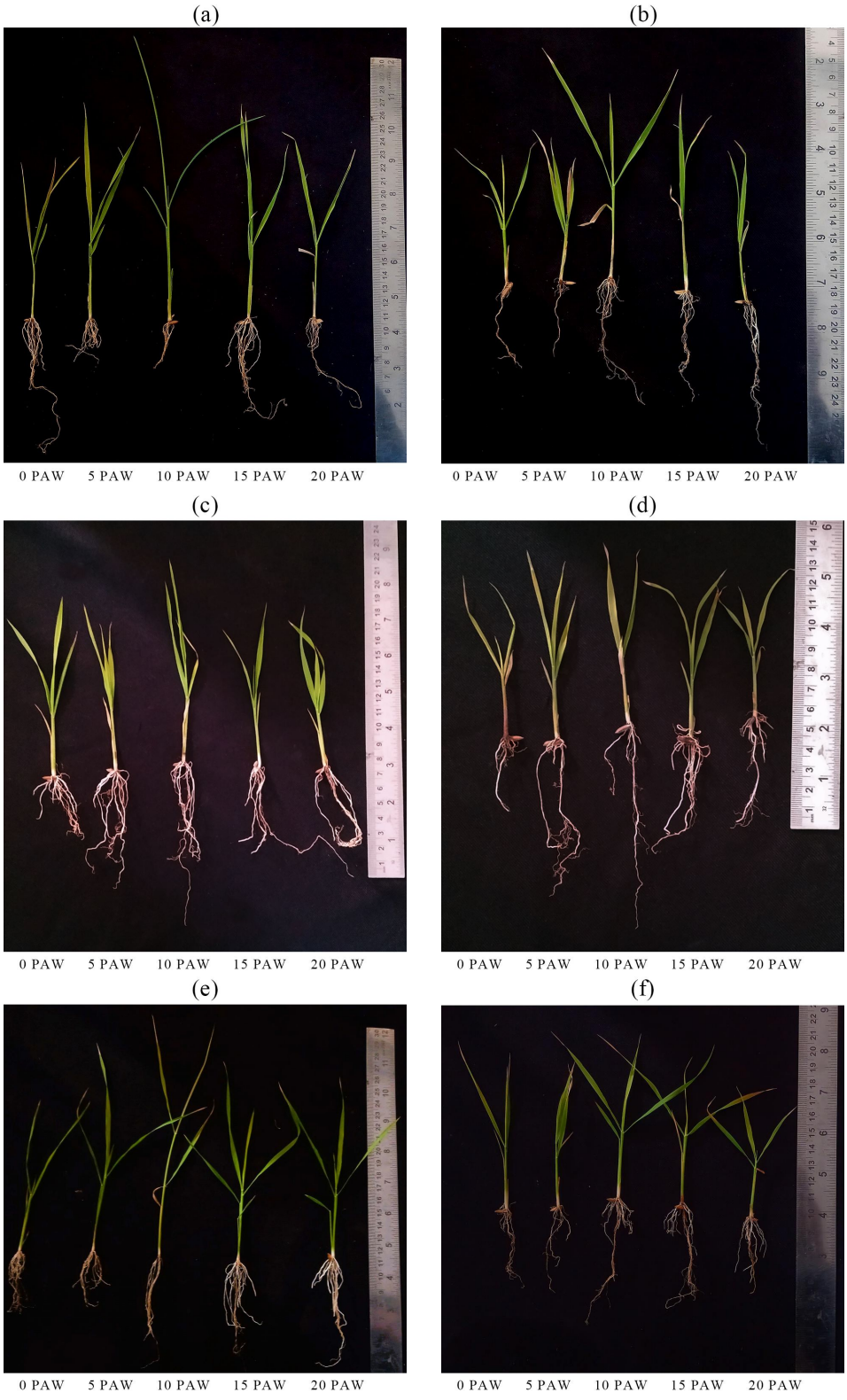

Figure 45: Longest and shortest shoots of every group; (a) and (b) of Basmati rice Khumal-14, (c) and (d) of Basmati rice Khumal-16, and (e) and (f) of Basmati rice Khumal-12 seedlings for PAW activation of 0-20 min after 21 days of plantation

seedlings treated with 10PAW recorded the highest shoot length. In Khumal-14, the 10PAW group demonstrated an average shoot length of (21.25 ± 1.31) cm which is

85.93% higher than the shoot length demonstrated by control group i:e (11.46 ± 0.98) cm. 10PAW group had highest shoot length in Khumal-16 too, with value of (9.63±0.56) cm while the control group demonstrated shoot length of (7.58 ± 0.35) cm. In the case of Khumal-12, the shoot length of the 10PAW group is 33.34% higher than that of the control. The shoot length for the 10PAW group and control are recorded as (16.46±0.63) cm and (12.32±0.50) cm respectively. The pattern in root length is not consistent but all samples had the highest root length in treated samples. Khumal-14 seeds demonstrated the longest root length in the 20PAW group, Khumal-16 in the 10PAW group, and Khumal-12 demonstrated the longest root in the 15PAW group. The root length of the control group in Khumal-14 is recorded to be (6.84 ± 1.23) cm while the 20PAW group had (9.64 ± 1.45) cm which is a 41.18% increment. In Khumal-16, the difference is notable with the control having (4.55 ± 0.57) cm while the 10PAW group had a root length of (10.59 ± 0.44) cm which is a 133.35% increment. Khumal-12 variety of seeds demonstrated the longest root length on the 15PAW group with (10.26 ± 0.72) cm while the control had a root length of (5.07 ± 0.64) cm. Thus, in the case of Khumal-12, the 15PAW group had 104% longer root length when compared with the control.

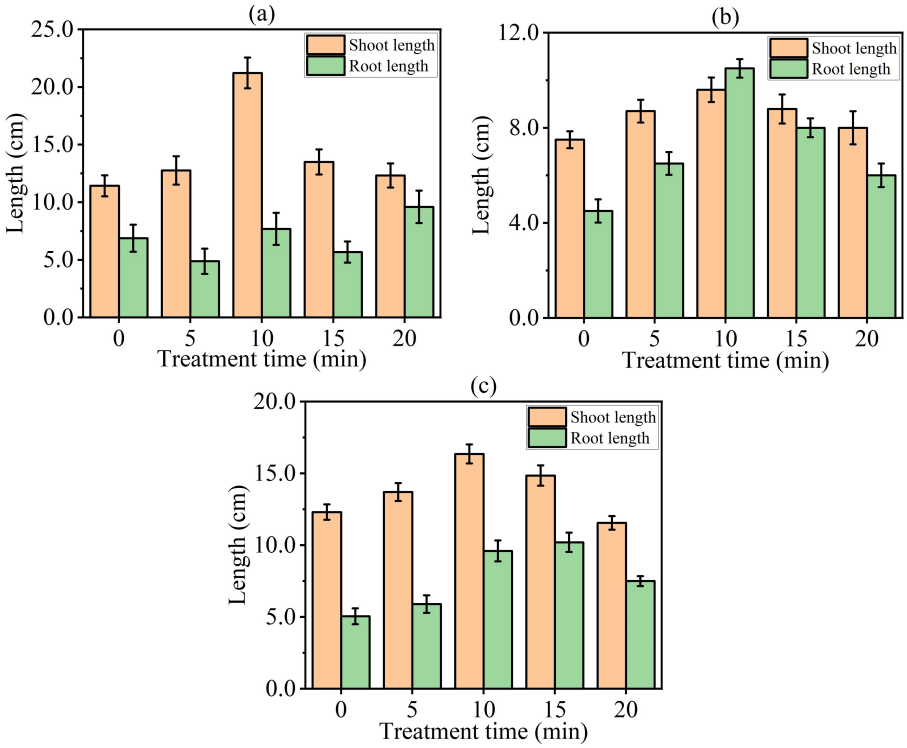

Figure 46: Average shoot and root length of Basmati rice (a) Khumal-14, (b) Khumal-16, and (c) Khumal-12 seedlings for 0-20 min of PAW activation after 21 days of plantation

These fresh weights per plant recorded after 21 days of plantation are depicted in Figure 47 (a), (b), and (c) of varieties of Basmati rice; Khumal-14, Khumal-16, and Khumal-12 seeds respectively. In all three varieties of Basmati rice, the 10PAW group is recorded with the highest average weight per plant value. In Khumal-14, the control

group weighed (152.4 ± 8.5) mg whereas the 10PAW group weighted (255.9 ± 7.5) mg which is a 33% increment. In Khumal-16, the control group weighed (330.4 ± 24.2) mg while the 10PAW group had (370.2 ± 26.4) mg which is a 12% increment. The khumal-16 group followed a similar pattern with the control group having (120.5 ± 9.1) mg whereas the 10PAW group demonstrated (201.4 ± 11.2) mg which is a 67% increase.

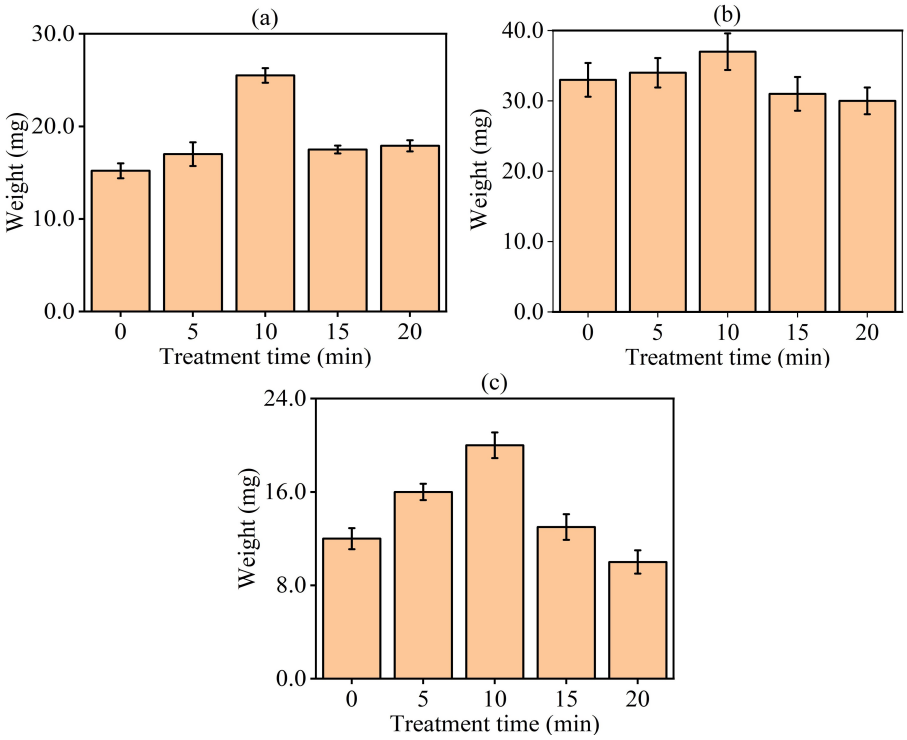

Figure 47: Average weight per plant recorded from 0-20 min PAW after 21 days of plantation of Basmati rice of (a) Khumal-14 (b) Khumal-16 (c) Khumal-12 seeds

4.3.2 Cash Crops

In this section, we presented the direct plasma treatment of seeds by DBD plasma and PAW application produced by GAD plasma in wheat crops brought from Pyuthan, the direct and indirect effect on oyster mushroom production, and PAW generated by GAD plasma applied on germination and seedling growth of cauliflower and dormancy breaking of potato brought from NARC, Khumaltar, Nepal.

4.3.2.1 Cauliflower

The germination conditions are maintained in a petri dish (without soil), and plastic glass with soil for seedling growth. For the petri dish, a single filter paper is used to retain the wet surface, and five replicates of 10 cauliflower seeds are sown in each petri dish with a total of 25 petri dishes used. The plants are cultivated near the window, in an isolated room, and the temperature and humidity are in the range 12-25°C and

55-81% respectively. During the experiment, 10.0 ml of control and plasma-treated water is dripped every day. The PAW is made below 10.0 mm from the lower point of the electrode by treating 50.0 ml of de-ionized water with treatment times 0, 5, 10, 15, and 20 min, which are denoted by 0PAW 5PAW, 10PAW, 15PAW, and 20PAW. On the other hand, 0PAW represents the control de-ionized water (untreated). Plastic glass is filled with 60.00 gm of a mixture of garden soil, vermicompost, and cocopeat in a ratio of 2:2:1, and the pH of the mixture is recorded as 7.8. The height of the soil level from the base of the glass is 46.0 mm.

4.3.2.1.1 Water Imbibition Rate: The estimation of the water uptaking rate is crucial for seed germination as it softens the outer coating layer of the seed. For measuring the imbibition rate, the weights of the cauliflower seeds for each group are taken, and placed in a petri dish, and then 10.0 ml of PAW is dripped for each group. After 24 hrs, the weight is taken and the average water imbibition rate is calculated by equation (3.16). The variation of water imbibition rate for different plasma exposure times on water is depicted in Figure 48. It is found that the water absorption rate of

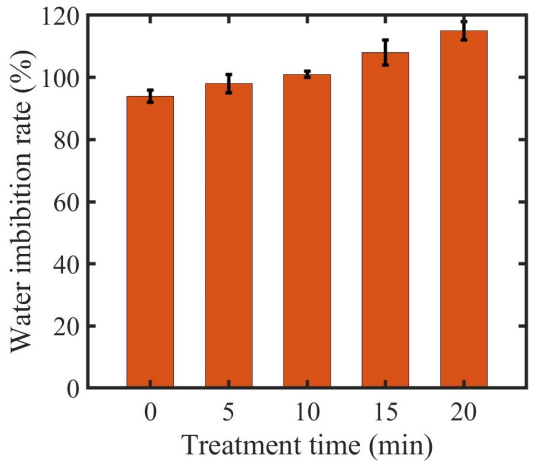

Figure 48: Water imbibition rate of cauliflower seeds soaked in 0-20 min of PAW generated by GAD plasma (Chalise et al., 2023)

cauliflower seeds increases with the increase in the plasma activation time of water. Water uptaking plays a crucial role in seed germination by providing sufficient water that softens the seed coats, raises the seed permeability, supplies dissolved oxygen for the outgrowth of the embryo, and enhances the activities of protoplasm (Thirumdas et al., 2018).

4.3.2.1.2 Effects of PAW Without Soil: In this work, the germination and growth rate parameters have been studied for two different conditions: petri dish and plastic glass with soil. The petri dish is used to reduce the effect of external environmental factors on germination; however, we have used plastic glass filling with soil to study

the germination and seedlings growth of seeds in the real field scenario. The final day germination of cauliflower seeds grown in a petri dish using control and PAW for different activation times is shown in Figure 49.

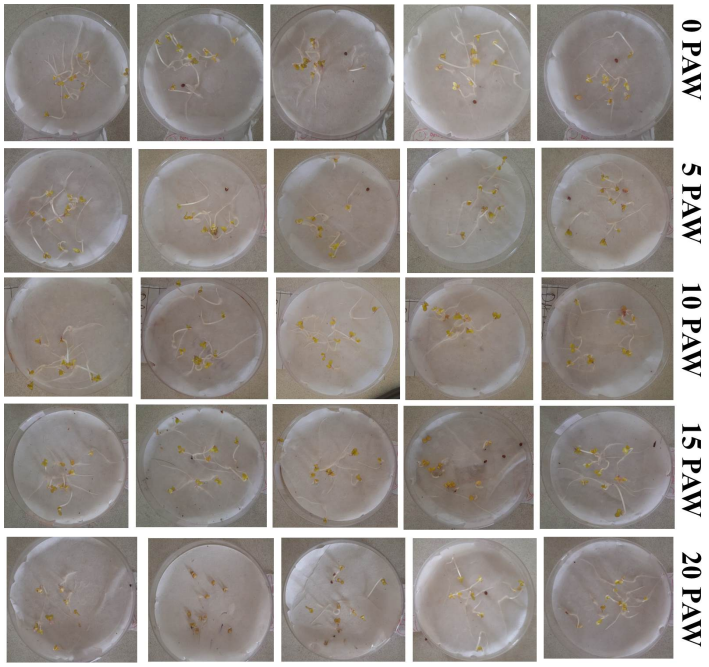

Figure 49: Final germination of cauliflower seeds grown in petri dish using control and PAW for different exposure times (Chalise et al., 2023)

The various germination characteristics are calculated using equations (3.20-3.28) which are presented in Table 10 and 11. In table 10, it is observed that the final germination percentage is found to increase by 5% when the activation time increases from 0 to 10 min. On further increasing the treatment time from 10 min to 20 min, FGP decreases by 5.44%; however, there is no significant change in the relativized percentage, MGT and MGR of the seedlings germinated using control and PAW of different activation times. In Table 11, it is seen that CVT is the maximum for 15PAW which is 39.99 ± 1.21 and is 2.46% greater than the control seeds. CVG is maximum for 5PAW which is 1.07% maximum than the control seeds. It decreases as the activation time increases and reaches 247.56 ± 16.56 for 20PAW. However, no significant change in the variance and uncertainty is observed in the case of seedlings germinated using PAW and control water.

Table 10: Final germination, relativized percentage, mean germination time and rate of cauliflower seeds for effect of PAW (Chalise et al., 2023)

Water	Final Germination (%)	Relativized (%)	MGT (day)	MGR(day^{-1})
0PAW	94.00 ± 1.26	97.93 ± 1.29	2.48 ± 0.16	0.40 ± 0.03
5PAW	95.30 ± 2.72	97.31 ± 2.75	2.51 ± 0.14	0.40 ± 0.02
10PAW	98.63 ± 1.39	98.71 ± 1.32	2.46 ± 0.15	0.41 ± 0.03
15PAW	98.06 ± 2.02	98.08 ± 2.09	2.45 ± 0.17	0.41 ± 0.03
20PAW	93.36 ± 2.93	95.26 ± 3.09	2.47 ± 0.16	0.18 ± 0.01

Table 11: Coefficient of variation of germination time, velocity of germination, variance of germination time, uncertainty of germination, and synchrony of germination of cauliflower seeds for effect of PAW (Chalise et al., 2023)

Water	CVT (%)	CVG (%)	S_t^2	U	Z
0PAW	39.03 ± 1.20	248.64 ± 16.71	0.97 ± 0.17	1.84 ± 0.14	0.28 ± 0.03
5PAW	38.23 ± 2.48	251.36 ± 14.38	0.96 ± 0.20	1.82 ± 0.16	0.86 ± 0.56
10PAW	39.65 ± 1.90	246.73 ± 15.81	0.99 ± 0.19	1.84 ± 0.15	0.28 ± 0.03
15PAW	39.99 ± 1.21	245.54 ± 17.12	0.99 ± 0.18	1.85 ± 0.14	0.28 ± 0.03
20PAW	39.31 ± 1.60	247.56 ± 16.46	0.98 ± 0.19	1.84 ± 0.14	0.28 ± 0.03

4.3.2.1.3 Effect of PAW With Soil: The seedling growth of cauliflower seeds in plastic glass for different plasma exposure times on water is shown in Figure 50. The

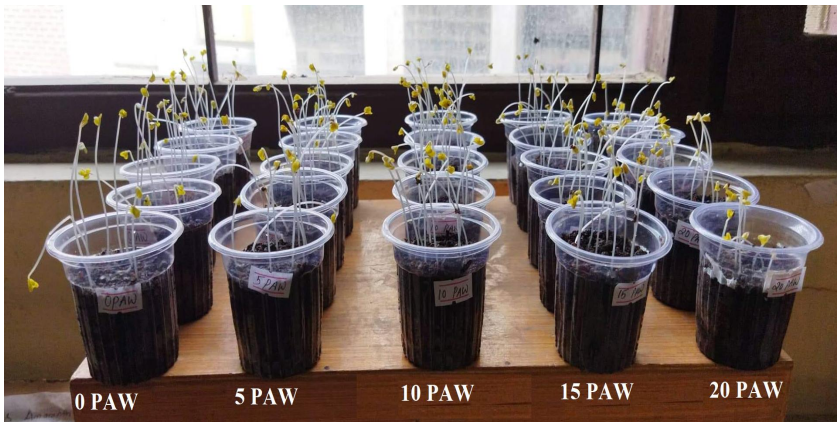

Figure 50: Seedling growth of cauliflower at 17 days of germination (Chalise et al., 2023)

germination parameters are calculated and obtained numerical values using equations (3.20-3.28) are tabulated in Table 12 and 13. It is observed that the final germination percentage and the relativized percentage are found to increase by 26.56% and 24.51% for the activation time increases from 0 to 15 min and from 0 to 5 min, respectively. However, there is no significant change in the MGT and MGR of the germination using control and PAW at different activation times. The CVT is found to be maximum for 0PAW and its numerical value is 30.03 ± 1.85. In Table 13, CVG is maximum for 15PAW which is 1.86% greater than that of control seeds. However, no significant changes in the variance, uncertainty, and synchrony are observed in seedling germination using PAW and a controlled environment. The impact of PAW on germination is correlated with PAW activity and chemical makeup, or RONS concentrations. These reactive species are believed to be crucial in seed germination (Subramanian et al., 2021).

The variation of average root and shoot lengths is illustrated in Figure 51 (a). After a 27-day germination period, measurements revealed that the average shoot length for control water (0PAW) is 8.06 cm. Notably, as the activation time increased to 15PAW, the average shoot length exhibited the highest value, surpassing the control case by 28.29%. Conversely, a decrease of 20.10% is observed for 20PAW. Additionally, the

Table 12: Final germination, relativized percentage, mean germination time and rate of cauliflower seeds for effect of soil and PAW (Chalise et al., 2023)

Water	Final Germination (%)	Relativized (%)	MGT (day)	MGR (day^{-1})
0PAW	65.31 ± 8.45	74.34 ± 16.69	5.42 ± 0.44	0.19 ± 0.02
5PAW	71.32 ± 3.34	92.42 ± 6.51	5.47 ± 0.46	0.19 ± 0.02
10PAW	72.76 ± 6.78	79.07 ± 12.64	5.54 ± 0.44	0.18 ± 0.02
15PAW	82.73 ± 5.65	86.14 ± 10.07	5.51 ± 0.39	0.18 ± 0.01
20PAW	67.34 ± 6.21	76.50 ± 12.24	5.50 ± 0.33	0.18 ± 0.01

Table 13: Coefficient of variation of germination time, velocity of germination, variance of germination time, the uncertainty of germination, and synchrony of germination of cauliflower seeds for effect of soil and PAW (Chalise et al., 2023)

Water	CVT (%)	CVG (%)	S_t^2	U	Z
0PAW	30.03 ± 1.85	541.51 ± 43.63	2.71 ± 0.55	1.80 ± 0.11	0.29 ± 0.02
5PAW	29.98 ± 1.45	546.75 ± 46.32	2.75 ± 0.55	1.82 ± 0.09	0.29 ± 0.02
10PAW	28.62 ± 1.18	533.66 ± 44.28	2.60 ± 0.54	1.80 ± 0.06	0.76 ± 0.24
15PAW	29.79 ± 2.31	551.40 ± 38.75	2.86 ± 0.72	1.85 ± 0.03	0.76 ± 0.24
20PAW	28.55 ± 3.33	549.95 ± 32.74	2.67 ± 0.78	1.81 ± 0.02	0.76 ± 0.24

root length of seedlings irrigated with 15PAW is as significantly greater, measuring 36.47% more than those irrigated with 0PAW. The absorption of nitrates from PAW through the seedling's roots plays a crucial role in promoting plant growth, acting as a plant growth enhancer (Subramanian et al., 2021; Kučerová et al., 2019). Two leaves for a single plant are chosen for the measurement of chlorophyll content. Chlorophyll is crucial for the conversion of light into chemical energy, which aids in determining the photosynthetic rate and primary production in plants. As a result, it has been widely utilized as an indicator for studies on plant growth (Li et al., 2019). The effect of PAW on chlorophyll content is shown in Figure 51 (b). It is found that the chlorophyll content in the leaf is maximum for the 10 min PAW used for plants. Once the chlorophyll content on the leaves is maximum for the 10PAW, it decreases when the plasma exposure time increases beyond 10 min.

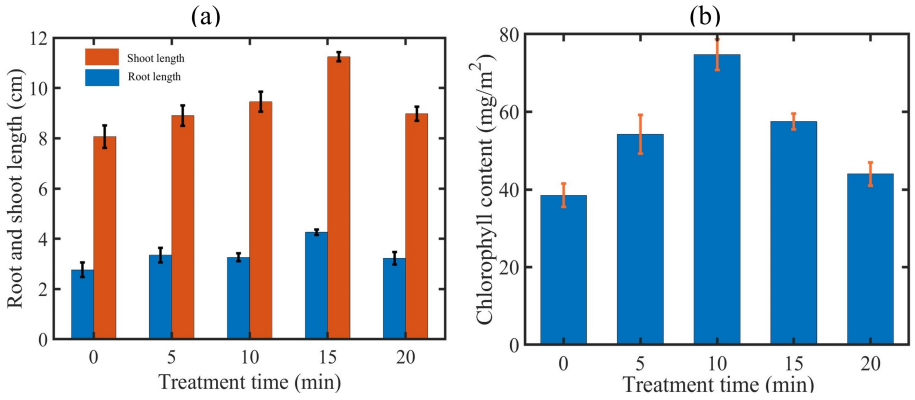

Figure 51: (a) Variation of root and shoot length of cauliflower's seedlings, and (b) chlorophyll content of leaves for PAW activation of 0-20 min (Chalise et al., 2023)

4.3.2.2 Oyster Mushroom

In this work, we have made a substrate in a plastic bag of 200.00 gm from rice straw for the production of the mushroom. The rice straws are chopped into small pieces (1-2 inches). They are soaked for 24 hrs, thoroughly washed with clean water, and allowed to drain until no water oozed out when squeezed by hand. Each substrate is individually sterilized by boiling it in a metallic pot for three hrs. It is then allowed to cool to room temperature before being filled into plastic bags. A total of 50 spawns are placed in each bag, with two layers of spawn per bag. After the bags are tied at the mouth, a few holes are made for aeration around the periphery of each bag. The mushroom spawn is directly treated by GAD plasma for one min (S-1), two min (S-2), and three min (S-3) adjusting the distance between the spawn and the electrode tip to 4.0 mm. For the indirect approach, we have taken two methods treated water and poured it every day from sprayed and another treated straw that is used for mushroom planting. PAW is created by pouring 200.0 ml of the tap water available in the Central Department of Physics. Kirtipur, Nepal. The water is treated with plasma for different time intervals, such as four min (LPAW-1), eight min (LPAW-2), and 12 min (LPAW-3). The straw is treated with plasma by placing it inside a glass block and allowing plasma to pass through the block for different time intervals, such as five min (ST-1), 10 min (ST-2), and 15 min (ST-3). We have carried out five replications in the ambient environment from 23 March 2022 to 08 May 2022. The obtained result agrees with the study carried out by Agun et al. (2020).

The different pictures of mushroom production after 29 days of spawning are presented in Figure 52, the colonization and budding time (days) from the spawning time of the mushroom in noted. Biological efficiency (BE) is calculated by equation (3.27), which represents the growth potential of the oyster mushroom.

The time duration required for the colonization started at 20 days for mushroom spawns two and three min treatment and straw 15 min treatment and more time taken by plasma treated water used. Similarly, the period required for the fruit initiation started at 25 days in the same mushroom category as shown in Figure 53 (a). Starting time is noted among the 3 replicas of the experiment so that error is included. The colonization period starts from 2^{nd} week and is completed within the 3^{rd} week. The fruit initiation period of plasma-treated spawn and straw is less than PAW sprayed. The colonization and budding time is faster than the plasma treatment on spawn and straw before packing than the spraying PAW. The observed delay in fruiting body initiation, despite accelerated colonization in some instances, may be attributed to treatment-induced alterations in the carbon-to-nitrogen (C/N) ratio. However, on average, plasma treatment is found to reduce the time required for both colonization and the initiation of fruiting bodies. The presence of RONS in the discharge, which is directly absorbed by the mushroom's spawn

and straw treatment is a good environment for faster colonization and budding (Agun et al., 2020). The increment of production of mushrooms in percentage is shown in Figure 53 (b). It is found that the plasma helps to enhance the production of the mushroom.

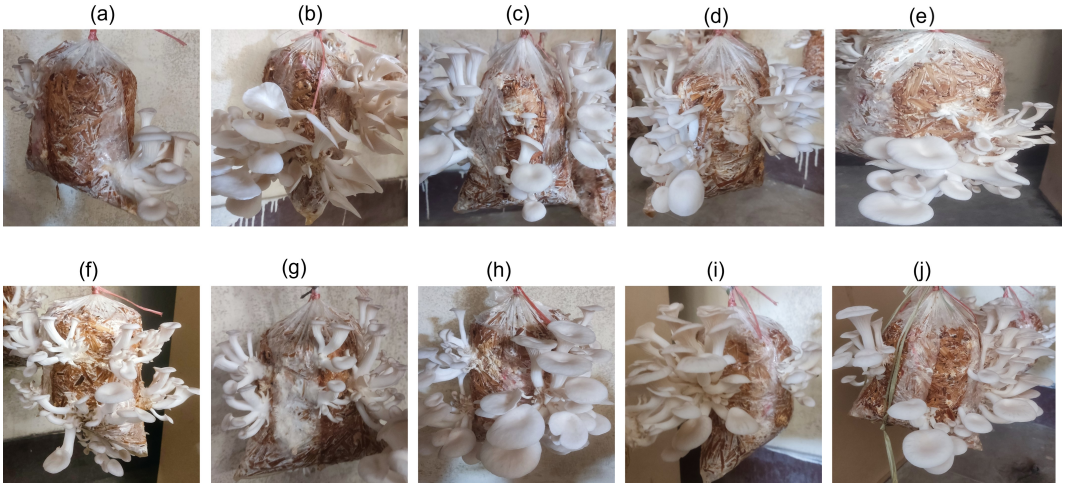

Figure 52: Pictures of mushroom before harvesting at 29 days after spawning (a) untreated sample, mushroom spawn treated (b) one min, (c) two min, (d) three min, water treated (e)four min, (f) eight min (g) 12 min, straw treatment (h) five min, (i) 10 min, and (j) 15 min

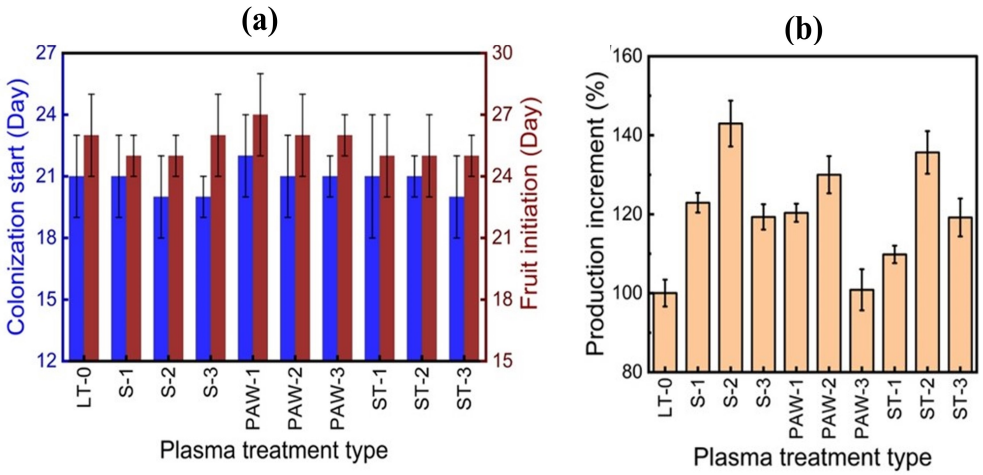

Figure 53: (a) Colonization and fruit initiation day and (b) total production of mushroom per bag in different configurations of oyster mushroom

Table 14 represents the comparison of mushroom stem length, stem and cap diameter, fresh weight, and biological efficiency of the produced mushroom. The length of the stem is found to be significantly higher for the mushroom spawn treated followed by three min, where the length of the stem is found to be significantly lowest for the straw treated in 15 min. The diameter of the stem is found to be the highest for eight min of PAW. However, the stem diameter is found to be significantly lower for 12 min PAW. In the same way, the cap diameter is found to be significantly higher for three min spawn treated and lowest for 12 min PAW. The total fresh weight and biological efficiency are

highest in two min spawn plasma-treated and lowest in the untreated case. Mushroom spawn treatment using cold plasma shows the mushroom fruiting body initiation cycle exhibits better results when producing almost 1.5 times more compared to control spawn. Similarly, for the straw treated with plasma and PAW used bag, the mushroom production is greater than the control spawn.

Table 14: Stem length and diameter, cap diameter, fresh weight of mushroom per bag, and biological efficiency of various treatments

Type	Lt. stem (cm)	Dia. Stem (cm)	Dia. Cap (cm)	Wt. (g)	BE (%)
LT_0	5.64^{c}	0.91^{d}	4.45^{c}	188.98^{d}	94.49^{d}
LMS_1	5.71^{c}	0.89^{d}	4.75^{c}	232.18^{b}	116.09^{b}
LMS_2	6.54^{a}	0.09^{d}	5.31^{b}	250.05^{a}	135.03^{a}
LMS_3	6.87^{a}	0.99^{b}	5.99^{a}	225.39^{b}	112.70^{b}
$LPAW_1$	5.76^{c}	1.22^{a}	5.51^{a}	227.36^{b}	113.68^{b}
$LPAW_2$	5.33^{d}	1.06^{b}	4.99^{b}	245.57^{b}	122.79^{b}
$LPAW_3$	5.16^{d}	0.83^{e}	4.18^{c}	190.53^{d}	96.27^{d}
LST_1	5.66^{c}	0.85^{d}	4.89^{b}	207.46^{e}	103.73^{c}
LST_2	6.13^{b}	0.95^{c}	5.36^{b}	256.22^{a}	128.11^{a}
LST_3	5.02^{e}	1.00^{b}	4.77^{c}	225.14^{b}	112.57^{b}

(Figure in a column having common letter(s) does not differ significantly at 5% level of significance.)

4.3.2.3 Wheat

The wheat *(Triticum aestivum)* seeds are procured from local farmers in the Pyuthan of Nepal. A total of 24 grow bags were prepared, each grow bag included similar 16 wheat grains, separated for each treatment time group. The temperature and humidity are in the range (10-25)°C and (56-80)% respectively.

4.3.2.3.1 Contact Angle: We measured the contact angle of the untreated and plasma-treated seeds using ImageJ software. The shape of the water drop on the seed before and after the direct plasma treatment is carried out from a locally made prototype goniometer by Chalise et al. (2023a) depicted in Figure 54 (a) and (b). The direct plasma exposure time explicitly affects the contact angle and its variation with direct plasma exposure time is shown in Figure 54 (c). The contact angle is measured 10 times and an average is taken. It is found that the contact angle of the seeds decreases with the increase in treatment time. The contact angle decreases from (76.27±1.12)° to (66.21±1.05)° when the plasma exposure time increases from about 0 to 5 min. The obtained results are agreed with similar work by Baldanov & Ranzhurov (2022). An R-squared value of 0.99 means that the independent variable accounts for 99% of the variance in the dependent variable. This suggests a good fit because the data points are extremely near to the fitted regression line.

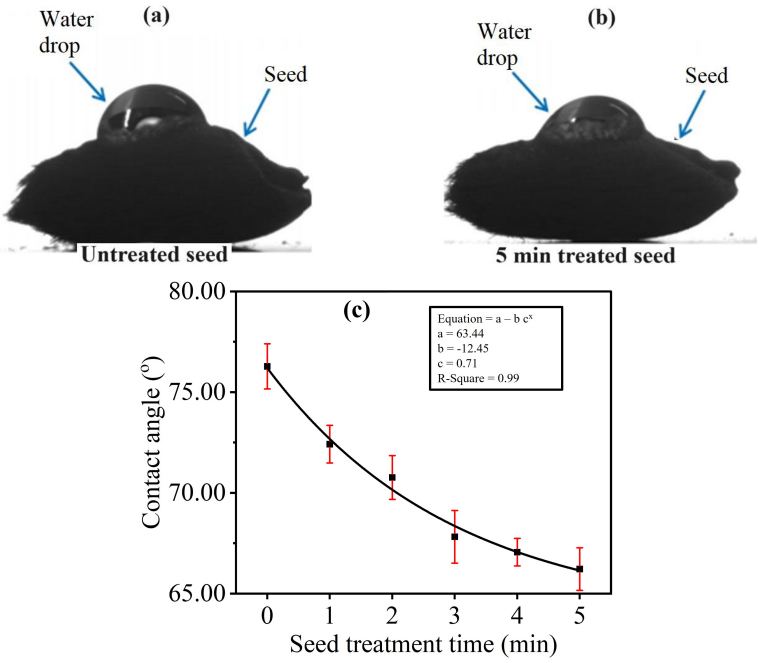

Figure 54: Image of water drop on the surface of (a) untreated (b) five min treated wheat seed, and (c) variation in the contact angle of wheat seeds with plasma treatment time (Chalise et al., 2023b)

Table 15 shows the one-way ANOVA test results at a $\alpha = 1$ level of significance, indicating the statistically significant differences between the treatment groups for the measured variables. The null hypothesis states that the plasma treatment has no effect, while the alternative hypothesis states that the plasma treatment has a positive impact on the results because of the significant difference in the means. The alternate hypothesis, that the plasma treatment has an effect on wheat yield, is proven to be true, indicating that the plasma treatment has a significant positive impact on the results.

Table 15: One-way ANOVA test between the measured variables of wheat (Chalise et al., 2023b)

S.N.	ANOVA test at α=1 level for measured variables of wheat	F-value	P-value
1	Growth rate after 7 days of germination	4.24	0.01
2	Germination Potential	0.68	0.64
3	Germination Index at 8^{th} day of plantation	0.67	0.65
4	Spike length	1.01	0.44
5	Fruit number	0.49	0.78
6	Root length	1.03	0.43

4.3.2.4 Potato

In this section, we present the effect of the PAW on potato dormancy-breaking enhancement. The potatoes are provided by NARC. In each experiment, 10/10 Janakdev and Khumal Ujjwal potatoes are dipped in 0PAW, 10PAW, and 20PAW for 48 hours.

Then placed in a dark environment the process is repeated five times and the obtained results are as shown in Figure 55. Potatoes that are immersed for 20 min begin to go dormant earlier than those in the control. On the other hand, Janakdev potato varieties exhibit faster dormancy onset than Khumal Ujjwal varieties. The dormancy breaking is faster due to the availability of NO in PAW (Šírová et al., 2011). The result obtained by faster dormancy breaking is supported by H. P. Sharma et al. (2021).

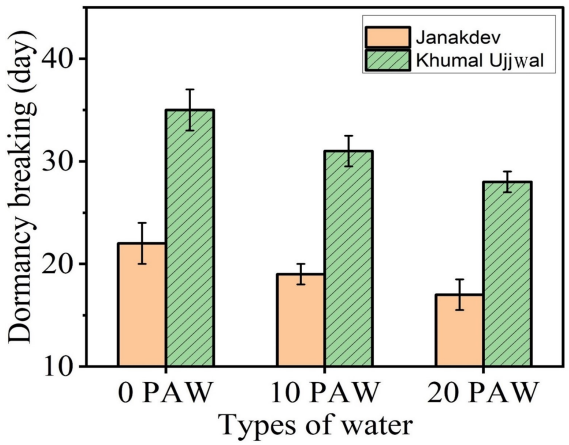

Figure 55: Dormancy breaking of Janakdev and Khumal Ujjwal potato after dipping for PAW activation of 0-20 min

4.3.3 Greenness and Freshness of Leaf

4.3.3.1 Green Leafy Vegetables

In this work the healthy and similar seeds of local green leafy vegetables; leaf mustard (*Brassica juncea*); (*Rayo* Manakamana and *Rayo* Marpha), spinach (*Spinacia oleracea*/*Palungo*) and garden cress (*Lepidium sativum*/*Chamasur*) is obtained from NARC. From the selected seeds, 30 seeds are soaked in 0, 5, 10, 15, and 20 min PAW, which is generated below 10.0 mm from the lower point of the electrode of GAD plasma by treating 40.0 ml of de-ionized water. Here 0 represents the control de-ionized water (not exposed by plasma). The seeds are weighed and placed in separate petri dishes for each experimental group and soaked in 40.0 ml of respective water. These soaked seeds are removed from the water and cleaned with tissue paper, and weight. The water imbibition rate by the seed is calculated by equation (3.16). 10 seeds are planted in plastic glasses, each with 80.00 gm of a mixture of 50% soil and 50% vermicompost. The planted seeds are kept in the window side of the room in an ambient environment and 10.0 ml of respective water is poured into a glass every two days. The temperature and humidity are in the range 5 to 18°C and 30 to 50% respectively of the environment. The germination rate is calculated by equation (3.17). The obtained results in germination and seedling growth are supported by Stoleru et al. (2020) and Hsu et al. (2023) which are presented here.

4.3.3.1.1 Wettability: The water absorbance rate of green leafy vegetables with increasing treatment time of plasma in water is calculated using equation (3.16) and depicted in Figure 56 (a), (b), (c) and (d) of *Chamsur*, *Rayo* Manakamana, *Rayo* Marpha, and *Palungo* respectively. Initially, the water imbibition of green leafy vegetable seeds shows an increase from 0 to 15 min of plasma treatment, followed by a decrease when soaked in water activated for 20 min. This observation indicates that seeds treated with PAW for 10-15 min exhibit a higher water imbibition capacity. Specifically, green leafy seeds soaked in water exposed to GAD plasma for 10-15 min demonstrate the greatest ability to absorb water. These results suggest that seed priming with plasma may trigger molecular processes within the seeds. It has been found that seed coverings undergo etching by oxygen radicals like O_2^+. This etching process leads to the generation of reactive oxygen species, altering the seed coat and facilitating gaseous and water exchange within the seed (Adhikari et al., 2020). As a result of this etching process, a higher water absorbance in the seed is observed when soaked in PAW for 10-15 min. This underscores the potential of plasma seed priming to enhance water imbibition capacity and promote efficient germination in green leafy vegetable seeds.

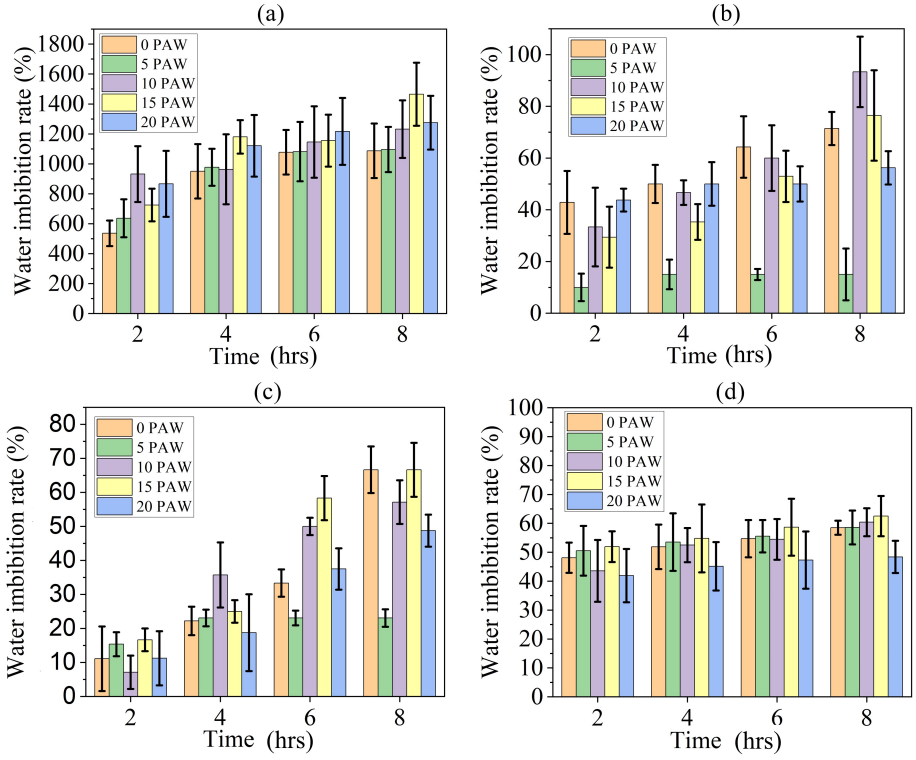

Figure 56: Water imbibition rate of (a) *Chamsur*, (b) *Rayo* Manakamana, (c) *Rayo* Marpha, and (d) *Palungo* of green leafy vegetables for PAW activation of 0-20 min (Chalise et al., 2024c)

4.3.3.1.2 Germination: Equation (3.17) is used to determine seed germination rate, which is started 72 hours after planting. Figure 57 (a), (b), (c) and (d) display the results of germination rate observed after 72 hours of plantation of *Chamsur*, *Rayo*

Manakamana, *Rayo* Marpha, and *Palungo* respectively. The germination rate exhibited a pattern of increase from 0 min of PAW exposure to 15 min, followed by a decrease at 20 min of PAW exposure across all four varieties of green leafy vegetables. Notably, the *Chamsur* variety displayed a higher germination rate. Seeds treated with 15 min

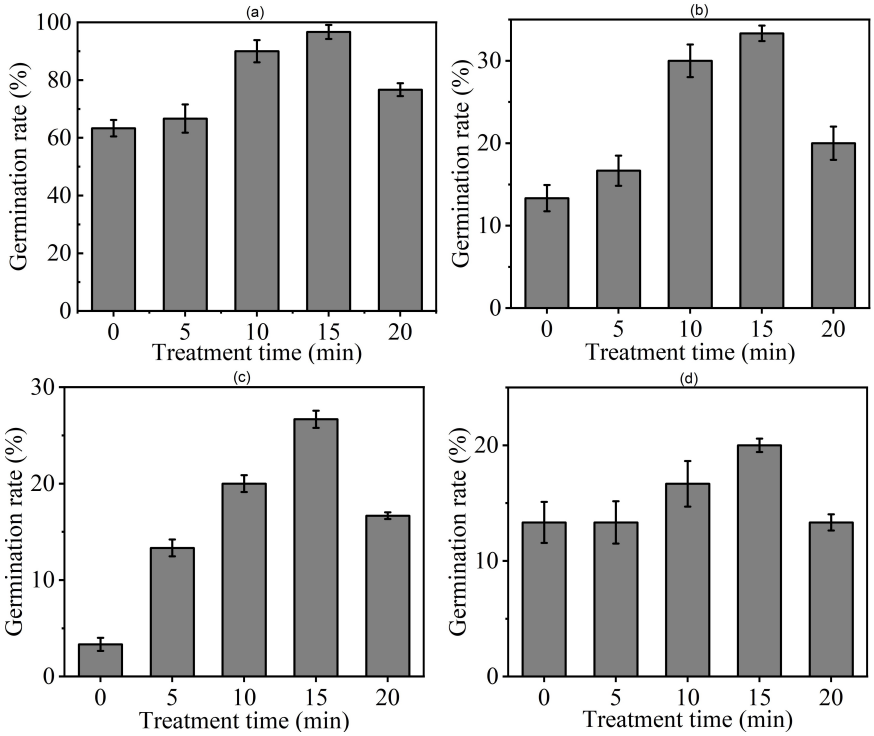

Figure 57: Germination rate of (a) *Chamsur*, (b) *Rayo* Manakamana, (c) *Rayo* Marpha, and (d) *Palungo* variety of green leafy vegetables for PAW activation of 0-20 min (Chalise et al., 2024c)

of PAW demonstrated the highest germination rate across all four vegetable varieties. For instance, in the *Rayo* Marpha variety, seeds exposed to 15 min of PAW achieved a germination rate of 26.67%, which is eight times higher than the control group. Similarly, in *Rayo* Manakamana and *Palungo* varieties, seeds treated with 15 min of PAW exhibited the highest germination rates of 33.33% and 20.00%, respectively, while the control groups showed lower germination rates. In the case of *Chamsur*, seeds treated with 15 min of PAW achieved an impressive germination rate of 96.67%, while those treated with 0 min of PAW exhibited a lower rate of 63.33%. These results underscore the direct influence of PAW on seed germination, with optimal germination observed at 15 min of plasma exposure, followed by 10 min of exposure. The use of PAW on seeds stimulates germination chemistry, activating the amylase enzyme, modulating phytohormone ratios, and enhancing reactive oxygen species, O_2^+, and water uptake. These reactive species function as signaling molecules within seed cells, promoting oxidative signaling and facilitating germination processes (Adhikari et al., 2020). The application of PAW during seed planting significantly impacts germination rates, with optimal results achieved at specific exposure times, highlighting the potential of PAW as a germination enhancer in agriculture.

4.3.3.1.3 Growth Parameters: A real picture of seedling growth of one of the green leafy vegetable varieties during the experiment is depicted in Figure 58 in an ambient environment at CDP, T.U. Figure 59 (a), (b), (c) and (d) show the average root and shoot length of *Chamsur*, *Rayo* Manakamana, *Rayo* Marpha, and *Palungo* plant respectively, after 21 days of plantation. It is found that the seeds treated with 10 min of PAW of the *Rayo* Marpha variety exhibited maximum root and shoot lengths.

Figure 58: Real picture of seedlings growth of a variety of green leafy vegetables plant along with Basmati rice

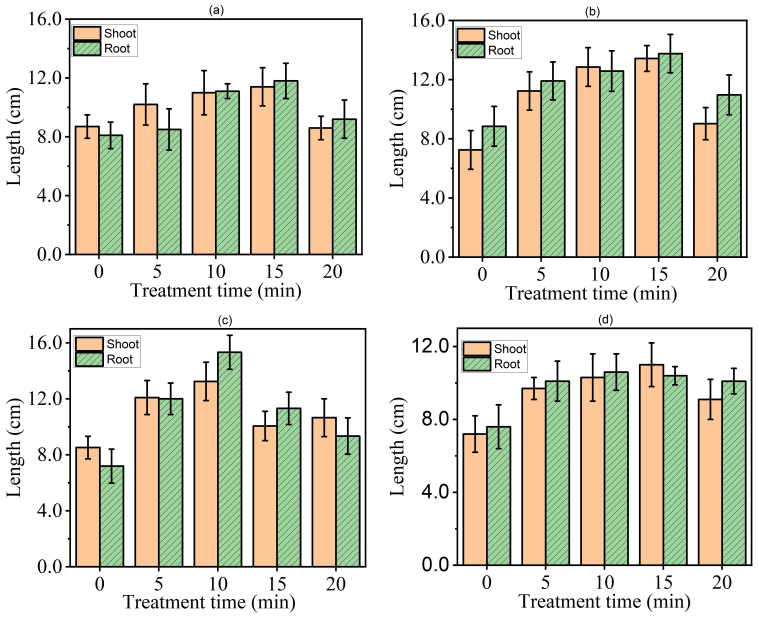

Figure 59: Average root and shoot length of per plant of (a) *Chamsur*, (b) *Rayo* Manakamana, (c) *Rayo* Marpha, and (d) *Palungo* seeds for PAW activation of 0-20 min (Chalise et al., 2024c)

Conversely, the other three varieties demonstrated maximum root and shoot lengths when treated with 15 min of PAW. A longer root length is advantageous for plants to search for nitrate and nitrite solubles in the soil, facilitated by the application of PAW into the plant. However, the presence of higher concentrations of hydrogen peroxide and nitrate, despite being primary sources of nitrogen for plants, may unfavorably slow down growth processes. Nitric oxide and ROS are known to influence plant growth and development at low concentrations positively. However, at higher concentrations,

these reactive species can become toxic and hinder various developmental processes (L. Fan et al., 2020). Furthermore, the low pH value observed in PAW-treated water, which approaches the lower limit of the ideal pH required for seed growth, may also contribute to smaller seedling growth. This phenomenon could explain the reduced growth observed in seedlings treated with PAW (Holmes et al., 2019). The average fresh weight of *Chamsur*, *Rayo* Manakamana, *Rayo* Marpha, and *Palungo* is presented in Figure 60 (a), (b), (c) and (d) respectively, where it is evident that green leafy vegetables treated with 15 min of PAW *Palungo*, *Rayo* Marpha, and *Chamsur* exhibited the maximum weight per plant. However, *Rayo* Manakamana plants demonstrated the highest weight when treated with 10 min of PAW. These findings collectively suggest that the optimal duration for PAW treatment in promoting green leafy vegetable production is 10-15 min, as it maximizes growth parameters and fresh weight per plant.

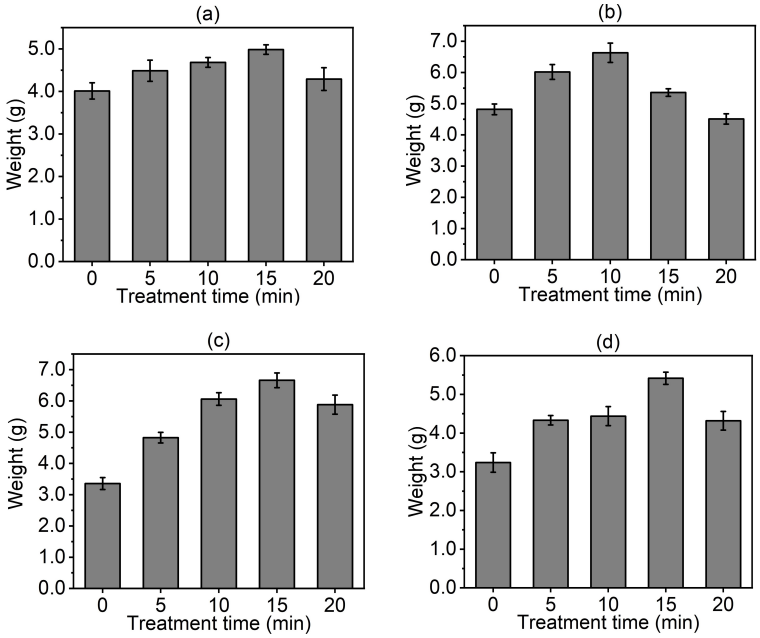

Figure 60: Average fresh weight of (a) *Chamsur*, (b) *Rayo* Manakamana, (c) *Rayo* Marpha, and (d) *Palungo* variety of green leafy vegetables measured after 21 days of plantation for PAW activation of 0-20 min (Chalise et al., 2024c)

4.3.3.1.4 Chlorophyll Content: The greenness of plant foliage is a major parameter in assessing the quality of green vegetables. Figure 61 (a), (b), and (c) illustrate the chlorophyll content on the leaves of green leafy vegetables of *Rayo* Manakamana, *Rayo* Marpha, and *Palungo* respectively measured by TYS-B chlorophyll meter. Due to the limitation of scan area of instrument less than 2μm $\times 2\mu$m *chamsur* leave is less than this size and can't succeed to measure. The results indicate that leaves treated with 15 min of PAW exhibit the highest greenness. However, in the case of *Rayo* Marpha, higher greenness on the leaves is observed when treated with 10 min of PAW. The higher chlorophyll content observed in plants treated with PAW can be attributed to the increased concentration of nitrate. Nitrate is not only essential for plant growth as

a primary source of nitrogen but also plays a crucial role in chlorophyll production. Consequently, the elevated nitrate levels in PAW-treated plants contribute to enhanced chlorophyll synthesis. Chlorophyll content serves as a critical quality indicator in leafy green vegetables, as changes in leaf color due to chlorophyll degradation can signify a reduction in product quality. Additionally, higher levels of chlorophyll are typically associated with increased rates of photosynthesis and overall plant metabolism (Ramalho et al., 2002). These findings suggest that PAW treatment, particularly for 15 min, enhances chlorophyll content in green leafy vegetables, contributing to improved plant quality and metabolic activity.

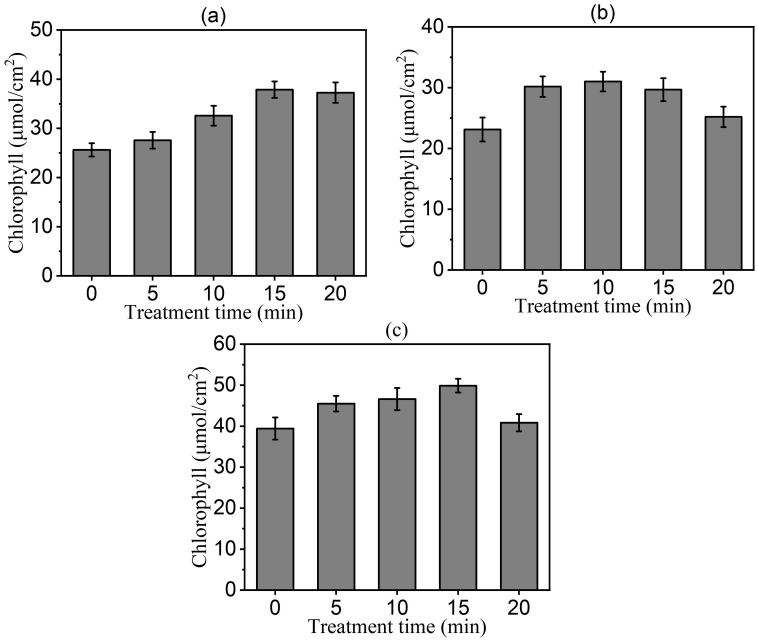

Figure 61: Chlorophyll content on leaf of (a) *Rayo* Manakamana, (b) *Rayo* Marpha, and (c) *Palungo* of green leafy vegetables for PAW activation of 0-20 min (Chalise et al., 2024c)

4.3.3.2 Detached Tejpat Leaf

This research is aimed at improving the longevity of the greenness of the leaves from the indirect application of plasma in Tejpat (*Cinnamomum tamala*) Leaves. The PAW is made from GAD plasma below 10.0 mm from the lower point of the electrode by treating 50.0 ml of de-ionized water with treatment times 0, 4, 8, 12, and 16 min, which are denoted by 0PAW 4PAW, 8PAW, 12PAW, and 16PAW. On the other hand, 0PAW represents the control de-ionized water (untreated). The physical parameters of PAW are measured every 24 hrs continuously until 5 days, where PAW is put in an ambient environment of plastic glass without covering it. Tejpat leaves are plucked from the Tejpat tree from the Central Department of Botany, TU, Kirtipur, Kathmandu, Nepal, and selected similar types of 25 leaves having petioles for each experiment divided into five leaves for each set of the experiment: control, 4 min, 8 min, 12 min, and 16 min

PAW, and repeated three times in same conditions. Each leaf is kept inside a plastic zip bag and wrapped in its petiole by tissue paper soaked in 10.0 ml of 0, 4, 8, 12, and 16 min PAW. These leaves are kept in a dark room where the temperature and humidity are in the range of 12 to 25°C and 55 to 81% respectively during the experiment. Before and after dipping the leaves in plasma-treated water, CCM-300 is used to measure the chlorophyll of the leaves based on the chlorophyll fluorescence (CFR) technique. This device measures chlorophyll content in leaves up to 675 mgm^{-2} and the measurement diameter of the device is 3.0 mm with its 4.0 mm outer diameter. However, the device works very accurately for the smaller plants as well. Unlike the absorption technique that requires full coverage of the aperture and a flat surface, this method does not need that (Gitelson et al., 1999) leaf is measured 5 times and averaged for a more accurate and precise result of the chlorophyll measurement. The chlorophyll content in these leaves is assessed every three days until it completely disappears, and the duration it takes for the chlorophyll to vanish is known as the greenness period. For chlorophyll retention, the measured chlorophyll is converted into a ratio with its initial value. The obtained results are presented here.

4.3.3.2.1 Aging Effect of Plasma Activated Water: To study the aging effect of PAW, the change in physical parameters is measured for up to 5 days. The variation of pH, EC, TDS, and ORP as the function of the number of storage days is shown in Figure 62. It is found that the pH and ORP have slowly regained their original value as shown in 62 (a) and (d), whereas the EC and TDS go on increasing for the increase in storage days from their initial value as shown in 62 (b) and (c). The regaining rate of pH and ORP is found to be slower for the 12PAW than that of other cases. For the same plasma exposure time (12PAW), the increasing rate of EC and TDS is also lower. The changes in the physical properties of PAW explicitly indicate that there should be a significant effect on leaves as they absorb treated water for nutrients.

4.3.3.2.2 Chlorophyll Retention: The chlorophyll retention of Tejpat leaves for different plasma treatment times is shown in Figure 63. The chlorophyll retention decreases with the increase in the number of storage days and the minimum value has been recorded in 21 days. The chlorophyll retention (%) is higher for the leaves that have been used with PAW for 12 min compared to the other various plasma-activated as well as untreated water. This indicates that the PAW can effectively preserve the chlorophyll content in the leaves, especially the PAW of 12 min, which is the best candidate for this purpose in our case. It is found that the nitrate and nitrite concentration of treated water increase with the increase in plasma treatment time. The concentrations are found to be maximum for the 16 PAW with numerical values of nitrite and nitrate concentrations are 150 and 60 ppm respectively. The primary method of absorbing nitrogen is nitrate (Wen

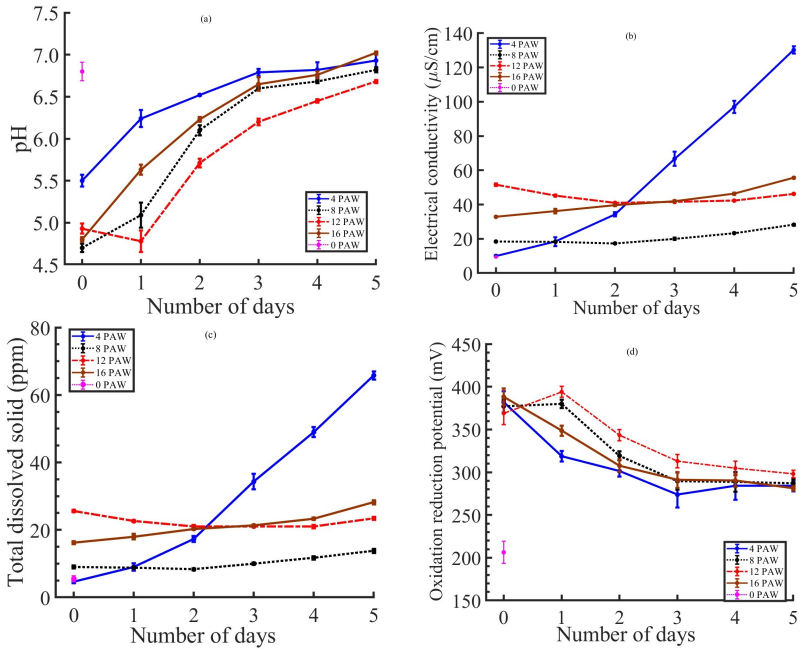

Figure 62: Variation of Aging (a) pH, (b) EC, (c) TDS, and (d) ORP during 5 days (Chalise et al., 2024)

et al., 2020), which has a key role in the synthesis of proteins, enzymes, nucleotides, and chlorophyll in plants, making it a crucial macronutrient for plant growth and development (Marschner, 2011). Nitrate is the primary form of nitrogen that plants receive, and it

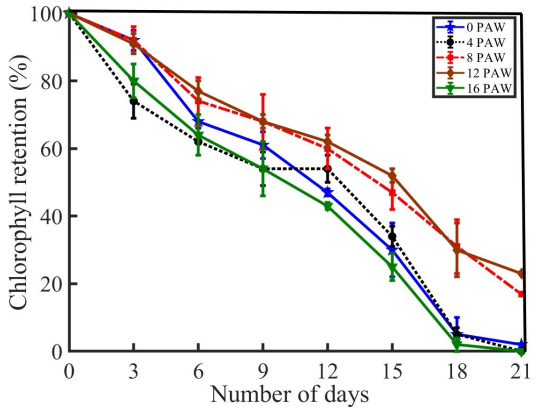

Figure 63: Variation of chlorophyll retention for increasing the storage days (Chalise et al., 2024)

is also the nutrient element that they absorb the fastest. As a result, most plants rely on nitrate as their primary nitrogen source for morphological development, growth, and maintenance. The ability of plants to respond to changing environmental conditions is enhanced by nitrate, which can quickly boost the transport and digestion of nutrients (Meng et al., 2016). The basis of plant growth and development is the process of nitrate absorption and transformation, and a deficiency in nitrate immediately causes decreased photosynthetic efficiency, inhibited root growth, and organ senescence, further impacting the fruit quality and output (Ruffel, 2018). Nitrate decreased reactive oxygen species generation by increasing photosynthetic pigments (Iqbal et al., 2015). Nitrate may

up-regulate anti-oxidative genes, increasing the synthesis of anti-oxidative enzymes. Additionally, nitrate increases the total nitrogen metabolism and continuously supplies nitrogen to produce chlorophyll and other photosynthetic enzymes (Agnihotri & Seth, 2016).

4.3.3.2.3 Freshness: The effect of PAW on chlorophyll retention, and consequently the greenness, of detached Tejpat leaves is investigated as illustrated in Figure 64. The average number of days for the leaves to reach zero chlorophyll content when treated with PAW is seen to be significantly prolonged compared to the leaves treated with normal water. Leaves treated with 12 min PAW retained their green color for an average of 576.00 ± 34.23 hrs (24 days), compared to leaves treated with untreated water, which retained their greenness for 456.34 ± 31.45 hrs (19 days). Likewise, leaves treated with four min PAW maintained their greenness for 504.45 ± 17.31 hrs (21 days), while those treated with eight min PAW retained greenness for 552.34 ± 23.36 hrs (23 days), and leaves treated with 16 min PAW stayed green for 408.76±19.35 (17 days). These findings demonstrate that a 12 min PAW treatment is most effective in preserving chlorophyll content in Tejpat leaves. Because fresh foods are high in vitamins, minerals, fiber, and bioactive substances, they are crucial for a balanced diet. However, these fresh goods are frequently contaminated by several things, such as handling tools, irrigation water, and manure. The effectiveness of bacterial inactivation is influenced by leaf health and freshness (Mao et al., 2021). The reason for the chlorophyll retention, and thus the prolonged freshness and greenness of leaves by PAW, is attributed to the considerable effect of plasma exposure on the physico-chemical properties of water against bacteria, viruses, fungi, and parasites.

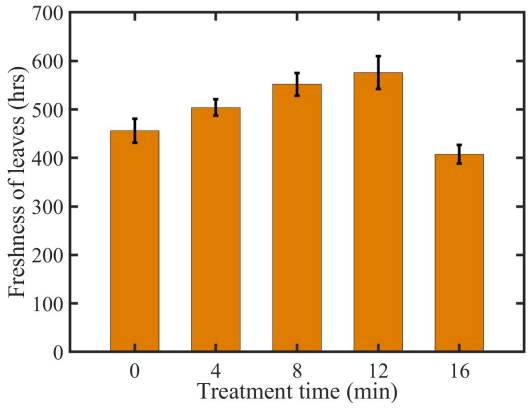

Figure 64: Longevity of greenness of leaves, whose petioles dip in 0-16 min PAW (Chalise et al., 2024)

4.3.4 Bacterial Inactivation of Water

The goal of this study is to investigate the efficacy of plasma in reducing bacterial activity. When normal water is applied to the plant to facilitate seedling growth, the

presence of water-associated bacteria leads to plant infection. Consequently, PAW is administered to plants harboring free bacteria, viruses, fungi, and parasites. The Central Department of Microbiology, Tribhuvan University, Nepal provided two different strains of bacteria, namely *S. aureus* (ATCC 292213) and *E. Coli* (ATCC 52922), which are utilized as test microorganisms. To prepare the bacterial suspension, the bacteria are cultured on nutrient agar and incubated for 24 hrs at 36°C. Subsequently, 10.0 ml of de-ionized water is added to a test tube containing a small number of bacterial colonies until the suspension reaches a density of 1.50×10^8 CFU ml^{-1}. Turbidity measurements are conducted using this suspension as a reference. In another test tube, a solution with a concentration of 1.50×10^4 CFU ml^{-1} is prepared by mixing 2.0 ml of the suspension with 18.0 ml of de-ionized water and serially diluting it three times. Next, the 20.0 ml solution is subjected to plasma treatment for two to eight min. Subsequently, 100 µl of the plasma-treated solution is cultivated for 24 hrs at 36°C in a nutritional agar medium. Bacterial colonies on petri dishes are then counted using a colony counter. The test liquids are arranged on a 10.00 cm-diameter petri dish, maintaining a constant liquid surface area of 78.50 cm^2. The effective gap between the high-voltage electrode and the liquid surface (20.0 ml) is 6.0 mm. The experiment is conducted at a room temperature of 18°C under atmospheric air conditions. Both *S. aureus* and *E. coli*, cultured at a specific concentration, are exposed to SDBD plasma. As the duration of plasma treatment increases, the quantity of colony-forming units (CFU) decreases, as illustrated in Figure 65. Plasma can eliminate germs through two mechanisms: physical

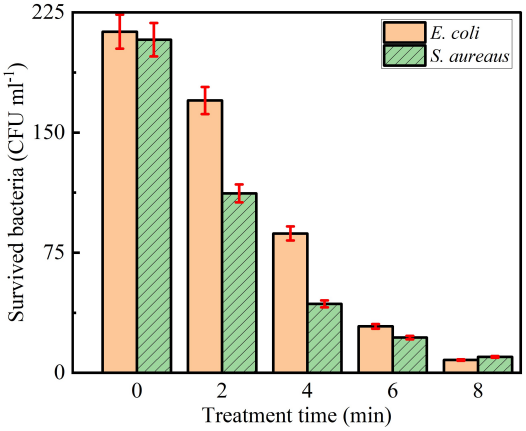

Figure 65: Effect of plasma treatment on reduction of bacteria that are in water (Dhakal et al., 2023)

reactions on the water's surface, generating heat, shock waves, a strong electric field, and other effects, as well as the chemical breakdown of cell walls and membranes due to RONS (Lukes et al., 2012a). The majority of bacteria in the medium can be eliminated with eight min of plasma treatment, and bacterial colonies are quantified on nutritional agar following a 24-hour incubation at 36°C.

CHAPTER 5

CONCLUSIONS AND RECOMMENDATIONS

5.1 Conclusions

The three types of atmospheric pressure plasma sources (GAD, DBD, and APJ) are successfully generated, characterized electrically and optically, and investigated for their effect on agricultural crop productivity. These plasma sources that operate using an inexpensive power supply are constructed from readily available local market materials, enabling atmospheric air pressure GAD plasma for various non-thermal plasma applications. Comprehensive electrical and optical characterizations are conducted on the GAD plasma to analyze the produced discharge, achieving temperatures and plasma densities agreed with the previous published GAD plasma. Most importantly, the relationship $T_{\text{exc}} > T_{\text{vib}} > T_{\text{rot}}$ indicates a non-equilibrium state in the plasma discharges. Additionally, the atmospheric pressure plasma (DBD and APJ) are generated using a commercial power supply and characterized electrically and optically through various methods.

When the plasma is directly or indirectly exposed to water, the plasma exposure time significantly affects various physico-chemical parameters, such as pH, electrical conductivity, oxidation-reduction potential, total dissolved solids, temperature, hydrogen peroxide, and nitrite and nitrate concentration. Specifically, the pH values of water decrease as the plasma exposure time increases, while other physico-chemical parameters increase respectively. We have also studied the aging effect of the physical parameters of PAW generated by GAD plasma in 0, 4, 8, 12, and 16 minutes. However, these changes in the physical properties did not last long for a long period. The pH value retains its original value for five days, whereas the electrical conductivity and total dissolved solids are found to be increasing. On the other hand, the oxidation-reduction potential gets reduced and shifted to a stable domain after five days. The change in physical parameters during the storage time is slower for 12 minutes of PAW than in other cases which indicates the activeness of these parameters for a longer period.

We have applied this plasma in germination, seedling growth, bacterial inactivation of

water, and longer-time greenness of detached leaves using direct and indirect methods. The study underscores the potential advantages of employing PAW in cereal crops (Basmati rice), and cash crops (wheat, cauliflower, oyster mushroom), particularly in its influence on the germination, seedling growth, and the quantity as well as quality of production. The findings demonstrate that the PAW treatment, specifically the 10-minute activation by GAD plasma, positively affected the germination and the subsequent growth of seedlings of Basmati rice. The seedlings treated with 10-minute PAW exhibited a notable 66.75% increase in weight compared to the control group in Basmati. Furthermore, when contrasted with control seeds, the seeds treated with PAW displayed superior germination, longer root and shoot length, and higher overall weight. However, it is important to note that extended exposure to plasma discharges negatively impacted the germination and development properties of Basmati seeds. The fruit initiation and colonization period of plasma-treated spawn and straw is faster than that of PAW sprayed. The presence of RONS in the discharge, which is directly absorbed by the mushroom's spawn and straw treatment is a good environment for faster colonization and budding. The length of the stem is found to be highest in the mushroom spawn treated for three minutes and lowest in the straw treated for 15 minutes. The diameter of the stem is found to be the highest for eight minutes of PAW. The cap diameter is highest for three-minute spawn treated and lowest for 12-minute PAW. The total fresh weight and biological efficiency are highest in the two-minute spawn treated and lowest in the untreated case. Similarly, for the straw treated with plasma and PAW, the mushroom production is greater than the control spawn.

Furthermore, we have investigated the effects of cold atmospheric pressure plasma on the seed germination of cash crops (wheat, and cauliflower) and its use for the production of green leafy vegetables, and enhanced dormancy breaking of potatoes. The results show that longer treatment times increase seed wettability, while the contact angle decreases. Notably, we found that the germination of seeds is enhanced when PAW generated from GAD plasma is applied for 10 minutes in cauliflower planted in a petri dish (effect of water only) and for 15 minutes in a plastic glass (water and soil effect), which is supported by various germination parameters. Furthermore, the root and shoot lengths are maximum while 15 minutes of PAW is irrigated. Another potential advantage of using PAW made from GAD is the enhancement of quantity and quality of green leafy vegetables. The water absorbency rate of green leafy vegetables is maximum in 15 minutes of PAW, which is applied to the germination rate too. Similarly, the root and shoot lengths as well as chlorophyll content of the vegetable plants are highest while using PAW for 15 minutes, except while using PAW for 10 minutes in *Rayo* Marpha. Likewise, the fresh weight measurement of the green leafy vegetable plants is also highest while using PAW for 15 minutes, except while using PAW for 10 minutes in

Rayo Manakamana. Hence, PAW has a positive effect on germination, seedling growth, production, and chlorophyll content of leaf in the *Rayo* Marpha, *Chamsur*, and *Rayo* Manakamana. Moreover, higher rates of photosynthesis and total plant metabolism are often associated with higher quantities of chlorophyll. Another benefit of the PAW is to shorten the dormancy breaking time of potatoes observed in Janakdev and Khumal Ujjwal by soaking them in the PAW generated by GAD plasma.

Another important application of SDBD is to reduce bacterial activation in water. After eight minutes of treatment by SDBD almost 95% of *E. coli* and *S. aureus* surviving in water are reduced. It proves that the SDBD plasma is highly effective at sterilizing water. Out of the PAW of 0, 4, 8, 12, and 16 minutes applied to the petiole of the detached Tejpat leaves, the chlorophyll retention percentage of the leaves is highest for PAW of 12 minutes, which lasted for 576 ± 34 hrs. This shows that PAW is crucial in preserving the freshness of leaves for a longer time.

In conclusion, our research highlights the potential applications of plasma and PAW in improving the quality and quantity of agricultural products. This will aid in addressing issues related to low water absorption, delayed germination, low production, and stress related to seedling growth in the plants, as well as the longevity of green products and bacterial activation in water.

Limitations

As we started the experimental works on plasma application in agriculture within the Department, we are facing several limitations, as follows

i) The need to irrigate a substantial quantity of PAW, which poses a challenge for sustaining the research.

ii) The analysis tools and methods required for tests such as nutritional assessments and microscopic surface morphology are not readily available.

iii) Strong collaboration with a diverse range of stakeholders is essential.

iv) Establishing a greenhouse or agricultural farmhouse environment is currently not feasible.

v) The focus on multiple seed varieties introduces numerous parameters to consider, such as chlorophyll "A" and "B", and various nutritional analyses.

5.2 Recommendations

Based on the results of our experimental research on a lab scale, it is recommended that farmers integrate PAW into their farming practices to enhance the quality and quantity of

agricultural commodities. Moreover, efforts should be directed towards industrial-level production of PAW, ensuring accessibility for farmers in sufficient quantity as per their needs. Being a multidisciplinary work, collaboration with experts from various fields such as physics, chemistry, microbiology, botany, agronomy, biotechnology, and food sciences, are to be considered for further work. Government agencies must prioritize funding for such research and industrial endeavors, aiming to expand the applications of physics in daily life and facilitate sustained farming.

In the future, the current work can be expanded by taking into account the following.

i) Comparative nutritional analysis of plasma treated and untreated agricultural products.

ii) Maintaining uniformity while direct plasma treatment of seeds.

iii) Challenges and issues for upscaling the findings for a large quantity of PAW and a large number of seeds.

iv) Analysis of both chlorophyll "A" and "B" before and after plasma treatments.

v) Designing and fabricating power supply for larger scale applications, particularly for generating DBD and APJ from locally available materials.

vi) Strong collaboration with other stakeholders (Chemistry, Microbiology, Botany, NAST, NARC, farmers, etc.) and government policy review to implement the findings in real agricultural conditions.

CHAPTER 6

SUMMARY

This section summarizes the findings from the production of cold atmospheric pressure plasma, and the direct and indirect application of the three kinds of produced cold atmospheric pressure plasma to the seeds of cash crops, cereal crops, and green leafy vegetables. It also covers the results of bacterial activation in water and the length of time that detached leaves remain green.

We have successfully developed a low-cost power supply using locally available materials, enabling the generation of GAD plasma for various non-thermal plasma applications. The produced three plasma are characterized through comprehensive electrical and optical characterizations. To calculate the energy from time-averaged and charge dissipation from the capacitor (Lissajous plot), more convergent results are found in the Lissajous plot method. Our produced plasma also follows the classical rules of temperature of plasma species. The obtained temperature and density values of produced plasma have been compared with previous studies and found to be in good agreement.

We have significantly observed PAW's physical and chemical changes such as pH, electrical conductivity, oxidation-reduction potential, total dissolved solids, temperature, hydrogen peroxide, and nitrite and nitrate concentration generated through cold atmospheric pressure plasma: GAD, DBD, and APJ. These changes in parameters positively influence seed germination, growth rate, and root and shoot lengths. The creation of various RONS and the acidity of suspensions produced by plasma are crucial elements of water sterilization and bacterial inactivation. Bacterial cells are susceptible to mechanical stress caused by an electric field generated by plasma. This mechanical stress can lead to bacterial cell rupture and altered permeability, which can let internal components leak out and ultimately cause cell death. Furthermore, the increment of treatment time results in higher concentrations of RONS and ORP, while lowering the pH value of water leading to improved germination characteristics and productivity as well. However, the germination of seeds and the growth of seedlings are highly dependent on the pH values of the water; an excessively high or low pH can impact enzyme activity.

Similarly, higher content of H_2O_2 and NO_3 which apart from being the main source of nitrogen for plants could have unfavorably slowed the growth processes. Nitric Oxide (NO) and RONS are known to positively impact plant growth and development when present in low concentrations. Reactive species can, however, become toxic at high concentrations and impede or slow down several developmental processes. The low pH value, which is at the lower limit of the ideal pH required for seed growth, may also have contributed to the smaller growth in seedlings treated with PAW. This highlights the significance of optimizing exposure times for realizing the positive effects of PAW on agricultural production.

Our findings reveal that the water absorbency rate of the seeds increases with longer plasma treatment time. The increment of wettability of treated seeds is attributed to ultraviolet light and OH radicals, which are considered to be the primary components of atmospheric plasma. By activating various stress-related signaling pathways and inducing stress-responsive chemicals inside the seeds and seedlings when exposed to plasma, seeds can boost their resilience to environmental challenges like salinity, drought, or severe temperatures. Therefore, it can be concluded that seedlings grow quite well when treated with plasma. Our findings demonstrate that changes in the physical and chemical properties of PAW have a crucial role in germination and seedling growth as well as production, preserving the greenness of detached leaves, production enhancement of oyster mushrooms, and enhancing the quality of green leafy production and plant metabolism, with practical implications for improving the shelf life of leafy vegetables and for enhancing the more qualitative production of green leafy vegetables.

Overall, our study demonstrates the potential benefits of plasma for enhancing the quality and quantity of agricultural products, thereby helping to meet future food demands.

REFERENCES

Adhikari, B., Adhikari, M., Ghimire, B., Adhikari, B. C., Park, G., & Choi, E. H. (2020). Cold plasma seed priming modulates growth, redox homeostasis and stress response by inducing reactive species in tomato (*Solanum lycopersicum*). *Free Radical Biology and Medicine*, *156*, 57-69. doi: https://doi.org/10.1016/j.freeradbiomed.2020.06.003

Adhikari, B., Adhikari, M., Ghimire, B., Park, G., & Choi, E. H. (2019). Cold atmospheric plasma-activated water irrigation induces defense hormone and gene expression in tomato seedlings. *Scientific Reports*, *9*(1), 16080-16095. doi: https://doi.org/10.1038/s41598-019-52646-z

Agnihotri, A., & Seth, C. S. (2016). Exogenously applied nitrate improves the photosynthetic performance and nitrogen metabolism in tomato (*Solanum lycopersicum L. cv Pusa Rohini*) under arsenic (v) toxicity. *Physiology and Molecular Biology of Plants*, *22*, 341-349. doi: https://doi.org/10.1007/s12298-016-0370-2

Agun, L., Ahmad, N., Redzuan, N., Ali, M. F. A. M., Zainal, M. N. F., Misnal, M. F. I., & Ibrahim, R. K. R. (2020). Spawn treatment by cold plasma for increase mushroom germination and production. *IOP Conference Series: Materials Science and Engineering*, *884*(1), 012004-012010. doi: https://doi.org/10.1088/1757-899X/884/1/012004

Alves Junior, C., de Oliveira Vitoriano, J., da Silva, D. L. S., de Lima Farias, M., & de Lima Dantas, N. B. (2016). Water uptake mechanism and germination of *Erythrina velutina* seeds treated with atmospheric plasma. *Scientific Reports*, *6*(1), 33722-7pp. doi: https://doi.org/10.1038/srep33722

Aragón, C., & Aguilera, J. A. (2008). Characterization of laser induced plasmas by optical emission spectroscopy: A review of experiments and methods. *Spectrochimica Acta Part B: Atomic Spectroscopy*, *63*(9), 893-916. doi: https://doi.org/10.1016/j.sab.2008.05.010

Baldanov, B., & Ranzhurov, T. V. (2022). Effect of plasma treatment on surface wettability of wheat seeds. *High Energy Chemistry*, *56*(4), 294-298. doi: https://doi.org/10.1134/S0018143922040038

Batak, I., Dević, M., Gibal, Z., Grubišić, D., Poff, K. L., & Konjević, R. (2002). The effects of potassium nitrate and NO-donors on phytochrome A-and phytochrome B-specific induced germination of Arabidopsis thaliana seeds. *Seed Science Research*, *12*(4), 253-259. doi: https://doi.org/10.1079/SSR2002118

Benard, N., & Moreau, E. (2014). Electrical and mechanical characteristics of surface AC dielectric barrier discharge plasma actuators applied to airflow control. *Experiments in Fluids*, *55*, 1-43. doi: https://doi.org/10.1007/s00348-014-1846-x

Billah, M., Karmakar, S., Mina, F. B., Haque, M. N., Rashid, M. M., Hasan, M. F., & Talukder, M. R. (2021). Investigation of mechanisms involved in seed germination enhancement, enzymatic activity and seedling growth of rice *(Oryza Sativa L.)* using LPDBD (Ar+Air) plasma. *Archives of Biochemistry and Biophysics*, *698*, 108726-10pp. doi: https://doi.org/10.1016/j.abb.2020.108726

Biloiu, C., Sun, X., Harvey, Z., & Scime, E. (2006). Determination of rotational and vibrational temperatures of a nitrogen helicon plasma. *Review of Scientific Instruments*, *77*, 10F117-5pp. doi: https://doi.org/10.1063/1.2219392

Bissell, C., & Chapman, D. (1992). *Digital signal transmission*. Cambridge University Press.

Blundell, S. J., & Blundell, K. M. (2010). *Concepts in thermal physics*. Oxford University Press, United Kingdom.

Bogaerts, A., Neyts, E., Gijbels, R., & Van der Mullen, J. (2002). Gas discharge plasmas and their applications. *Spectrochimica Acta Part B: Atomic Spectroscopy*, *57*(4), 609-658. doi: https://doi.org/10.1016/S0584-8547(01)00406-2

Bradu, C., Kutasi, K., Magureanu, M., Puač, N., & Živković, S. (2020). Reactive nitrogen species in plasma-activated water: generation, chemistry and application in agriculture. *Journal of Physics D: Applied Physics*, *53*(22), 223001-55pp. doi: https://doi.org/10.1088/1361-6463/ab795a

Bruggeman, P. J., Sadeghi, N., Schram, D., & Linss, V. (2014). Gas temperature determination from rotational lines in non-equilibrium plasmas: A review. *Plasma Sources Science and Technology*, *23*(2), 023001-18pp. doi: https://doi.org/10.1088/0963-0252/23/2/023001

Chalise, R., Bhandari, P., Sharma, S., Basnet, S., Subedi, D. P., & Khanal, R. (2023b). Enhancement of wheat yield by atmospheric pressure plasma treatment. *AIP Advances*, *13*(6), 065105-7pp. doi: https://doi.org/10.1063/5.0156552

Chalise, R., Dahal, A., Basnet, S., Sharma, S., Pant, D. R., & Khanal, R. (2024). Effect of plasma-activated water on chlorophyll retention in detached Tejpat (*Cinnamomum tamala*) leaves. *Heliyon*, *10*, e24480-11pp. doi: https://doi.org/10.1016/j.heliyon.2024.e24480

Chalise, R., Niroula, A., Shrestha, P., Paudel, B., Subedi, D., & Khanal, R. (2023a). A low-cost goniometer for contact angle measurements using drop image analysis: Development and validation. *AIP Advances*, *13*(8), 085123-6pp. doi: https://doi.org/10.1063/5.0164668

Chalise, R., Regmi, K., Nepal, S., Sharma, S., Basnet, S., & Khanal, R. (2024d). Characterization of atmospheric pressure circular dielectric barrier discharge via electrical and optical methods. *BIBECHANA*, *21*(3), 187. doi: https://doi.org/10.3126/bibechana.v21i3.62034

Chalise, R., Shrestha, P., Sharma, S., Basnet, S., Mishra, L. N., & Khanal, R. (2023). Enhancing seed germination and growth parameters of cauliflower (*Brassica oleracea*, variety *Botrytis*) using plasma-activated water. *Journal of Physics D: Applied Physics*, *56*(50), 505201-12pp. doi: https://doi.org/10.1088/1361-6463/acf588

Chalise, R., Tamang, A., Kattel, A., Sharma, S., Basnet, S., & Khanal, R. (2024c). Impact of plasma-activated water on germination, growth, and production of green leafy vegetables. *AIP Advances*, *14*(6), 065318. doi: https://doi.org/10.1063/5.0205372

Chen, F. (2016). *Introduction to plasma physics and controlled nuclear fusion* (3rd ed.). Springer International Publishing, Switzerland.

Chen, H., Yuan, D., Wu, A., Lin, X., & Li, X. (2021). Review of low-temperature plasma nitrogen fixation technology. *Waste Disposal & Sustainable Energy*, *3*, 201-217. doi: https://doi.org/10.1007/s42768-021-00074-z

Chen, H. H., Chen, Y. K., & Chang, H. C. (2012). Evaluation of physicochemical properties of plasma treated brown rice. *Food Chemistry*, *135*(1), 74-79. doi: https://doi.org/10.1016/j.foodchem.2012.04.092

Chen, K., Li, G.-J., Bressan, R. A., Song, C.-P., Zhu, J.-K., & Zhao, Y. (2020). Abscisic acid dynamics, signaling, and functions in plants. *Journal of Integrative Plant Biology*, *62*(1), 25-54. doi: https://doi.org/10.1111/jipb.12899

Chen, Z., Lin, L., Cheng, X., Gjika, E., & Keidar, M. (2016). Effects of cold atmospheric plasma generated in deionized water in cell cancer therapy. *Plasma Processes and Polymers*, *13*(12), 1151-1156. doi: https://doi.org/10.1002/ppap.201600086

Chiappim, W., Sampaio, A. d. G., Miranda, F., Fraga, M., Petraconi, G., da Silva Sobrinho, A., & Pessoa, R. (2021). Antimicrobial effect of plasma-activated tap water on *staphylococcus aureus, escherichia coli*, and *Candida* albicans. *Water*, *13*(11), 1480-16pp. doi: https://doi.org/10.3390/w13111480

Choi, E. H. (2015). Plasma bioscience and medicines. *Vacuum Magazine*, *2*(4), 9-15. doi: https://doi.org/10.5757/vacmac.2.4.9

Choi, E. H., Kaushik, N. K., Hong, Y. J., Lim, J. S., Choi, J. S., & Han, I. (2022). Plasma bioscience for medicine, agriculture and hygiene applications. *Journal of the Korean Physical Society*, *80*(8), 817-851. doi: https://doi.org/10.1007/s40042-022-00442-w

Cui, D., Yin, Y., Wang, J., Wang, Z., Ding, H., Ma, R., & Jiao, Z. (2019). Research on the physio-biochemical mechanism of non-thermal plasma-regulated seed germination and early seedling development in Arabidopsis. *Frontiers in Plant Science*, *10*, 1322-12pp. doi: https://doi.org/10.3389/fpls.2019.01322

Debye, P., & Hückel, E. (1923). The theory of electrolytes. I. freezing point depression and related phenomena. *Phyikalishce Zeitschrift.*, *24*, 185-206. Retrieved from `http://digital.library.wisc.edu/1793/79225`

Dhakal, O. B., Dahal, R., Acharya, T. R., Lamichhane, P., Kaushik, N. K., Choi, E. H., & Chalise, R. (2023). Effects of spark dielectric barrier discharge plasma on water sterilization and seed germination. *Current Applied Physics*, *54*, 49-58. doi: https://doi.org/10.1016/j.cap.2023.08.006

Dimitrakellis, P., Giannoglou, M., Zeniou, A., Gogolides, E., & Katsaros, G. (2021). Food container employing a cold atmospheric plasma source for prolonged preservation of plant and animal origin food products. *MethodsX*, *8*, 101177-12pp. doi: https://doi.org/10.1016/j.mex.2020.101177

Dobrin, D., Magureanu, M., Mandache, N. B., & Ionita, M. D. (2015). The effect of non-thermal plasma treatment on wheat germination and early growth. *Innovative Food Science & Emerging Technologies*, *29*, 255-260. doi: https://doi.org/10.1016/j.ifset.2015.02.006]

Dubinov, A., Lazarenko, E., & Selemir, V. (2000). Effect of glow discharge air plasma on grain crops seed. *IEEE Transactions on Plasma Science*, *28*(1), 180-183. doi: 10.1109/27.842898

Eliasson, B., & Kogelschatz, U. (1991). Nonequilibrium volume plasma chemical processing. *IEEE Transactions on Plasma Science*, *19*(6), 1063-1077. doi: 10.1109/27.125031

El-Maarouf-Bouteau, H., & Bailly, C. (2008). Oxidative signaling in seed germination and dormancy. *Plant Signaling & Behavior*, *3*(3), 175-182. doi: https://doi.org/10.4161/psb.3.3.5539

El-Maarouf-Bouteau, H., Sajjad, Y., Bazin, J., Langlade, N., Cristescu, S. M., Balzergue, S., Baudouin, E., & Bailly, C. (2015). Reactive oxygen species, abscisic acid and ethylene interact to regulate sunflower seed germination. *Plant, Cell & Environment*, *38*(2), 364-374. doi: https://doi.org/10.1111/pce.12371

Ercan, U. K., Wang, H., Ji, H., Fridman, G., Brooks, A. D., & Joshi, S. G. (2013). Nonequilibrium plasma-activated antimicrobial solutions are broad-spectrum and retain their efficacies for extended period of time. *Plasma Processes and Polymers*, *10*(6), 544-555. doi: https://doi.org/10.1002/ppap.201200104

Fan, L., Liu, X., Ma, Y., & Xiang, Q. (2020). Effects of plasma-activated water treatment on seed germination and growth of mung bean sprouts. *Journal of Taibah University for Science*, *14*(1), 823-830. doi: https://doi.org/10.1080/16583655.2020.1778326

Fan, Z., Qi, H., Liu, Y., Yan, H., & Ren, C. (2016). Effects of airflow on the distribution of filaments in atmospheric AC dielectric barrier discharge. *Physics of Plasmas*, *23*(12), 123520-10pp. doi: https://doi.org/10.1063/1.4972095

Finch-Savage, W. E., & Leubner-Metzger, G. (2006). Seed dormancy and the control of germination. *New Phytologist*, *171*(3), 501-523. doi: https://doi.org/10.1111/j.1469-8137.2006.01787.x

FNCCI. (2024). *Agriculture*. Retrieved 2024 January 15, from `https://www.fncci.org/agriculture-148.html`.

Fridman, A. (2012). *Plasma decontamination of gases and liquids*. Cambridge University Press, United Kingdom.

Fridman, A., & Kennedy, L. A. (2004). *Plasma physics and engineering*. CRC press, United States. doi: https://doi.org/10.1201/9781482293630

Gharagozalian, M., Dorranian, D., & Ghoranneviss, M. (2017). Water treatment by the AC gliding arc air plasma. *Journal of Theoretical and Applied Physics*, *11*, 171-180. doi: https://doi.org/10.1007/s40094-017-0254-z

Ghimire, B. (2018). *Characteristics of low temperature atmospheric pressure plasma jets interacting with liquids and transport mechanism of reactive species* (Ph.D. Thesis). Department of Electrical and Biological Physics, Kwangwoon University, Seoul, South Korea.

Gitelson, A. A., Buschmann, C., & Lichtenthaler, H. K. (1999). The chlorophyll fluorescence ratio F735/F700 as an accurate measure of the chlorophyll content in plants. *Remote Sensing of Environment*, *69*(3), 296-302. doi: https://doi.org/10.1016/S0034-4257(99)00023-1

Goussous, S. J., Samarah, N. H., Alqudah, A. M., & Othman, M. O. (2010). Enhancing seed germination of four crop species using an ultrasonic technique. *Experimental Agriculture*, *46*(2), 231-242. doi: https://doi.org/10.1017/S0014479709991062

Graves, D. B. (2012). The emerging role of reactive oxygen and nitrogen species in redox biology and some implications for plasma applications to medicine and biology. *Journal of Physics D: Applied Physics*, *45*(26), 263001-42pp. doi: https://doi.org/10.1088/0022-3727/45/26/263001

Grill, A. (1994). *Cold plasma in materials fabrication* (Vol. 151). IEEE Press, New York.

Guangwu, Z., & Xuwen, J. (2014). Roles of gibberellin and auxin in promoting seed germination and seedling vigor in *Pinus massoniana*. *Forest Science*, *60*(2), 367-373. doi: https://doi.org/10.5849/forsci.12-143

Gulec, A., Bozduman, F., & Hala, A. M. (2015). Atmospheric pressure 2.45-GHz microwave helium plasma. *IEEE Transactions on Plasma Science*, *43*(3), 786–790. doi: https://doi.org/10.1109/TPS.2015.2403280

Guofeng, X., & Xinwei, D. (2012). Electrical characterization of a reverse vortex gliding arc reactor in atmosphere. *IEEE Transactions on Plasma Science*, *40*(12), 3458-3464. doi: 10.1109/TPS.2012.2219557

Guragain, R. P., Baniya, H. B., Pradhan, S. P., Dhungana, S., Chhetri, G. K., Sedhai, B., Panta, G.P., Joshi, U.M., Pandey, B.P., & Subedi D.P. (2021a). Impact of non-thermal plasma treatment on the seed germination and seedling development of carrot (*Daucus carota sativus L.*). *Journal of Physics Communications*, *5*(12), 125011-17pp. doi: https://doi.org/10.1088/2399-6528/ac4081

Guragain, R. P., Baniya, H. B., Pradhan, S. P., Pandey, B. P., & Subedi, D. P. (2021d). Influence of plasma-activated water (PAW) on the germination of

radish, fenugreek, and pea seeds. *AIP Advances*, *11*(12), 125304-10pp. doi: https://doi.org/10.1063/5.0070800

Guragain, R. P., Baniya, H. B., Shrestha, B., Guragain, D. P., & Subedi, D. P. (2023). Germination enhancement of mustard (*Brassica nigra*) seeds using dielectric barrier discharge (DBD). *AIP Advances*, *13*(3), 035338-14pp. doi: https://doi.org/10.1063/5.0146955

Guragain, R. P., Baniya, H. B., Shrestha, B., Guragain, D. P., & Subedi, D. P. (2023b). Improvements in germination and growth of sprouts irrigated using plasma activated water (PAW). *Water*, *15*(4), 744-12pp. doi: https://doi.org/10.3390/w15040744

Guragain, R. P., Pradhan, S. P., Baniya, H. B., Pandey, B. P., Basnet, N., Sedhai, B., Dhungana, S., Chhetri, G.K., Joshi, U.M., & Subedi, D. P. (2021c). Impact of plasma-activated water (PAW) on seed germination of soybean. *Journal of Chemistry*, *2021*, 1-9 doi: https://doi.org/10.1155/2021/7517052

Hashizume, H., Kitano, H., Mizuno, H., Abe, A., Yuasa, G., Tohno, S.,Tanaka H., Ishikawa, K., Matsumoto, S., Sakakibara, H., & Nikawa S. (2021). Improvement of yield and grain quality by periodic cold plasma treatment with rice plants in a paddy field. *Plasma Processes and Polymers*, *18*(1), 181-11pp. doi: https://doi.org/10.1002/ppap.202000181

Holmes, S. C., Wells, D. E., Pickens, J. M., & Kemble, J. M. (2019). Selection of heat tolerant lettuce (*Lactuca sativa L.*) cultivars grown in deep water culture and their marketability. *Horticulturae*, *5*(3), 50-61. doi: https://doi.org/10.3390/horticulturae5030050

Hsu, S. C., Kong, T. K., Chen, C. Y., & Chen, H. L. (2023). Plasma-activated water affects the antioxidant contents in water spinach. *Applied Sciences*, *13*(5), 3341. doi: https://doi.org/10.3390/app13053341

Huang, H., Ullah, F., Zhou, D.-X., Yi, M., & Zhao, Y. (2019). Mechanisms of ros regulation of plant development and stress responses. *Frontiers in plant science*, *10*, 800. doi: https://doi.org/10.3389/fpls.2019.00800

Huang, S., Li, T., Zhang, Z., & Ma, P. (2019). Rotational and vibrational temperatures in the spark plasma by various discharge energies and strategies. *Applied Energy*, *251*, 113358-11pp. doi: https://doi.org/10.1016/j.apenergy.2019.113358

Indarto, A., Choi, J. W., Lee, H., & Song, H. K. (2008). Decomposition of greenhouse gases by plasma. *Environmental Chemistry Letters*, *6*, 215-222. doi: https://doi.org/10.1007/s10311-008-0160-3

Indumathy, B., Ananthanarasimhan, J., Rao, L., Yugeswaran, S., & Ananthapadmanabhan, P. V. (2022). Catalyst-free production of ammonia by means of interaction between a gliding arc plasma and water surface. *Journal of Physics D: Applied Physics*, *55*(39), 395501-11pp. doi: https://doi.org/10.1088/1361-6463/ac7b52

Iqbal, N., Umar, S., & Khan, N. A. (2015). Nitrogen availability regulates proline and ethylene production and alleviates salinity stress in mustard (*Brassica juncea*). *Journal of Plant Physiology*, *178*, 84-91. doi: https://doi.org/10.1016/j.jplph.2015.02.006

Iqdiam, B. M., Abuagela, M. O., Boz, Z., Marshall, S. M., Goodrich-Schneider, R., Sims, C. A., MacIntosh, A. J., & Welt, B. A. (2020). Effects of atmospheric pressure plasma jet treatment on aflatoxin level, physiochemical quality, and sensory attributes of peanuts. *Journal of Food Processing and Preservation*, *44*(1), e14305-11pp. doi: https://doi.org/10.1111/jfpp.14305

Ivankov, A., Nauciene, Z., Zukiene, R., Degutyte-Fomins, L., Malakauskiene, A., Kraujalis, P., ... Mildaziene, V. (2020). Changes in growth and production of non-psychotropic cannabinoids induced by pre-sowing treatment of hemp seeds with cold plasma, vacuum and electromagnetic field. *Applied Sciences*, *10*(23), 8519-14pp. doi: https://doi.org/10.3390/app10238519

Jaeger, G. (1998). The Ehrenfest classification of phase transitions: Introduction and evolution. *Archive for History of Exact Sciences*, *53*, 51-81. doi: https://doi.org/10.1007/s004070050021

Jones, K. W., & Sanders, D. (1987). The influence of soaking pepper seed in water or potassium salt solutions on germination at three temperatures. *Journal of Seed Technology*, *11*(1), 97-102. Retrieved from `https://www.jstor.org/stable/23432941`

Kaushik, N. K., Ghimire, B., Li, Y., Adhikari, M., Veerana, M., Kaushik, N., Masur, K. (2019). Biological and medical applications of plasma-activated media, water and solutions. *Biological Chemistry*, *400*(1), 39-62. doi: https://doi.org/10.1515/hsz-2018-0226

Kawano, A., Yamasaki, R., Sakakura, T., Takatsuji, Y., Haruyama, T., Yoshioka, Y., & Ariyoshi, W. (2020). Reactive oxygen species penetrate persister cell membranes of Escherichia coli for effective cell killing. *Frontiers in Cellular and Infection Microbiology*, *10*, 496-505. doi: https://doi.org/10.3389/fcimb.2020.00496

Khatun, M., Islam, M., & Haque, M. (2016). Studies of thunderstorms and lightning on human health, agriculture and fisheries in Mymensingh and Jamalpur district

of Bangladesh. *Progressive Agriculture*, *27*(1), 57-63. Retrieved from `http://www.banglajol.info/index.php/PA`

Kim, S. H., Seo, J., Hong, Y., Shin, Y., Chung, H., An, H., Kim, C., & Lee, H.s (2023). Construction of an underwater plasma and fenton hybrid system for the rapid oxidation of organic dyes and antibiotics. *Journal of Water Process Engineering*, *52*, 103519-10pp. doi: https://doi.org/10.1016/j.jwpe.2023.103519

Kramida, A., Yu. Ralchenko, Reader, J., & and NIST ASD Team. (2023). *Nist atomic spectra database (ver. 5.10)*. National Institute of Standards and Technology, United States. Retrieved 2023 November 28, from `https://physics.nist.gov/asd` doi: https://dx.doi.org/10.18434/T4W30F

Krapivina, S., Filippov, A., Levitskaya, T., & Bakhvalov, A. (1994). Gas plasma treatment of plant seeds. 5, 281, 315. *US Patent*.

Kučerová, K., Henselová, M., Slováková, L., & Hensel, K. (2019). Effects of plasma activated water on wheat: Germination, growth parameters, photosynthetic pigments, soluble protein content, and antioxidant enzymes activity. *Plasma Processes and Polymers*, *16*(3), 1800131-14pp. doi: https://doi.org/10.1002/ppap.201800131

Kunhardt, E. E. (2000). Generation of large-volume, atmospheric-pressure, nonequilibrium plasmas. *IEEE Transactions on Plasma Science*, *28*(1), 189-200. doi: 10.1109/27.842901

Lamichhane, P., Acharya, T. R., Park, J., Amsalu, K. A., Park, B., & Choi, E. H. (2023). Surface activation of thin polyvinyl alcohol films by atmospheric pressure plasma jet: Influence of electron temperature. *Plasma Processes and Polymers*, *20*(11), e2300102. doi: https://doi.org/10.1002/ppap.202300102

Langmuir, I. (1928). Oscillations in ionized gases. *Proceedings of the National Academy of Sciences of the United States of America*, *14*(8), 627-637. doi: https://doi.org/10.1073/pnas.14.8.627

Le, T. Q. X., Nguyen, L. N., Nguyen, T. T., Choi, E. H., Nguyen, Q. L., Kaushik, N. K., & Dao, N. T. (2022). Effects of cold plasma treatment on physical modification and endogenous hormone regulation in enhancing seed germination and radicle growth of mung bean. *Applied Sciences*, *12*(20), 10308-12pp. doi: https://doi.org/10.3390/app122010308

Lee, Y., Lee, Y. Y., Kim, Y. S., Balaraju, K., Mok, Y. S., Yoo, S. J., & Jeon, Y. (2021). Enhancement of seed germination and microbial disinfection on *ginseng*

by cold plasma treatment. *Journal of Ginseng Research*, *45*(4), 519-526. doi: https://doi.org/10.1016/j.jgr.2020.12.002

Li, Y., Sun, Y., Jiang, J., & Liu, J. (2019). Spectroscopic determination of leaf chlorophyll content and color for genetic selection on sassafras tzumu. *Plant Methods*, *15*, 1-11. doi: https://doi.org/10.1186/s13007-019-0458-0

Ling, L., Jiafeng, J., Jiangang, L., Minchong, S., Xin, H., Hanliang, S., & Yuanhua, D. (2014). Effects of cold plasma treatment on seed germination and seedling growth of soybean. *Scientific Reports*, *4*(1), 5859-7pp. doi: https://doi.org/10.1038/srep05859

Ling, L., Jiangang, L., Minchong, S., Chunlei, Z., & Yuanhua, D. (2015). Cold plasma treatment enhances oilseed rape seed germination under drought stress. *Scientific Reports*, *5*(1), 13033-10pp. doi: https://doi.org/10.1038/srep13033

Liu, B., Honnorat, B., Yang, H., Arancibia, J., Rajjou, L., & Rousseau, A. (2018). Non-thermal DBD plasma array on seed germination of different plant species. *Journal of Physics D: Applied Physics*, *52*(2), 025401-33pp. doi: 10.1088/1361-6463/aae771

Liu, C., Chen, C., Jiang, A., Sun, X., Guan, Q., & Hu, W. (2020). Effects of plasma-activated water on microbial growth and storage quality of fresh-cut apple. *Innovative Food Science & Emerging Technologies*, *59*, 102256-25pp. doi: https://doi.org/10.1016/j.ifset.2019.102256

Liu, Y., Ye, N., Liu, R., Chen, M., & Zhang, J. (2010a). H_2O_2 mediates the regulation of ABA catabolism and GA biosynthesis in Arabidopsis seed dormancy and germination. *Journal of Experimental Botany*, *61*(11), 2979-2990. doi: https://doi.org/10.1093/jxb/erq125

Lofthus, A., & Krupenie, P. H. (1977). The spectrum of molecular nitrogen. *Journal of Physical and Chemical Reference Data*, *6*(1), 113-307. doi: https://doi.org/10.1063/1.555546

Lotfy, K., Al-Harbi, N. A., & Abd El-Raheem, H. (2019). Cold atmospheric pressure nitrogen plasma jet for enhancement germination of wheat seeds. *Plasma Chemistry and Plasma Processing*, *39*, 897-912. doi: https://doi.org/10.1007/s11090-019-09969-6

Lukes, P., Brisset, J. L., & Locke, B. R. (2012a). Biological effects of electrical discharge plasma in water and in gas-liquid environments. *Plasma Chemistry and Catalysis in Gases and Liquids*, 309-352. doi: 10.1002/9783527649525

Lukes, P., Locke, B. R., & Brisset, J. L. (2012). Aqueous-phase chemistry of electrical discharge plasma in water and in gas-liquid environments. *Plasma Chemistry and Catalysis in Gases and Liquids*, *1*, 243-308. doi: https://doi.org/10.1002/9783527649525

Ma, R., Wang, G., Tian, Y., Wang, K., Zhang, J., & Fang, J. (2015). Non-thermal plasma-activated water inactivation of food-borne pathogen on fresh produce. *Journal of Hazardous Materials*, *300*, 643-651. doi: https://doi.org/10.1016/j.jhazmat.2015.07.061

Mangolini, L., Orlov, K., Kortshagen, U., Heberlein, J., & Kogelschatz, U. (2002). Radial structure of a low-frequency atmospheric-pressure glow discharge in helium. *Applied Physics Letters*, *80*(10), 1722-1724. doi: https://doi.org/10.1063/1.1458684

Manley, T. (1943). The electric characteristics of the ozonator discharge. *Transactions of the Electrochemical Society*, *84*(1), 83-14pp. doi: 10.1149/1.3071556

Mao, L., Mhaske, P., Zing, X., Kasapis, S., Majzoobi, M., & Farahnaky, A. (2021). Cold plasma: Microbial inactivation and effects on quality attributes of fresh and minimally processed fruits and ready-to-eat vegetables. *Trends in Food Science & Technology*, *116*, 146-175. doi: https://doi.org/10.1016/j.tifs.2021.07.002

Marschner, H. (2011). *Marschner's mineral nutrition of higher plants* (3rd ed.). Academic press, United States.

Matějka, F., Galář, P., Khun, J., Scholtz, V., & Ksová, K. (2023). Mechanisms leading to plasma activated water high in nitrogen oxides. *Physics Scripta*, *98*(4), 045619-12pp. doi: https://doi.org/10.1088/1402-4896/acc48e

Meng, S., Peng, J.-S., He, Y.-N., Zhang, G.-B., Yi, H.-Y., Fu, Y.-L., & Gong, J.-M. (2016). Arabidopsis NRT 1.5 mediates the suppression of nitrate starvation-induced leaf senescence by modulating foliar potassium level. *Molecular Plant*, *9*(3), 461-470. doi: http://dx.doi.org/10.1016/j.molp.2015.12.015

Mhamdi, A., & Van Breusegem, F. (2018). Reactive oxygen species in plant development. *Development*, *145*(15), dev164376. doi: https://doi.org/10.1242/dev.164376

Miano, A. C., Forti, V. A., Abud, H. F., Gomes-Junior, F. G., Cicero, S. M., & Augusto, P. E. D. (2015). Effect of ultrasound technology on barley seed germination and vigour. *Seed Science and Technology*, *43*(2), 297-302. doi: https://doi.org/10.15258/sst.2015.43.2.10

Milhan, N. V. M., Chiappim, W., Sampaio, A. d. G., Vegian, M. R. d. C., Pessoa, R. S., & Koga-Ito, C. Y. (2022). Applications of plasma-activated water in dentistry:

A review. *International Journal of Molecular Sciences*, *23*(8), 4131-26pp. doi: https://doi.org/10.3390/ijms23084131

Mitra, A., Li, Y.-F., Klämpfl, T. G., Shimizu, T., Jeon, J., Morfill, G. E., & Zimmermann, J. L. (2014). Inactivation of surface-borne microorganisms and increased germination of seed specimen by cold atmospheric plasma. *Food and Bioprocess Technology*, *7*(3), 645-653. doi: https://doi.org/10.1007/s11947-013-1126-4

Møller, I. M., Jensen, P. E., & Hansson, A. (2007). Oxidative modifications to cellular components in plants. *Annual Review of Plant Biology*, *58*, 459-481. doi: https://doi.org/10.1146/annurev.arplant.58.032806.103946

Moon, J.-D., & Chung, H.-S. (2000). Acceleration of germination of tomato seed by applying AC electric and magnetic fields. *Journal of electrostatics*, *48*(2), 103-114. doi: https://doi.org/10.1016/S0304-3886(99)00054-6

Motrescu, I., Ciolan, M. A., Calistru, A. E., & Jitareanu, G. (2023). Germination and growth improvement of some micro-greens under the influence of reactive species produced in a non-thermal plasma (NTP). *Agronomy*, *13*(1), 150-12pp. doi: https://doi.org/10.3390/agronomy13010150

Murray, L. T. (2016). Lightning NO_x and impacts on air quality. *Current Pollution Reports*, *2*(2), 115-133. doi: https://doi.org/10.1007/s40726-016-0031-7

Mutaf-Yardimci, O., Saveliev, A. V., Fridman, A. A., & Kennedy, L. A. (2000). Thermal and nonthermal regimes of gliding arc discharge in air flow. *Journal of Applied Physics*, *87*(4), 1632-1641. doi: 10.1063/1.372071

Nelson, E. B. (2018). The seed microbiome: origins, interactions, and impacts. *Plant and Soil*, *422*, 7-34. doi: https://doi.org/10.1007/s11104-017-3289-7

Obaisi, A. (2017). Overpopulation: a threat to sustainable agriculture and food security in developing countries? A review. *International Journal of Agriculture and Food Security*, *6*, 921-927. doi: 10.13140/RG.2.2.20613.04325

Oehmigen, K., Hähnel, M., Brandenburg, R., Wilke, C., Weltmann, K.-D., & Von Woedtke, T. (2010). The role of acidification for antimicrobial activity of atmospheric pressure plasma in liquids. *Plasma Processes and Polymers*, *7*(3), 250-257. doi: https://doi.org/10.1002/ppap.200900077

Ollegott, K., Wirth, P., Oberste-Beulmann, C., Awakowicz, P., & Muhler, M. (2020). Fundamental properties and applications of dielectric barrier discharges in plasma-catalytic processes at atmospheric pressure. *Chemistry Engineering Tecnology*, *92*(10), 1542-1558. doi: https://doi.org/10.1002/cite.202000075

Osawa, N., & Yoshioka, Y. (2012). Basic processes in fully and partially ionized plasmas-generation of low-frequency homogeneous dielectric barrier discharge at atmospheric pressure. *IEEE Transactions on Plasma Science*, *40*(1), 2-8. doi: 10.1109/TPS.2011.2172634

Panth, M., Hassler, S. C., & Baysal-Gurel, F. (2020). Methods for management of soilborne diseases in crop production. *Agriculture*, *10*(1), 1-21. doi: https://doi.org/10.3390/agriculture10010016

Paschen, F. (1889). On the potential difference required for spark transfer in air, hydrogen and carbonic acid at different pressures. *Annals of Physics*, *273*(5), 69-75.

Pawłat, J., Starek, A., Sujak, A., Terebun, P., Kwiatkowski, M., Budzeń, M., & Andrejko, D. (2018). Effects of atmospheric pressure plasma jet operating with DBD on *Lavatera Thuringiaca L.* seeds germination. *PLoS One*, *13*(4), e0194349-12pp. doi: https://doi.org/10.1371/journal.pone.0194349

Pourali, N., Lai, K., Gregory, J., Gong, Y., Hessel, V., & Rebrov, E. V. (2023). Study of plasma parameters and gas heating in the voltage range of nondischarge to full-discharge in a methane-fed dielectric barrier discharge. *Plasma Processes and Polymers*, *20*(1), 2200086-10pp. doi: https://doi.org/10.1002/ppap.202200086

Puač, N., Škoro, N., Spasić, K., Živković, S., Milutinović, M., Malović, G., & Petrović, Z. L. (2018). Activity of catalase enzyme in paulownia tomentosa seeds during the process of germination after treatments with low pressure plasma and plasma activated water. *Plasma Processes and Polymers*, *15*(2), 1700082-12pp. doi: https://doi.org/10.1002/ppap.201700082

Ramalho, J., Marques, N., Semedo, J., Matos, M., & Quartin, V. (2002). Photosynthetic performance and pigment composition of leaves from two tropical species is determined by light quality. *Plant Biology*, *4*(01), 112-120. doi: https://doi.org/10.1055/s-2002-20443

Ranal, M. A., Santana, D. G. d., Ferreira, W. R., & Mendes-Rodrigues, C. (2009). Calculating germination measurements and organizing spreadsheets. *Brazilian Journal of Botany*, *32*, 849-855. doi: https://doi.org/10.1590/S0100-84042009000400022

Rathore, V., Patel, D., Butani, S., & Nema, S. K. (2021). Investigation of physicochemical properties of plasma activated water and its bactericidal efficacy. *Plasma Chemistry and Plasma Processing*, *41*, 871-902. doi: https://doi.org/10.1007/s11090-021-10161-y

Roth, J. R. (2001). *Industrial plasma engineering: Applications to nonthermal plasma processing* (Vol. 2). CRC Press,United States.

Roy, N., & Talukder, M. (2018). Effect of pressure on the properties and species production in gliding arc Ar, O_2, and air discharge plasmas. *Physics of Plasmas*, *25*, 093502-18pp. doi: https://doi.org/10.1063/1.5043182

Ruffel, S. (2018). Nutrient-related long-distance signals: common players and possible cross-talk. *Plant and Cell Physiology*, *59*(9), 1723-1732. doi: https://doi.org/10.1093/pcp/pcy152

Russ, S., Strykowski, P. J., & Pfender, E. (1994). Mixing in plasma and low density jets. *Experiments in Fluids*, *16*(5), 297-307. doi: https://doi.org/10.1007/BF00195428

Sansan, P., Dehui, X., Miao, Q., Rong, L., Zhang, X., Zhang, H., & Liu, D. (2021). Investigation of optimum discharge characteristics and chemical activity of AC driven air plasma jet and its anticancer effect. *Plasma Science and Technology*, *23*(12), 125401-12pp. doi: https://doi.org/10.1088/2058-6272/ac2482

Selcuk, M., Oksuz, L., & Basaran, P. (2008). Decontamination of grains and legumes infected with *Aspergillus spp.* and *Penicillum spp.* by cold plasma treatment. *Bioresource Technology*, *99*(11), 5104-5109. doi: https://doi.org/10.1016/j.biortech.2007.09.076

Sharma, H. P., Patel, A. H., & Pal, M. (2021). Effect of plasma activated water (PAW) on fruits and vegetables. *American Journal of Food and Nutrition*, *9*, 60-68. doi: https://doi.org/10.12691/ajfn-9-2-1

Sharma, S., Chalise, R., Basnet, S., Lamichahane, H. P., & Khanal, R. (2024). Development of a low-cost plasma source using fly-back transformer for atmospheric pressure gliding arc discharge. *Physics of Plasmas*, *31*, 043509-10pp. doi: https://doi.org/10.1063/5.0187159

Shelar, A., Singh, A. V., Dietrich, P., Maharjan, R. S., Thissen, A., Didwal, P. N., Shindee, M., Lauxl., P., Luch., A., Mathe., V., Jahnkeg, T., Chaskar, M., & Patil, R.(2022). Emerging cold plasma treatment and machine learning prospects for seed priming: a step towards sustainable food production. *RSC Advances*, *12*(17), 10467-10488. doi: https://doi.org/10.1039/D2RA00809B

Shelar, A., Singh, A. V., Maharjan, R. S., Laux, P., Luch, A., Gemmati, D., Shelar, A. Chaskar, M., Singh, S.P, & Patil., R. (2021). Sustainable agriculture through multidisciplinary seed nanopriming: prospects of opportunities and challenges. *Cells*, *10*(9), 2428-22pp. doi: https://doi.org/10.3390/cells10092428

Shi, M. F., Fan, J. J., Li, S. J., Yu, X. L., & Liang, X. M. (2014). The influence of high voltage electric field for barley seed germination and its mechanism. *Applied Mechanics and Materials*, *675*, 1142-1145. doi: https://doi.org/10.4028/www.scientific.net/amm.675-677.1142

Šírová, J., Sedlářová, M., Piterková, J., Luhová, L., & Petřivalskỳ, M. (2011). The role of nitric oxide in the germination of plant seeds and pollen. *Plant Science*, *181*(5), 560-572. doi: https://doi.org/10.1016/j.plantsci.2011.03.014

Stoleru, V., Burlica, R., Mihalache, G., Dirlau, D., Padureanu, S., Teliban, G.-C., Patras, A. (2020). Plant growth promotion effect of plasma activated water on Lactuca sativa L. cultivated in two different volumes of substrate. *Scientific Reports*, *10*(1), 20920-15pp. doi: https://doi.org/10.1038/s41598-020-77355-w

Su, L., Lan, Q., Pritchard, H. W., Xue, H., & Wang, X. (2016). Reactive oxygen species induced by cold stratification promote germination of hedysarum scoparium seeds. *Plant physiology and biochemistry*, *109*, 406-415. doi: https://doi.org/10.1016/j.plaphy.2016.10.025

Subramanian, P., Rao, H., Shivapuji, A. M., Girard Lauriault, P. L., & Rao, L. (2021). Plasma-activated water from DBD as a source of nitrogen for agriculture: Specific energy and stability studies. *Journal of Applied Physics*, *129*(9), 093303-11pp. doi: https://doi.org/10.1063/5.0039253

Takeuchi, N., & Yasuoka, K. (2020). Review of plasma-based water treatment technologies for the decomposition of persistent organic compounds. *Japanese Journal of Applied Physics*, *60*, SA0801-13pp. doi: https://doi.org/10.35848/1347-4065/abb75d

Tendero, C., Tixier, C., Tristant, P., Desmaison, J., & Leprince, P. (2006). Atmospheric pressure plasmas: A review. *Spectrochimica Acta Part B: Atomic Spectroscopy*, *61*(1), 2-30. doi: https://doi.org/10.1016/j.sab.2005.10.003

Thakur, G., Khanal, R., & Narayan, B. (2019). Characterization of arc plasma by movable single and double langmuir probes. *Fusion Science and Technology*, *75*(4), 324-329. doi: https://doi.org/10.1080/15361055.2019.1579623

Thirumdas, R., Deshmukh, R., & Annapure, U. (2016). Effect of low temperature plasma on the functional properties of Basmati rice flour. *Journal of Food Science and Technology*, *53*(6), 2742-2751. doi: https://doi.org/10.1007/s13197-016-2246-4

Thirumdas, R., Kothakota, A., Annapure, U., Siliveru, K., Blundell, R., Gatt, R., & Valdramidis, V. P. (2018). Plasma activated water (PAW): Chemistry, physico-

chemical properties, applications in food and agriculture. *Trends in Food Science & Technology*, *77*, 21-31. doi: https://doi.org/10.1016/j.tifs.2018.05.007

Thirumdas, R., Kothakota, A., Kiran, K. C. S. S., Pandiselvam, R., & Prakash, V. U. B. (2017). Exploitation of cold plasma technology in agriculture. *Advances in Research*, *12*, 1-7. doi: https://doi.org/10.9734/AIR/2017/38044

Tian, Y., Guan, B., Zhou, D., Yu, J., Li, G., & Lou, Y. (2014). Responses of seed germination, seedling growth, and seed yield traits to seed pretreatment in maize (*Zea mays L.*). *The Scientific World Journal*, *2014*, 1-8. doi: https://doi.org/10.1155/2014/834630

Tonks, L., & Langmuir, I. (1929). A general theory of the plasma of an arc. *Physical Review*, *34*(6), 876-924. doi: https://doi.org/10.1103/PhysRev.34.876

Townsend, J. (1900). The conductivity produced in gases by the motion of negatively-charged ions. *Nature*, *62*(1606), 340-341. doi: https://doi.org/10.1038/062340b0

Townsend, J. S. E. (1900). The diffusion of ions into gases. *Philosophical Transactions of the Royal Society of London. Series A, Containing Papers of a Mathematical or Physical Character*, *193*, 129-158. Retrieved from `https://www.jstor.org/stable/116121,Accessed19May2024`

Tyata, R. B., Subedi, D. P., Shrestha, A., & Baral, D. (2012). Development of atmospheric pressure plasma jet in air. *Kathmandu University Journal of Science, Engineering and Technology*, *8*(1), 15-22.

Unnikrishnan, V. K., Alti, K., Kartha, V. B., Santhosh, C., Gupta, G. P., & Suri, B. M. (2010). Measurements of plasma temperature and electron density in laser-induced copper plasma by time-resolved spectroscopy of neutral atom and ion emissions. *Pramana*, *74*, 983-993. doi: https://doi.org/10.1007/s12043-010-0089-5

Volin, J. C., Denes, F. S., Young, R. A., & Park, S. M. (2000). Modification of seed germination performance through cold plasma chemistry technology. *Crop Science*, *40*(6), 1706-1718. doi: https://doi.org/10.2135/cropsci2000.4061706x

Völker, T., & Gornushkin, I. B. (2022). Importance of physical units in the Boltzmann plot method. *Journal of Analytical Atomic Spectrometry*, *37*(10), 1972-1974. doi: https://doi.org/10.1039/D2JA00241H

Voráč, J., Kusỳn, L., & Synek, P. (2019). Deducing rotational quantum-state distributions from overlapping molecular spectra. *Review of Scientific Instruments*, *90*(12), 123102-10pp. doi: https://doi.org/10.1063/1.5128455

Voráč, J., Synek, P., Potočňáková, L., Hnilica, J., & Kudrle, V. (2017a). Batch processing of overlapping molecular spectra as a tool for spatio-temporal diagnostics of power modulated microwave plasma jet. *Plasma Sources Science and Technology*, *26*(2), 025010-12pp. doi: https://doi.org/10.1088/1361-6595/aa51f0

Voráč, J., Synek, P., Procházka, V., & Hoder, T. (2017). State-by-state emission spectra fitting for non-equilibrium plasmas: OH spectra of surface barrier discharge at argon/water interface. *Journal of Physics D: Applied Physics*, *50*(29), 294002-28pp. doi: https://doi.org/10.1088/1361-6463/aa7570

Wang, X.-Q., Zhou, R.-W., Groot, G. d., Bazaka, K., Murphy, A. B., & Ostrikov, K. (2017). Spectral characteristics of cotton seeds treated by a dielectric barrier discharge plasma. *Scientific Reports*, *7*(1), 5601-9pp. doi: https://doi.org/10.1038/s41598-017-04963-4

Waskow, A., Howling, A., & Furno, I. (2021). Mechanisms of plasma-seed treatments as a potential seed processing technology. *Frontiers in Physics*, *9*, 617345-23pp. doi: https://doi.org/10.3389/fphy.2021.617345

Wen, B., Xio, W., Mu, Q., Li, D., Chen, X., Wu, H., Li, L., & Peng, F. (2020). How does nitrate regulate plant senescence? *Plant Physiology and Biochemistry*, *157*, 60-69. doi: https://doi.org/10.1016/j.plaphy.2020.08.041

Worldometers. (2024). *Current world population.* Retrieved 2024 January 11, from `https://www.worldometers.info/population`.

Wu, A. J., Zhang, H., Li, X. D., Lu, S. Y., Du, C. M., & Yan, J. H. (2015). Determination of spectroscopic temperatures and electron density in rotating gliding arc discharge. *IEEE Transactions on Plasma Science*, *43*(3), 836-845. doi: 10.1109/TPS.2015.2394441

Xu, D., Wang, S., Li, B., Qi, M., Feng, R., Li, Q., Chen, H., & Kong, M. G. (2020). Effect of plasma activated water on skin wound healing in mice. *Microorganisms*, *8*(7), 1091-14pp. doi: https://doi.org/10.3390/microorganisms8071091

Xu, G., Wang, X.-t., Gan, C.-l., Fang, Y.-q., & Zhang, M. (2012). Biological effects of low energy nitrogen ion implantation on *Jatropha curcas L.* seed germination. *Nuclear Instruments and Methods in Physics Research Section B: Beam Interactions with Materials and Atoms*, *287*, 76-84. doi: https://doi.org/10.1016/j.nimb.2012.05.038

Yadav, S., Modi, P., Dave, A., Vijapura, A., Patel, D., & Patel, M. (2020). *Effect of abiotic stress on crops* (Vol. 3). IntechOpen, United Kingdom. doi:

http://dx.doi.org/10.5772/intechopen.8352

Yao, W., & Shen, Y. (2015). Effect of magnetic treatment on seed germination of loblolly pine *(Pinus taeda L.)*. *Scandinavian Journal of Forest Research*, *30*(8), 639-642. doi: https://doi.org/10.1080/02827581.2015.1048717

Zhang, J. J., Jo, J. O., Huynh, D. L., Mongre, R. K., Ghosh, M., Singh, A. K. & Jeong, D. K. (2017). Growth-inducing effects of argon plasma on soybean sprouts via the regulation of demethylation levels of energy metabolism-related genes. *Scientific Reports*, *7*(1), 41917. doi: https://doi.org/10.1038/srep41917

Zhang, M., Yunhu, L., Yao, L., Shuqi, L., Hao, Y., Liang, J., Xigfeng, Z., & Dezheng, Y. (2023).Generation of atmospheric pressure air diffuse discharge plasma in oxygen enriched working gas with floating electrode. *Plasma Science and Technology*, *25*(4), 045405-8pp. doi: https://doi.org/10.1088/2058-6272/aca5f3

Zhao, T. L., Xu, Y., Song, Y. H., Li, X. S., Liu, J. L., Liu, J. B., & Zhu, A. M. (2013). Determination of vibrational and rotational temperatures in a gliding arc discharge by using overlapped molecular emission spectra. *Journal of Physics D: Applied Physics*, *46*(34), 345201-12pp. doi: https://doi.org/10.1088/0022-3727/46/34/345201

Zhao, Y.-M., Patange, A., Sun, D.-W., & Tiwari, B. (2020). Plasma-activated water: Physicochemical properties, microbial inactivation mechanisms, factors influencing antimicrobial effectiveness, and applications in the food industry. *Comprehensive Reviews in Food Science and Food safety*, *19*(6), 3951-3979. doi: https://doi.org/10.1111/1541-4337.12644

Zhou, R., Zhou, R., Wang, P., Xian, Y., Mai-Prochnow, A., Lu, X., Cullen, P.J., Ostrikov, K.K. & Bazaka, K. (2020). Plasma-activated water: Generation, origin of reactive species and biological applications. *Journal of Physics D: Applied Physics*, *53*(30), 303001-28pp. doi: https://doi.org/10.1088/1361-6463/ab81cf

APPENDIX

Academic Activities

A. Attended courses offered by IoST

First semester:

PHS 911, Philosophy of Science (Cr. Hrs. 3)

PHS 912, Research Methodology (Cr. Hrs. 3)

PHS 913, Seminar (Cr. Hrs. 3)

Second semester:

PHS 951, Advanced Research Methodology (Cr. Hrs. 3)

PHS 957, Advanced Plasma Physics (Cr. Hrs. 3)

PHS 952, Seminar (Cr. Hrs. 3)

B. Paper publications

International

1) Chalise, R., Bhandari, P., Sharma, S., Basnet, S., Subedi, D. P., & Khanal, R. (2023). Enhancement of wheat yield by atmospheric pressure plasma treatment. *AIP Advances*, *13*, 065104.

2) Chalise, R., Shrestha, P., Sharma, S., Basnet, S., Mishra, L. N., & Khanal, R. (2023). Enhancing seed germination and growth parameters of cauliflower (*Brassica oleracea*, variety *Botrytis*) using plasma-activated water. *Journal of Physics D: Applied Physics*, *56*, 505201.

3) Chalise, R., Dahal, A., Basnet, S., Sharma, S., Panta, D. R., & Khanal, R. (2023). Effect of plasma-activated water on chlorophyll retention in detached Tejpat (*Cinnamomum tamala*) leaves. *Heliyon*, *10*, e24480.

4) Chalise, R., Niroula, A., Shrestha, P., Paudel, B., Subedi, D., & Khanal, R. (2023). A low-cost goniometer for contact angle measurements using drop image analysis: Development and validation. *AIP Advances*, *13*, 085123.

5) Dhakal, O. B., Dahal, R., Acharya, T. R., Lamichhane, P., Gautam, S., Lama, B., Kaushik, N. K., Choi, E. H., and Chalise, R. (2023). Effects of spark dielectric barrier discharge plasma on water sterilization and seed germination. *Current Applied Physics*, *54*, 49.

6) Pudasaini, A., Chaudhary, D. K., Chalise, R., Shrestha, P., Joshi, L. P., & Khanal, R. (2023). Effect of atmospheric dielectric barrier discharge on optical, electrical, and surface properties of ZnO thin film. *Advanced Materials Research*, *1176*, 43.

7) Sharma, S., Chalise, R., Basnet, S., Lamichhane, H. P., & Khanal, R. (2024). Development of a low-cost plasma source using a fly-back transformer for atmospheric pressure gliding arc discharge. *Physics of Plasmas*, *31*, 043509.

8) Chalise, R., Tamang, A., Kattel, A., Sharma, S., Basnet, S., & Khanal, R. (2024). Impact of plasma-activated water on germination, growth, and production of green leafy vegetables. *AIP Advances*, *14*(6), 065318.

9) Chalise, R., Dhungana, S., Sharma, S., Basnet, S., Baniya, H.B., Acharya, T.R., Lamichhane, P., & Khanal R. (2024). Development and characterization of atmospheric pressure gliding arc plasma jet. *Physica Scripta*, *99*(10), 105611.

10) Dahal, R., Dhakal, O. B., Acharya, T. R., Lamichhane, P., Gautam, S., Chalise, R., Kaushik N., Choi E.H., & Kaushik, N. K. (2024). Investigating plasma activated water as a sustainable treatment for improving growth and nutrient uptake in maize and pea plant. *Plant Physiology and Biochemistry*, 216, 109203.

National

1) Chalise R., Regmi K., Nepal S., Sharma S., Basnet S.,& Khanal R. (2024). Characterization of atmospheric pressure circular dielectric Barrier discharge via electrical and optical methods. *BIBECHANA*, *21*(3), 187

2) Mishra, L. N., Dahal, R., & Chalise, R. (2022). Impact of plasma treatment on coriander seeds for germination and growth. *Patan Pragya*, *10*(01), 86.

Under Review

1) Chalise, R., Lamichhane, P., Niure, D., Khan A.K., Sharma, S., Basnet, S., Lamichhane, P., Acharya, T.R., Lamichhane, P., & Khanal R., *Enhancing Oyster Mushroom Growth and Yield using Air Gliding Arc Discharge*. *Journal of Physics D: Applied Physics*

2) Chalise R., Rijal O.S, Oli D., Regmi K., Nepal S., Sharma S., Basnet S., and Khanal R., *Physical Properties of Natural and Processed Water Using Dielectric Barrier and Gliding Arc Discharges*. *IEEE Transactions on Plasma Science*

3) Chalise R., Kattel, A., Yadav, A.K., Sharma S., Basnet S., and Khanal R., *Plasma-activated water from gliding arc discharge and its application on germination and seedling growth of Basmati rice*. *Special Issue of JNPS*

C. Participation

1) Roshan Chalise, Bhagirath Ghimire, and Raju Khanal, Oral Presentation entitled in the conference “Effect of plasma treatment on the sprouting of Kwati beans" NAST 9^{th} National Conference on Science and Technology, during 26-28 June 2022 Kathmandu, Nepal

2) Roshan Chalise, Bhagirath Ghimire, and Raju Khanal, Participating and presenting our research work entitled “Enhancement of Agricultural Productivity by using Cold Atmospheric Pressure Plasma” in the 20^{th} International Congress on Plasma Physics (ICPP 2022), in Gyeongju, Korea, from November 27^{th} to December 2nd, 2022.

3) One month of Ph.D. training at Plasma Bioscience Research Center (PBRC), Kwangwoon University, Seoul, South Korea from Dec-3, 2022 to Jan-3, 2023.

4) Roshan Chalise, Bhagirath Ghimire, and Raju Khanal, Oral presentation entitled “Enhancement of Agricultural Commodities by Using Atmospheric Pressure Plasma" Plasma Theory and Simulation (PTS-2023) 21-23 September 2023 organized by JNU, New Delhi, India.

5) Roshan Chalise, Bhagirath Ghimire, and Raju Khanal, Oral and poster presentation entitled “Characterization and Application of Atmospheric Pressure Plasma for Enhanced Seed Germination and Agricultural Growth” in a Ph.D. festival organized by IOST, Tribhuvan University, Kathmandu, during 9-10, October 2023

Award

Nepal Physical Society Award (Prof. Dr. Shankar Prasad and Sudakshina Pradhan Award 2024).

D. Co-supervision of M.Sc. dissertations under Prof. Raju Khanal

Deepak Niure: Effect of Gliding Arc Discharge Plasma on Germination and Production of Oyster Mushroom (*Pleurotus ostreatus*)

Asish Dahal: Effect of Plasma Activated Water using Gliding Arc Discharge on Chlorophyll of Tejpatta Leaves (*Cinnamomum tamala*)

E. Co-supervision of B.Sc. project works under Prof. Raju Khanal

Avash Kattel: Germination and Seedling Growth of Khumal-14 Paddy Seeds using Plasma Activated Water

Abdul K Khan: Effect of Activated Water on the Yield of Oyster Mushroom

Asish Tamang: Germination and Seedling Growth of Green Leafy Vegetables using Plasma Activated Water

F. Research Work on PBRC, Korea

Characterization of Plasma Source

During the third semester, I got an opportunity for a one-month training at Plasma Bioscience Research Center (PBRC), Kwangwoon University, South Korea under Prof. Eun Ha Choi. Where learned generation of plasma sources, characterization and application techniques of plasma in agricultural field. I am confidential that with out his one months training, I can not published in renowned journal and complete Ph.D. within 3 years. Some tof the work which are done in PBRC presented here. The achievement at the one month, generation of plasma sources and its electrical and optical characterization, and germination of paddy and leafy mustard seeds provided by NARC, Khumaltar, Nepal. We have chosen the FDBD for the non-thermal plasma to uniform seed treatment and to treat multiple seeds simultaneously, and APJ for making PAW as shown in Figure 66. The plasma-activated water is activated by an APJ as shown in Figure 66(b). Figure 67 shows the schematic diagram of the floating DDB, the

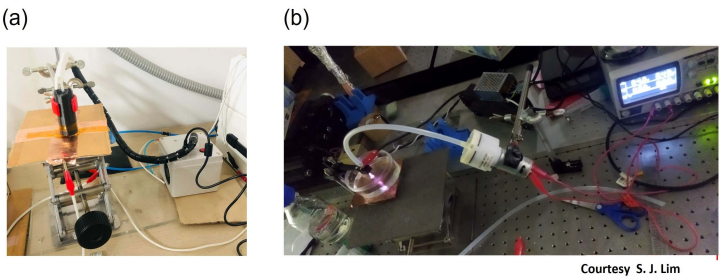

Figure 66: (a) Floating DBD that is used for direct seeds treatment, and (b) APJ for making PAW

current-voltage waveform of FDBD, and the optical emission spectroscopic spectrum of the FDBD source. It is observed that the peak-to-peak applied voltage is 15.62 kV, the root mean square voltage is 5.52 kV, the first discharge current is 16.61 mA, and the corresponding discharge voltage is 2.05 kV. Charge in one full cycle is 106.33 nC, energy is 586.94 µJ, the applied source's frequency is 34 kHz, the circuit's duty cycle is 14%, and the power is 0.45 W. Since air is the feeder gas and contains 78% nitrogen, nitrogen

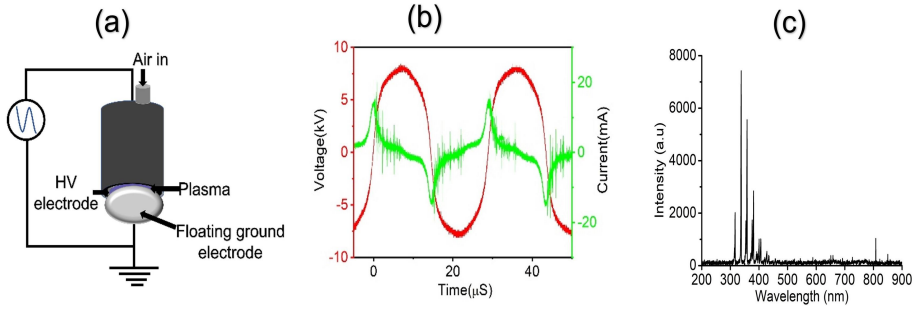

Figure 67: (a) Schematic diagram of FDBD, (b) I-V waveform, and (c) Optical emission spectra

species are mainly visible in the spectrum. Nitrogen N_2(C-B) species and OH(A-X) band

are observed. The electron excitation temperature (T_{exc}) of the floating DBD plasma source is 1.37 eV from the emission ratio method and 1.12 eV from the Boltzmann plot approach, with electron density $N_e = 9.2\times10^{14}$ cm^{-3}, rotational temperature $T_{rot} = 432.5 \pm 87.8$ K, and vibrational temperature $T_v = 2140.5\pm351.3$ K.

Direct Application of Plasma

For this study, we have chosen the Basmati rice Khumal-12, Khumal-14, Khumal-16, and *Brassica juncea* native seeds that NARC, Khumaltar recommended. This paddy seed is widely used in Nepal. The seeds for Basmati rice Khumal-12, and *Brassica juncea* are treated by FDBD at one, three, five, and seven min before being sown in a petri dish and placed in a plant growth chamber at 25°C and 60% humidity. Each dish has 3.0 ml of ultra-pure water with two filter papers already soaked in it, followed by treated 20 dry seeds of paddy as shown in Figure 68 (a), and 100 dry seeds of *Brassica juncea*. The dormancy and germination situation is considered if one stem and two stems appeared in seeds correspondingly as shown in Figure 68 (b). The dormancy and germination data

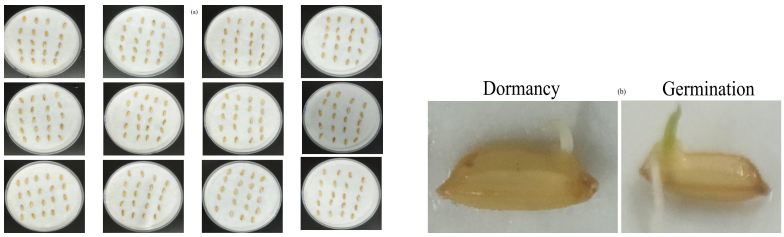

Figure 68: Seed preparation for placing the plant growth chamber, dormancy, and germination situation

is carried out at the end of the second and third days after seedling. Figure 69 shows the outcomes that are obtained. Although plasma-treated seeds are found to have higher dormancy and germination results than untreated seeds, longer-time plasma treatment does not show an advantageous result. In the case of *Brassica juncea* (leaf mustard), plasma direct treatment is not advantageous for germination because seeds are very tiny, and direct treatment damages the embryo of the seed.

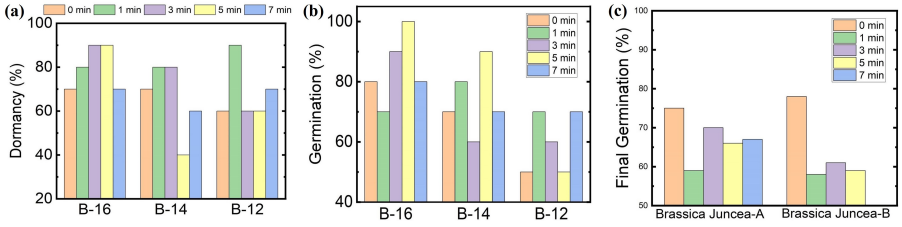

Figure 69: (a) Dormancy of Basmati rice at of the 2^{nd} day, (b) germination at the 3^{rd} day, and (c) the final germination of *Brassica juncea* at the 5^{th} day after planting

Indirect Applications of Plasma

Figure 70 illustrates the mechanism of the planting process. We have used the PAW in the process of sowing prepared by APJ at 10 LPM. To enhance seed germination through the use of PAW, we have chosen only Basmati rice Khumal-12 and 90.0 ml of ultra-pure

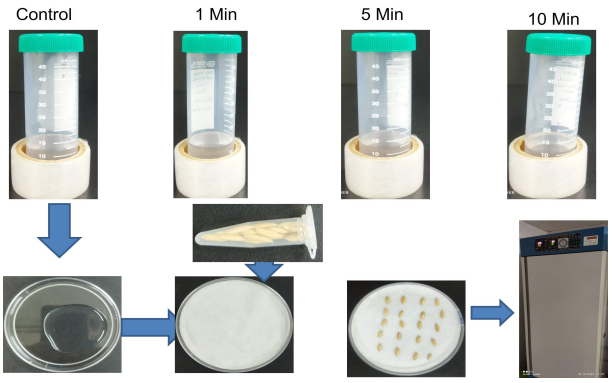

Figure 70: Sowing process of seeds

water that is treated for one min, five min, and 10 min at one time and used throughout the entire experiment. For each of the three petri dishes, three pieces of filter paper are wet with 5.0 ml of water, and 20 seeds are put in. Data are collected every 12 hours, and 1.0 ml of corresponding water is used for maintaining the wet environment every 24 hours. When compared to control water, one min plasma-treated water exhibits good results, while longer exposure water exhibits adverse effects on Basmati rice Khumal-12 germination and dormancy as shown in Figure 71. Based on the findings, the 10 min

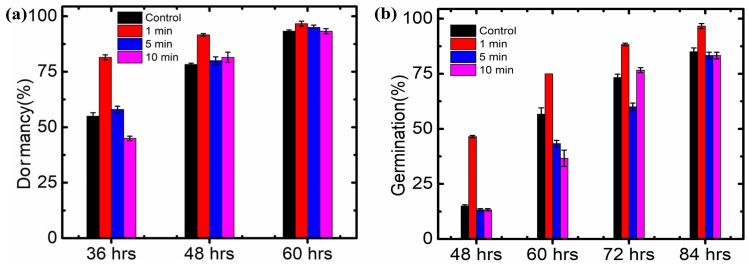

Figure 71: (a) Dormancy of Basmati rice Khumal-12 at the 2^{nd} days after sowing, and (b) germination at the 3^{rd} days after sowing

PAW is leaved, and one, two, three, four, and five min PAW is chosen for the next study as shown in Figure 72 (a) and (b). The PAW that has been treated for two min observed the higher germination of Basmati rice.

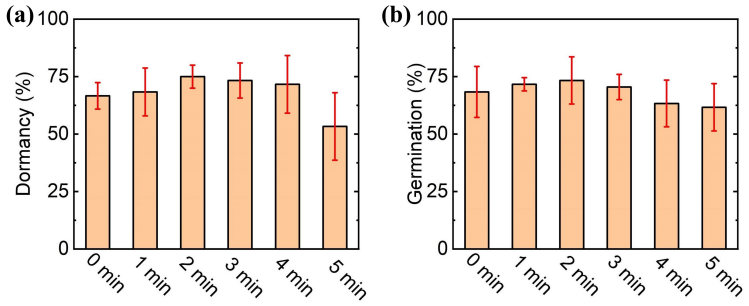

Figure 72: (a) Dormancy of Basmati rice Khumal-12 at the 2^{nd} day after sowing, and (b) germination at the 3^{rd} day after sowing